การใช้ดินเหนียวธรรมชาติดัดแปลงเป็นวัสดุดูดซับราคาประหยัด
สำหรับการกำจัดสารหนูในน้ำ

นายโบราโณ แด

วิทยานิพนธ์นี้เป็นส่วนหนึ่งของการศึกษาตามหลักสูตรปริญญาวิศวกรรมศาสตรดุษฎีบัณฑิต
สาขาวิชาวิศวกรรมสิ่งแวดล้อม
มหาวิทยาลัยเทคโนโลยีสุรนารี
ปีการศึกษา 2560

USING MODIFIED NATURAL COMMON CLAY AS

LOW-COST ADSORBENTS FOR ARSENIC REMOVAL

FROM AQUEOUS SOLUTION

Borano Te

A Thesis Submitted in Partial Fulfillment of the Requirements for the

Degree of Doctor of Philosophy in Environmental Engineering

Suranaree University of Technology

Academic Year 2017

USING MODIFIED NATURAL COMMON CLAY AS LOW-COST

ADSORBENTS FOR ARSENIC REMOVAL

FROM AQUEOUS SOLUTION

Suranaree University of Technology has approved this thesis submitted in partial fulfillment of the requirements for the Degree of Doctor of Philosophy.
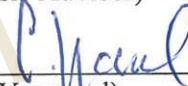
Thesis Examining Committee

_____
(Dr. Apichon Watcharenwong)

Chairperson

_____
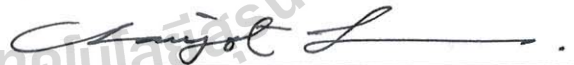(Asst. Prof. Dr. Boonchai Wichitsathian)

Member (Thesis Advisor)

_____
(Dr. Chatpet Yossapol)

Member

_____
(Asst. Prof. Dr. Sudjit Karuchit)

Member

_____
(Prof. Dr. Chaiyot Tangsathitkulchai)

Member

_____
(Assoc. Prof. Dr. Patiparn Punyapalakul)

Member

_____
(Assoc. Prof. Flt. Lt. Dr. Kontorn Chamniprasart)

_____
(Prof. Dr. Santi Maensiri)

Vice Rector for Academic Affairs

and Internationalization

Dean of Institute of Engineering

โบราโณ แด : การใช้ดินเหนียวธรรมชาติดัดแปลงเป็นวัสดุดูดซับราคาประหยัดสำหรับการกำจัด
สารหนูในน้ำ (USING MODIFIED NATURAL COMMON CLAY AS LOW-COST
ADSORBENTS FOR ARSENIC REMOVAL FROM AQUEOUS SOLUTION)
อาจารย์ที่ปรึกษา : ผู้ช่วยศาสตราจารย์ ดร.บุญชัย วิจิตรเสถียร, 187 หน้า.

คนนับล้านทั่วโลกในกว่า 70 ประเทศนั้นอยู่ในภาวะความเสี่ยงต่อการเกิดโรคพิษสารหนูเรื้อรังหรือ
โรคมะเร็งเนื่องจากการบริโภคน้ำที่มีการปนเปื้อนสารหนูในปริมาณสูง เทคโนโลยีการบำบัดน้ำที่ใช้กันอยู่นั้น
ล้วนแต่เป็นวิธีที่ใช้พลังงานสูงและสิ้นค่าใช้จ่ายมาก การพัฒนาวัสดุดูบซับราคาประหยัดและมีประสิทธิผลใน
การกำจัดสารหนูนั้นน่าจะเป็นแนวทางแก้ปัญหาที่นำไปใช้ประโยชน์ได้จริงเนื่องจากเป็นวิธีที่ง่าย ประหยัด
ยืดหยุ่น ง่ายต่อการดำเนินการ และมีประสิทธิภาพสูง งานวิจัยนี้มีจุดมุ่งหมายเพื่อเตรียมวัสดุดูดซับจากดินเหนียว
ธรรมชาติดัดแปลง และเพื่อศึกษาถึงสมรรถนะของวัสดุดูดซับนี้ในการกำจัดสารหนูในน้ำ โดยวัสดุดูดซับที่ได้
เตรียมขึ้นได้แก่ดินเหนียวเผาและดินเหนียวเผาดัดแปลงผสมเหล็กเฟอรัสและเหล็กเฟอริก ในการทดลองแบบกะ
นั้นพบว่าความสามารถในการดูดซับสูงสุดนั้นอยู่ในช่วง 250-747 µg/g และ 46.7-355 µg/g สำหรับการกำจัดอาร์เซ
เนตและอาร์เซไนต์ตามลำดับ และได้ใช้วิธี Mixture Design ในการกำหนดสัดส่วนที่เหมาะสมของเหล็กสำหรับ
การทำเม็ดตัวกลาง ซึ่งพบว่าสัดส่วนที่เหมาะสมได้แก่การเตรียมเม็ดตัวกลางด้วยดินเหนียวธรรมชาติ 52.15%
เหล็กออกไซด์ 19.22% และเหล็กผง 28.63% ซึ่งให้ค่าความสามารถในการดูดซับสูงสุดที่ 13 mg/g และ 19 mg/g
สำหรับการกำจัดอาร์เซเนตและอาร์เซไนต์ตามลำดับ และในการศึกษาถึงอิทธิพลของประจุลบนั้นพบว่าประจุลบ
ของฟอสเฟตมีผลทำให้ประสิทธิผลและ ประสิทธิภาพในกำจัดอาร์เซเนตและอาร์เซไนต์ด้อยลงในทุกวัสดุดูดซับ
และในการวิเคราะห์แบบ Pareto ด้วย Response Surface ถึงปัจจัยที่มีอิทธิพลต่อการบำบัดน้ำที่มีทั้งอาร์เซเนตและ
อาร์เซไนต์ร่วมกันนั้นพบว่าปัจจัยที่มีอิทธิพลมากที่สุด ได้แก่ค่าความเป็นกรดเป็นด่าง ความเข้มข้นเริ่มต้นของมล
สาร และปริมาณของวัสดุดูดซับ ซึ่งคิดเป็นสัดส่วน 47% 37% และ 14% ตามลำดับ ส่วนในการทดลองแบบ
คอลัมน์ที่มีการไหลต่อเนื่องนั้นดำเนินการ โดยใช้เม็ดตัวกลางดินเหนียวดัดแปลงผสมเหล็ก ให้ค่าความสามารถ
ในการดูดซับสูงสุดที่ 431 µg/g และ 509 µg/g สำหรับการกำจัดอาร์เซเนตและอาร์เซไนต์ตามลำดับ และการเตรียม
ชั้นวัสดุดูดซับ สำหรับการทดสอบภาคสนามนั้นประกอบไปด้วยการใช้เม็ดตัวกลางดินเหนียวดัดแปลงผสมเหล็ก
แทรกในตอนกลางระหว่างชั้นทรายและชั้น bio-sand น้ำหนักเบา ซึ่งพบว่ามีความสามารถในการกำจัดสารหนูที่มี
ความเข้มข้นระหว่าง 354-587 µg/L ด้วยประสิทธิภาพระหว่าง 97% ถึง 99% ซึ่งโดยสรุปแล้ววัสดุดูดซับดินเหนียว
ดัดแปลงน่าจะถือได้ว่ามีประสิทธิภาพและมีราคาประหยัดสำหรับใช้ในการกำจัดสารหนูในน้ำ ด้วยเหตุผลว่าเป็น
วัตถุดิบที่สามารถหาได้ทั่วไป ใช้เทคนิคที่ง่ายในการดัดแปลงวัสดุดูดซับ และมีการดูดซับด้วยประสิทธิภาพสูง

สาขาวิชาวิศวกรรมสิ่งแวดล้อม   ลายมือชื่อนักศึกษา_____
ปีการศึกษา 2560   ลายมือชื่อของที่ปรึกษา_____
   ลายมือชื่อของที่ปรึกษาร่วม_____

BORANO TE : USING MODIFIED NATURAL COMMON CLAY AS

LOW-COST ADSORBENTS FOR ARSENIC REMOVAL FROM AQUEOUS

SOLUTION. THESIS ADVISOR : ASST. PROF. BOONCHAI

WICHITSATHIAN, Ph.D., 187 PP.

ADSORPTION/ARSENIC/NATURAL CLAY/MESOPOROUS ADSORBENT

Millions of people in more than 70 countries are at risk of developing arsenicosis or cancer due to consuming elevated arsenic contaminated water. A failure of most applied remediation technologies is due to energy consumption and high cost. Developing low-cost and effective adsorbents for arsenic removal can provide a promising solution because the adsorption technique is simple, cost-effective, more flexible, easily operated and more efficient. The present research mainly aims to prepare modified natural clay adsorbents and to investigate their performance toward arsenic adsorption from aqueous solution. Calcined, ferrous and ferric-impregnated calcined clay adsorbents were prepared and characterized. In the batch experiments, the maximum adsorption capacities of the adsorbents were in the range of 250-747 µg/g and 46.7-355 µg/g for arsenate and arsenite, respectively. On the other hand, iron mixed porous clay pellet was developed in accordance with the mixture design approach. The optimum ratio was found to be 52.15% (natural clay):19.22% (iron oxide):28.63% (iron powder) and the maximum adsorption capacities were approximately 13 mg/g and 19 mg/g for arsenate and arsenite, respectively. Among coexisting anions, phosphate showed a significant negative effect on the removal efficiency of either arsenate or arsenite for all adsorbents. With central composite design under response surface methodology, the Pareto analysis suggested that the initial solution pH, initial adsorbate concentration, and adsorbent dosage had contributing percentage effects of around 47%,

37% and 14%, respectively, for the coexisting arsenite and arsenate removal. In the continuous fixed-bed column with iron mixed porous pellet, the highest adsorption capacities were approximately 431µg/g and 509µg/g for arsenate and arsenite, respectively. Adding iron mixed porous pellet in the middle of sand layer of lightweight bio-sand filter to treat polluted groundwater with arsenic ranging from 354-587µg/L improved the removal efficiency to about 97 and 99 %. Overall, with regard to a wide availability of raw materials, the simplicity of modification techniques, and the improvement of adsorption efficiencies, modified natural clay adsorbents could be considered to be effective and low-cost for arsenic removal from water.
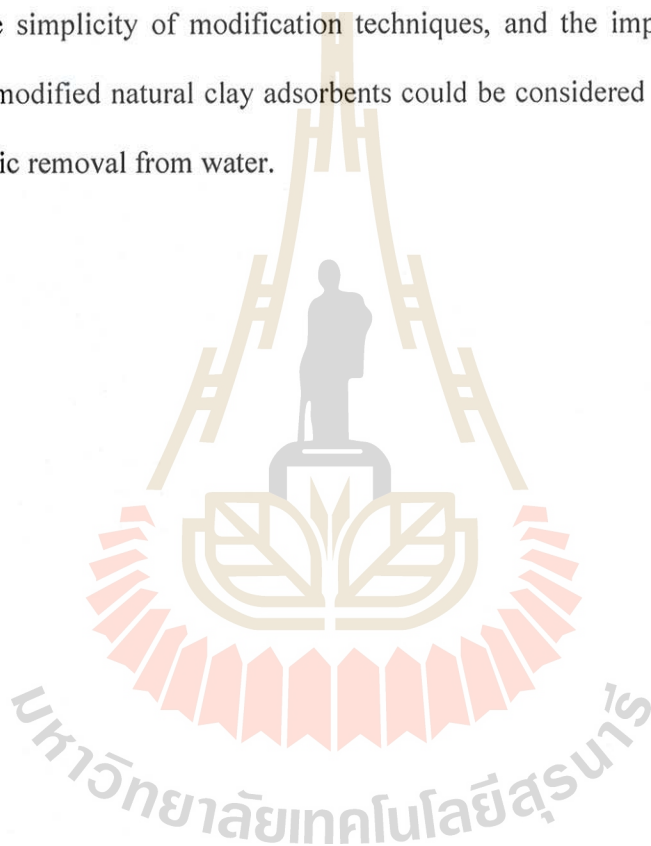
School of <u>Environmental Engineering</u>   Student's Signature _____

Academic Year 2017   Advisor's Signature _____

                                                     Co-Advisor's Signature _____

ACKNOWLEDGMENTS

I am very grateful to be awarded into SUT-ASEAN PhD scholarship program initiated by Suranaree University of Technology (SUT). Without this program, I would not even have been able to start and have a memorable graduate student life at SUT.

I would like to express my deeply gratitude to my advisor, Asst. Prof. Dr. Boonchai Wichitsathian, and co-advisor, Dr. Chatpet Yossapol, for their guidance, advice, comment, support, time and effort to make me able to initiate the research project and bring it to completion.

I greatly acknowledge and thank all faculty members of the School of Environmental Engineering for their kind help in both academic and administrative works. Extensive thanks go to my seniors and all friends at SUT for their warm friendship and encouragement to make my study life comfortable and joyful.

Special thanks go to Prof. Dr. Kevin D. Curry and Elizabeth A. Curry for their respectable kindness, friendship and recommendation. Without such supports, I would not have an opportunity for taking this graduate education. Plus, it would be my privilege to get help and support in the research project from all friends at Preah Kossomak Polytechnic Institute (PPI) and Paññāsāstra University of Cambodia (PUC) in Cambodia.

Finally, I would like to dedicate this to Dr. Anita Pattnaik, a former dean of Faculty of Science, Mathematics and Engineering, PUC.

Borano Te

TABLE OF CONTENTS

Page

TABLE OF CONTENTS (Continued)

TABLE OF CONTENTS (Continued)

TABLE OF CONTENTS (Continued)

TABLE OF CONTENTS (Continued)

IRON MIXED CLAY POROUS PELLET IN

A FIXED-BED COLUMN………………………………………..108

7.1   Introduction…………………………………............108

7.2   Materials and methods…………………………............ 109

        7.2.1 Reagents………………………………………109

        7.2.2 Adsorbent preparation and its characterization…………… 109

        7.2.3 Fixed-bed adsorption experiments…………………………110

        7.2.4 Application to the real arsenic contaminated

                groundwater……………………………………111

        7.2.5 Fixed-bed column data analysis……………………....111

7.3   Results and discussion…………………………............113

        7.3.1 Adsorbent characterization……………………………..113

        7.3.2 Continuous fixed-bed column studies……………............ 114

        7.3.3 Effect of flow rate……………………………………115

        7.3.4 Effect of bed height……………………………............ 118

        7.3.5 Effect of initial concentration…………………………..119

        7.3.6 Effect of initial pH……………………………………121

        7.3.7 Kinetic models of the fixed-bed column adsorption……….122

                7.3.7.1 The Thomas kinetic model………………………..123

                7.3.7.2 The Adams-Bohart model………………………..125

TABLE OF CONTENTS (Continued)

TABLE OF CONTENTS (Continued)

LIST OF TABLES

LIST OF TABLES (Continued)

LIST OF FIGURES

LIST OF FIGURES (Continued)

LIST OF FIGURES (Continued)

LIST OF FIGURES (Continued)

LIST OF FIGURES (Continued)

LIST OF FIGURES (Continued)

LIST OF FIGURES (Continued)

CHAPTER I

INTRODUCTION

1.1   Background

Water is a key element of life. People need to access to safe and clean drinking water, but majority of the world population cannot afford it due to water pollution. The presence of excess toxins and pathogens in water is a major issue and limits the availability of drinkable water. One of highly toxic and carcinogenic pollutants is arsenic. Its existence in soil, air and water results from both natural processes and human activities, e.g., weathering reactions, biological activities, geochemical reactions, volcanic emissions, mining activities, fossil fuel combustions, and utilizations of arsenic pesticides and additives (Mohan and Pittman, 2007). In recent decades, arsenic contamination in water has become a global concern because it causes a serious threat to human health at a large scale. Arsenic is regarded as the number one toxin in the United States Environmental Protection Agency (USEPA) list of prioritized pollutants and also classified as a class I of human carcinogen by the International Agency for Research on Cancer (IARC) (Chen et al., 2009; Ng et al., 2003). Consumption of arsenic contaminated water is one of the main pathways for its accumulation in human body (Singh et al., 2015). Health problems associated with excessive and long-term exposure to arsenic are skin problems, skin cancers, internal cancers (bladder, kidney and lung), leg and feet blood vessel diseases, diabetes, high blood pressures, reproductive disorders, adverse pregnancy outcomes, and intellectual malfunction in children (Chen et al., 2009; Sharma et al., 2014).

The World Health Organization (WHO) has newly set the maximum contaminant level (MCL) of arsenic in drinking water to 10 ppb brought down from 50 ppb (Glocheux et al., 2013; Ng et al., 2003). More than 70 countries have been reported with elevated arsenic concentration (>10 ppb) in water sources that poses a health risk to more than 150 million people, most of whom live in countries as follow: Bangladesh, Cambodia, China, India, Laos, Myanmar, Nepal, Pakistan, Taiwan and Vietnam (Brammer and Ravenscroft, 2009). In coming years, the consumption of arsenic contaminated groundwater can result in a direct cause of around 6500 deaths a year, and over 2.5 million people may develop arsenicosis in the next 50 years (Glocheux et al., 2013). In some circumstances, the only solution to provide clean and safe drinking water to local people is to treat contaminated water via an affordable purification technique.

Remediation technologies applied for arsenic removal from water include coagulation-flocculation, ion exchange, membrane filtration, reverse osmosis, and adsorption process (Singh et al., 2015). Many arsenic affected areas are in countryside lacking of infrastructures, electricity supplies, and high educated people. This makes some treatment technologies inapplicable. For instance, reverse osmosis and membrane technologies are energy-requiring methods with technical skill operators and pose a high cost (Muniz et al., 2009; Sabbatini et al., 2010). Coagulation-flocculation is not suitable for household scale and has difficulties with a sludge production and a complete separation of flocs. Ion-exchange is considered to be relatively high cost and possibly releases back harmful chemicals into the environment when the resin is regenerated (Lenoble et al., 2005; Sabbatini et al., 2010). Adsorption has more advantages over other techniques in terms of simplicity, economy, removal efficiency, easiness in operation and maintenance, flexibility to be scaled up (from the point of use to a community based treatment plant), and avoidance of liquid waste generation on site (Dousova et al., 2006; Masih et al., 2007; Sabbatini et al., 2010).

The adsorption technique primarily depends on adsorbent materials that can be either natural or synthetic to obtain high affinities toward pollutants (Muniz et al., 2009). Clay has gained much attention to be used for removing pollutants such as metal ions, organic pollutants and bacteria due to its large specific surface area, chemical and mechanical stability, layer structure, and high cation exchange capacity (Dousova et al., 2006; Sdiri et al., 2011). However, the adsorption capacity of clays for arsenic is low compared to that of iron containing minerals. For example, clay minerals such as kaolinite, montmorillonite, and illite exhibit arsenate adsorption in the range of 0.15 to 8.4 µmol/g as compared to ferrihydrite and goethite that can adsorb arsenate in the range of 200 µmol/g to 700 µmol/g (Luengo et al., 2011). Furthermore, clay is difficult for application in a column adsorption due to its fine particle size that creates a permeability problem (Mohapatra et al., 2007). To improve the adsorption capacity and permeability, clays can be modified or used as a binder to iron oxides, iron particles, or other metal oxides (Jiang et al., 2009; Mohapatra et al., 2007).

Pure iron oxides or particles are well-known for a strong adsorption affinity toward arsenic (Dousova et al., 2009; Dousova et al., 2006; Mohan and Pittman, 2007). However, their direct use for arsenic treatment from water is not really popular or plausible under some circumstances because they are not cost-effective in their synthetic forms, difficult to apply for a column study in a fine powdery form, and not easily separated from effluent after adsorption (Dousova et al., 2009; Liu et al., 2012; Maiti et al., 2010).

Low cost materials such as alumina, bauxite, carbon, calcined bauxite, cellulose bead, and clay have been used to support iron oxides or particles to improve pollutant removal efficiency from aqueous solution, and to extend the application in a continuous flow system (Maiti et al., 2010). Previous researchers have observed a significant improvement of the pollutant treatment using iron-clay-based adsorbents. Dousova et al. (2006) has modified some clay minerals with iron salts to adsorb arsenic from aqueous

solution and found that the sorption capacity increased from about 0.5 mg/g to around 20 mg/g. Bhowmick et al. (2014) indicated that montmorillonite-supported nanoscale zero-valent iron (Mt-nZVI) expressed the arsenic adsorption capacity of more than 45 mg/g that is much higher than montmorillonite (only 0.64 mg/g found by Mohapatra et al. (2007)). This may imply that clays could stabilize and disperse iron species on their surface to improve the adsorption capacity.

Most previous studies, however, focus only on using specific pure clay minerals such as kaolinite, montmorillonite, illite and smectite as direct adsorbents or iron modified clay mineral adsorbents for treating arsenic from water. So far of reviewing literatures, no study has completely addressed the use of natural clays for hosting iron species to produce a more cost-effective and efficient adsorbent toward arsenic removal from aqueous solution or treating real elevated arsenic contaminated water in both batch equilibrium and column dynamic systems. Therefore, in this research, natural clay manually collected from the field was used to support iron species to be the novel modified clay based adsorbent for being investigated the arsenic adsorption performance from water, especially the application to treating real contaminated groundwater in an arsenic-affected area.

1.2   Objectives of the research

The overall goals of this research are 1) to develop an efficient iron-based adsorbent through a modification of natural common clay with iron species for a better arsenic adsorption from water and 2) to apply the new developed adsorbent to treat groundwater bearing elevated arsenic concentration in the arsenic-affected area in Cambodia. This is achieved through the following specific objectives:

i)   To prepare, investigate and characterize iron impregnated calcined natural clay adsorbents for arsenic removal from aqueous solution.

ii) To apply a mixture design approach for developing an efficient iron mixed porous pellet adsorbent with a characterization and an investigation for arsenic adsorption from aqueous solution.

iii) To determine optimal condition of contact time, initial solution pH, adsorbent dosage, and initial arsenic concentration for arsenic adsorption with iron mixed porous pellet adsorbent via the application of response surface methodology.

iv) To investigate the arsenic removal from water by iron mixed porous pellet adsorbent in a continuous fixed-bed column study.

v) To add iron mixed porous pellet as active media in a filter to treat real arsenic contaminated groundwater in Cambodia.

1.3 Scopes of the research

This research has been undertaken within scopes as follow:

i) Natural common clay in Thailand is used to impregnate with ferrous and ferric solutions to be iron impregnated calcined natural clay adsorbents for conducting adsorption experiments on arsenite and arsenate from aqueous solution via a batch mode in a laboratory. The characterization of the adsorbent is conducted using X-ray fluorescence (XRF), X-ray diffraction (XRD), the Brunauer-Emmett-Teller (BET) and Scanning electron microscope (SEM) techniques.

ii) Iron mixed porous pellet adsorbent is designed by the augmented simplex-centroid mixture design method for obtaining high adsorption efficiency on both arsenite and arsenate via a batch mode. Regeneration and leaching test of the adsorbent are included.

iii) Central composite design under response surface methodology is applied for optimize the condition of contact time, initial solution pH, adsorbent dosage and adsorbate initial concentration in batch mode experiments.

iv) Performance of the continuous fixed-bed column in terms of breakthrough curve analyses is investigated with the variation of influent flow rate, adsorbent bed height, initial solution pH and initial adsorbate concentration in a laboratory.

v) The real arsenic contaminated groundwater in Kandal Province, Cambodia, is fed to lightweight bio-sand filter embedded with iron mixed porous pellet adsorbent. The main target is to have effluent arsenic concentration less than 10 ppb and to produce daily 30 L of arsenic free drinking water for a household.

CHAPTER II

LITERATURE REVIEW

2.1   Arsenic

Arsenic is a heavy metal occurring in group 15 of the elemental periodic table, the 20th most abundant element in the earth's crust, and a component of more than 245 minerals (Mandal and Suzuki, 2002). In natural environment, arsenic can exist in several oxidation states such as -III, 0, III and V, but the (-III) oxidation state is found only in an extremely reduced environment and (0) arsenic metal rarely occurs (Choong et al., 2007; Wang and Mulligan, 2006). Thus, the occurrence of arsenic is primarily in the oxidation states of (III) and (V) as inorganic and organic forms. The structures of some inorganic and organic arsenic forms identified in water are presented in Figure 2.1. The organic forms include monomethylarsonous acid (MMA$^{(III)}$), monomethylarsonic acid (MMA$^{(V)}$), dimethylarsinous acid (DMA$^{(III)}$), and dimethylarsinic acid (DMA$^{(V)}$), and the major inorganic forms include arsenous acid or arsenite and arsenic acid or arsenate (Smedley and Kinniburgh, 2002; Wang and Mulligan, 2006). Arsenite is reported 10 times more toxic than arsenate and 70 times more toxic than MMA$^{(V)}$ and DMA$^{(V)}$; however, it is less toxic than MMA$^{(III)}$ and DMA$^{(III)}$ in terms of causing DNA breakdown (Katsoyiannis and Zouboulis, 2002). The quantitative presence of arsenite and arsenate in natural water and their toxicity seem to be more significant. Therefore, this research would interest more for the review on arsenite and arsenate.
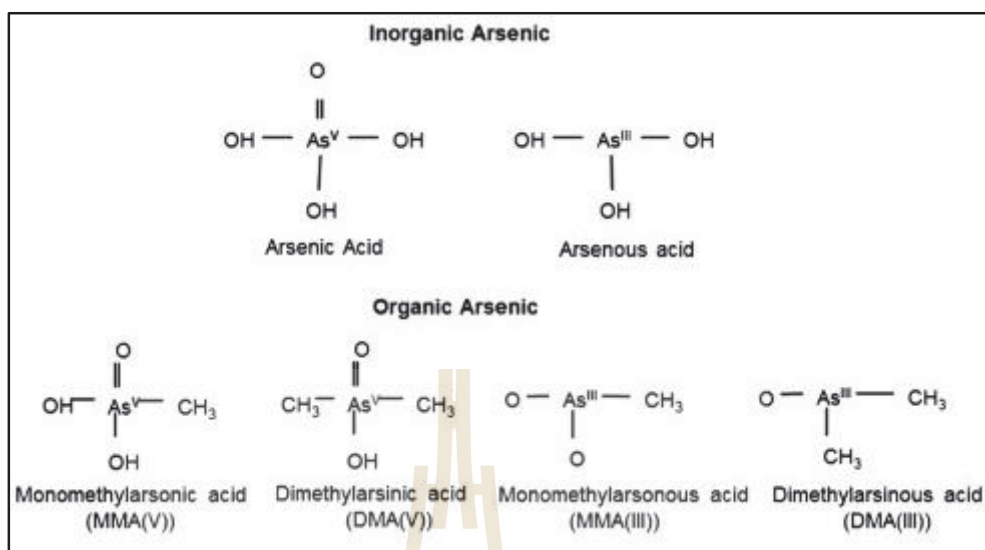
Figure 2.1 Structures of some arsenic forms found in natural water (Hughes, 2002)

Arsenate [As(V)] is a thermodynamically stable form of inorganic arsenic species and predominates in oxygen-rich environments like surface water, whereas arsenite [As(III)] favors and predominates in a moderate reducing environment like anaerobic groundwater (Villaescusa and Bollinger, 2008; Wang and Mulligan, 2006). In water with the influence of redox potential (Eh) and pH value, As(V) can be derivative into species H_3AsO_4, $H_2AsO_4^-$, $HAsO_4^{2-}$ and AsO_4^{3-}, while As(III) species can be converted into H_3AsO_3, $H_2AsO_3^-$, $HAsO_3^{2-}$, and AsO_3^{2-} (Mohan and Pittman, 2007; Mondal et al., 2013).

As shown in Figure 2.2, the arsenite species occur in a low redox potential, and the arsenate species exist in a higher redox potential conditions. Under an oxidizing condition, $H_2AsO_4^-$ is dominant at pH less than 6.9, $HAsO_4^{2-}$ becomes dominant at higher pH, and $H_3AsO_4^0$ and AsO_4^{3-} present in either extremely acidic or alkaline conditions, respectively. Under a reducing condition, the uncharged arsenite specie ($H_3AsO_3^0$) dominates at pH less than 9.2.
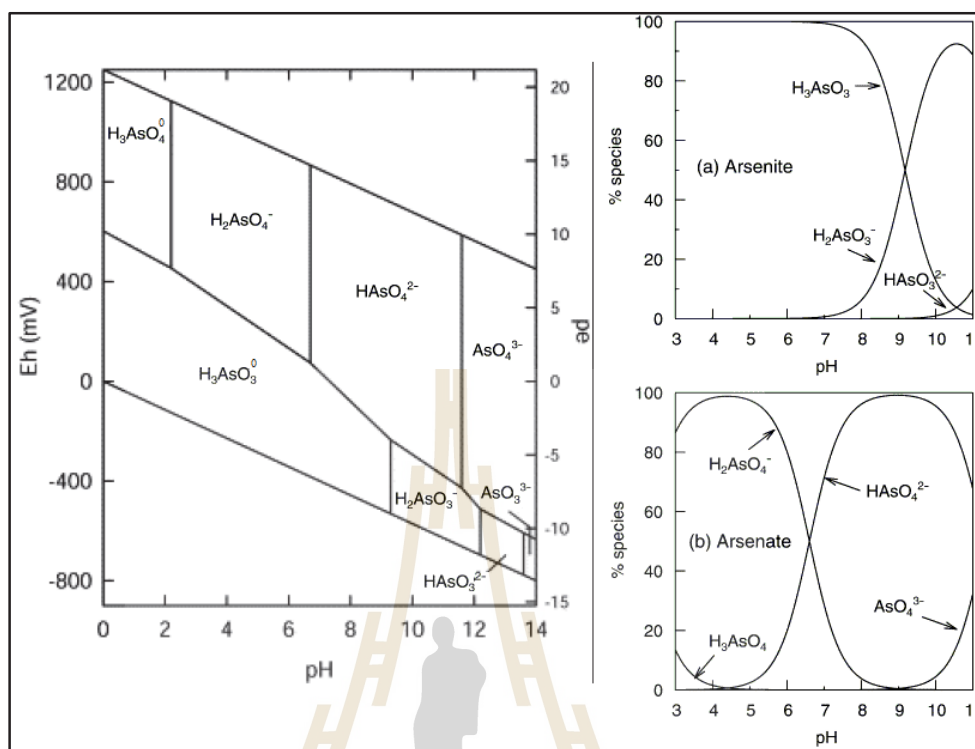
Figure 2.2 Eh-pH diagram for aqueous arsenic species at 25 °C and 1 bar (Left) and arsenic speciation as a function of pH (Right) (Smedley and Kinniburgh, 2002)

Arsenic can mobilize through different flow paths in the environmental media like soil, air and water via various mechanisms (Figure 2.3). Sorption-desorption and precipitation-dissolution are the two principal mechanisms to release arsenic into water from soils, sediments and rocks (Sullivan et al., 2010). Arsenic can be adsorbed to the surface of various materials such as iron oxides, aluminum oxides, and clay minerals under certain conditions. For instance, in acidic and near-neutral conditions (pH = 4 or pH = 7 to 8.5), As(III) or As(V) are strongly adsorbed by iron oxides, but desorption process occurs and results in releasing arsenic into water when pH of the solution becomes more alkaline (Hossain and Piantanakulchai, 2013).

Many ores of transition metals like arsenopyrite (FeAsS) dissolve under reducing conditions, leaving arsenic into the system (Sullivan et al., 2010). Arsenic cannot be easily

destroyed and can be converted into different forms or transformed into insoluble compounds in combination with other elements (Choong et al., 2007). Figure 2.4 shows the detail of arsenic transformation in reducing and oxidizing sediments in aqueous environments.
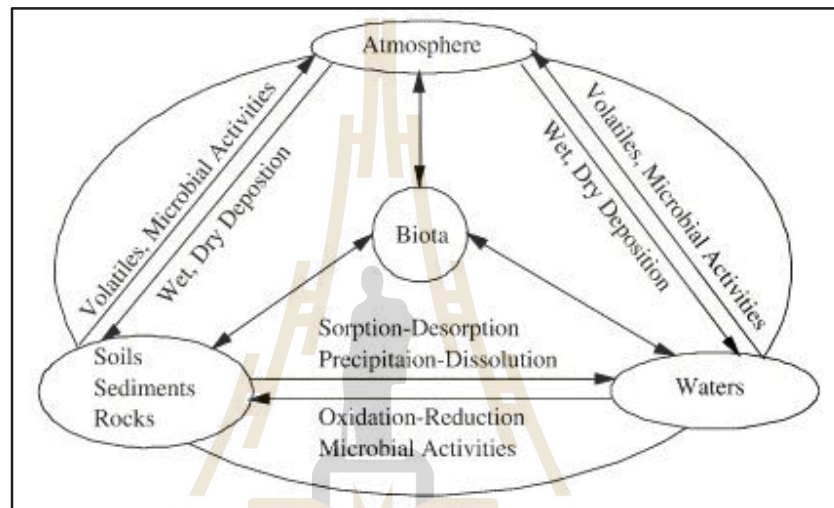
Figure 2.3 A modified diagram of arsenic mobilizing in the environment (Wang and Mulligan, 2006)
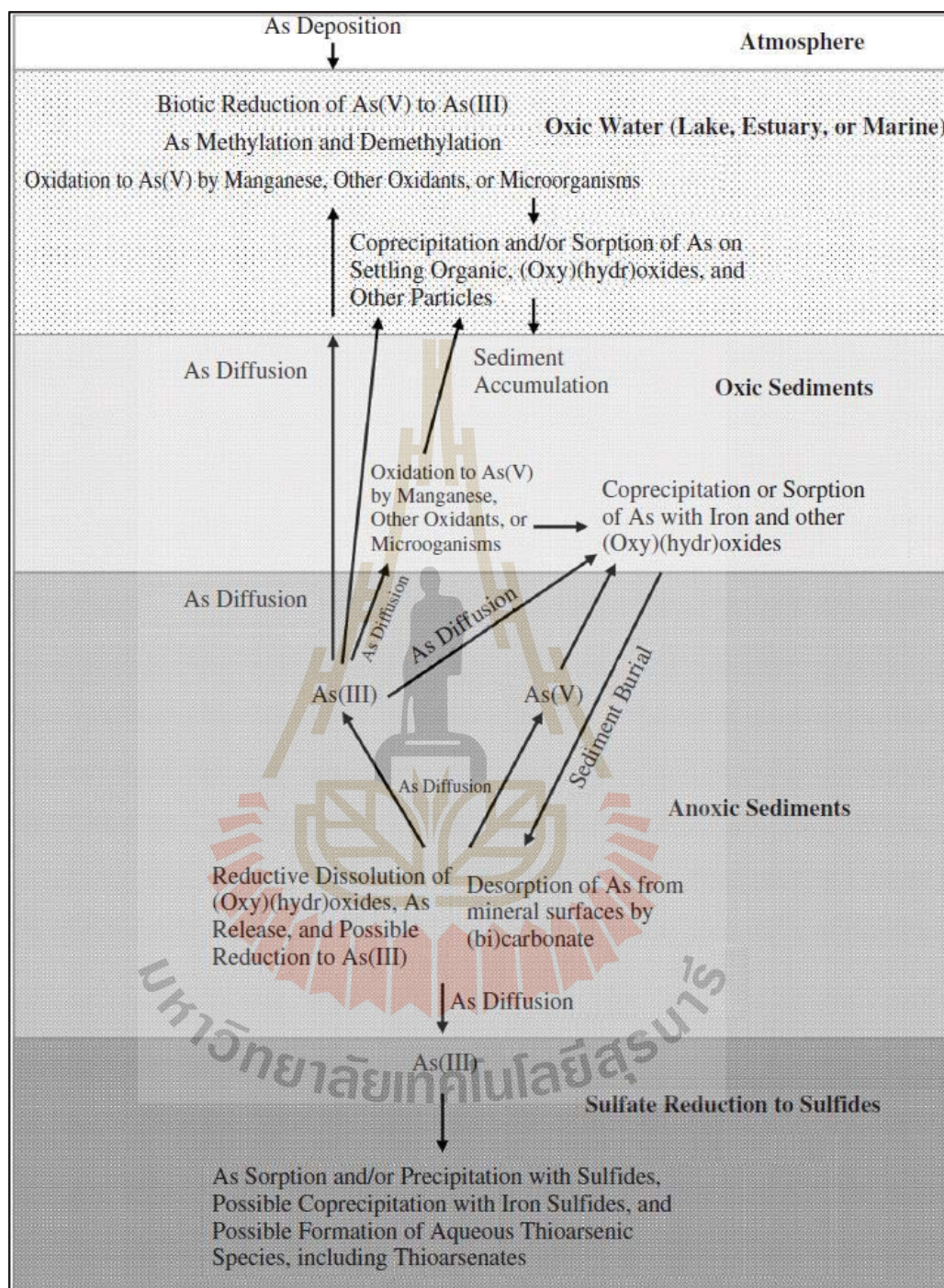
Figure 2.4 Arsenic transformations in oxidizing and reducing sediments in aqueous environments (Henke, 2009)

2.2   Technologies for removing arsenic from water

Arsenic remediation technologies based on the physical-chemical processes include oxidation, coagulation-flocculation, ion exchange, membrane filtration, and adsorption (Figure 2.5).
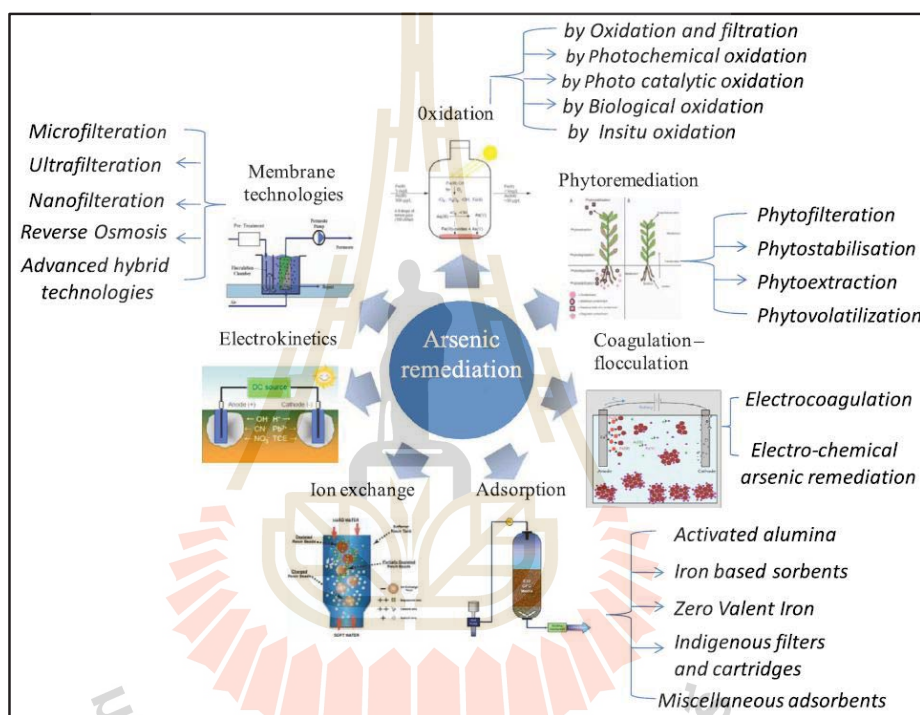
Figure 2.5 Schematic diagram of various methods for arsenic removal from soil and water (Singh et al., 2015)

Oxidation is considered as a pre-treatment rather than a treatment technology of arsenic from water. The main purpose of applying this method is to covert As(III) to As(V), which adsorbs easily onto solid surfaces (Garelick et al., 2005; Malik et al., 2009). Oxidants such as chlorine, chlorine dioxide, chloramine, hydrogen peroxide, ozone and permanganate have been used for oxidizing As(III) (Sharma et al., 2007). More than 95% of As(III) could be oxidized within less than 20s by MnO_4 (Ghurye and Clifford, 2004). More than 96% oxidation of As(III) by ozone occurs within 10 min whereas 5 day oxidation is required to

oxidize around 50% of As(III) by air and pure oxygen (Kim and Nriagu, 2000). The efficiency of As(III) oxidation in water is influenced by interfering ions or compounds such as Fe(II), Mn(II), sulfide (HS$^-$ and S^{2-}), total organic carbon (TOC) and dissolved organic carbon (DOC) (Dodd et al., 2006).

Coagulation-flocculation is a method that uses coagulants for transforming dissolved arsenic into insoluble solids or for co-precipitating with arsenic. The solids or precipitates are then removed from liquid phase by a clarification, sedimentation or filtration. Das and Anand (1999) found that around 82-93% arsenic could be precipitated within 15 min in Fe(II)-NH$_3$-(NH$_4$)$_2$SO$_4$-O$_2$ system. Pallier et al. (2010) observed that using kaolinite and FeCl$_3$ as coagulants and flocculants could remove over 90% and 77% of As(V) and As(III), respectively. Hu et al. (2012) used aluminum chloride and poly-aluminum chloride coagulants and reduced 280 ppb As(V) to less than 10 ppb. Initial arsenic concentration, dosage of coagulants, pH and arsenic species are the main factors affecting the removal efficiency through the coagulation-flocculation process (Garelick et al., 2005). For this method, the negative effects occur for the presence of anions such as phosphate, silicate, bicarbonate, and organic matter, whereas Ca^{2+} and Mg^{2+} provide positive effects (Sharma et al., 2014). The major limitation of this method is the generation of considerable amount of arsenic contaminated sludge, which is possibly the secondary pollution to the environment (Mondal et al., 2013).

Ion exchange is a process of exchanging between ions in the solution and similar ions on the surface of a solid, typically a synthetic ion exchange resin (Chiban et al., 2012). Resins are generally coated with hydrochloric acid (HCl) to hold ion Cl$^-$ on their surface, which later exchanges with anion arsenic in the solution (Mondal et al., 2013). The efficiency of the method has been proved to be able to reduce elevated arsenic concentration to below the WHO's MCL. Barakat and Ismat-Shah (2013) used anion exchange resin Spectra/Gel eluted by 2M NaCl to remove arsenic from water and the results

showed that As(III) was poorly adsorbed whereas As(V) was 99.2% removed. Arsenic removal efficiency through ion exchange method is relatively pH and initial influent concentration independent, and the presence of competing anions or compounds such as sulfate, phosphate, fluoride, and nitrate, total dissolved solid, and precipitated iron results in a negative effect (Jain and Singh, 2012; Litter et al., 2010; Mondal et al., 2013).

Membrane filtration can remove contaminants by excluding them from passing a barrier or membrane that is driven by a difference in pressure. Membrane filtration are commonly developed as a microfiltration (MF) (possibly removing bacteria and suspended solids with pore sizes of 0.1 micron or higher), ultrafiltration (UF) (possibly removing colloids, viruses and certain protein with pore sizes of 0.003 to 0.1 micron), nano-filtration (NF) (possibly rejecting molecular size in the range of 0.001 to 0.003 microns), and reverse osmosis (RO) (possibly used for desalination with pore size of about 0.0005 microns) (Chiban et al., 2012). Arsenic in water has relatively low molecular weight that can pass through MF and UF membranes; therefore, only NF and RO membranes are able to remove arsenic from water (Jain and Singh, 2012). The efficiency of arsenic removal for NF are in the range of 60% to >95%, while As(V) and As(III) removal efficiency was achieved by >95% and 74%, respectively, using RO experiments (Holl, 2010).

Adsorption is a process to remove contaminants from water by adhering a molecular pollutant (an adsorbate) onto the solid surface (an adsorbent or sorbent) driven by physical and chemical forces (Ali, 2012). The adsorbent reported for arsenic remediation from water include modified sands, natural sorbents, carbon based sorbents, agricultural wastes, industrial wastes, bio-sorbents, and other miscellaneous adsorbents (Baig et al., 2015; Mohan and Pittman, 2007). Among those applied adsorbents, iron based adsorbents have gained more popularity for arsenic treatment from water (Mondal et al., 2013) most probably due to their widely availability, low-cost, and high adsorption capacity. The adsorbents express a certain level of arsenic adsorption capacity based on their nature and

the experimental conditions, and the arsenic removal efficiency can be in the range of 30-90% for some adsorbents, and can be higher than 90% for some cases.

Each removal technology has advantages and disadvantages over its application for pollutant treatment, as shown in Table 2.1. From the Table 2.1, a low-cost technique is with oxidation and adsorption technologies, coagulation-flocculation has a cost from medium to high, and ion exchange and membrane pose high to very high cost. Although an oxidation method has a low cost, it does not technically remove arsenic from water without a help of other physical or chemical transformations (Litter et al., 2010). On the other hand, sophisticated and expensive techniques cannot work sustainably when people in the affected regions cannot afford or maintain the treatment system in a long run. For domestic or community treatments in rural or urban isolated populations, low-cost technologies using non-expensive materials should be developed (Litter et al., 2010). Sharma et al. (2014) suggested that the adopted arsenic technologies in the rural areas lacking of main infrastructure should meet following criteria: low initial and maintenance cost, giving clear water with no color and odour, sufficient capacity per day of producing safe drinking water, ability to function without electricity, only dependent on local resources and skill, and no use of dangerous chemicals and no extra added contamination to the water.

Therefore, the adsorption technique using natural clays modified with iron seem to be a good solution for arsenic removal from water and easily applied in the real arsenic contaminated areas in many developing countries like Cambodia.

Table 2.1 Comparison of some arsenic removal technologies (Mohan and Pittman, 2007; Mondal et al., 2013)

Methods	Advantages	Disadvantages	Removal (%)	Relative costs
Oxidation	1) Relatively simple process 2) *In situ* arsenic removal 3) Oxidizes other inorganic and organic constituents in water 4) Kills microbes and applicable for large water volume	1) Possible toxic chemicals and carcinogens are produced by-products 2) Interfering substances decreases the removal efficiency 3) Additional removal process is essential	-	Low
Coagulation -flocculation	1) Effective over a wider range of pH 2) Chemicals are widely available 3) Relatively simple in operation 4) Effective for the system with hard water and applicable for large water volume	1) Very high amount of coagulant dose is required 2) Additional separation step is necessary 3) As contaminated sludge is produced that may become a concern of environmental recontamination	20-90 & ≥90	Medium - high
Adsorption	1) More suitable for household application 2) Typically inexpensive with simple replacement requirements 3) Improves test and odour 4) High removal efficiencies	1) Interferences from competitive anions may decreases removal efficiency 2) Problems might occur regarding regeneration and multiple uses of the adsorbents 3) As spent adsorbent possibly become environmental recontamination	30-90 & ≥90	Low-Medium
Ion exchange	1) The removal efficiency is pH independent 2) Well-defined media and capacity, which possibly developed as exclusive ion specific resin to remove arsenic	1) High-tech operation and maintenance 2) Regeneration creates a sludge disposal problem 3) As(III) is difficult to remove 4) Interference from other anions	≥90	High
Membrane filtration	1) Good purification and no toxic solid waste are produced 2) High removal efficiency for arsenate from water along with other contaminants	1) Low removal for As(III) 2) High electrical energy needs to operate 3) Pretreatment steps are often required 4) Efficiency is decrease with increasing As concentration	≥90	High

2.3   A brief concept of adsorption for liquid-solid phase

Accumulation of an adsorbate at the liquid-solid interface refers to the adsorption process. The process of adsorption proceeds by migrating the concentration of adsorbate to the surface of adsorbent, diffusing on the external surface characterized by the available external surface area on the adsorbent, and later diffusing on the available pores of the adsorbent (Figure 2.6). Adsorption process can occur as either chemical adsorption or physical adsorption (Sarkar and Paul, 2016). Chemical adsorption or chemisorption is characterized by forming strong chemical associations between molecules or ions of adsorbate and the surface of adsorbent, generally involves the exchange of electrons, and thus is normally irreversible (Yagub et al., 2014). Physical adsorption or physisorption is illustrated by weak van der Waals bonds between an adsorbate and adsorbent, reversible in
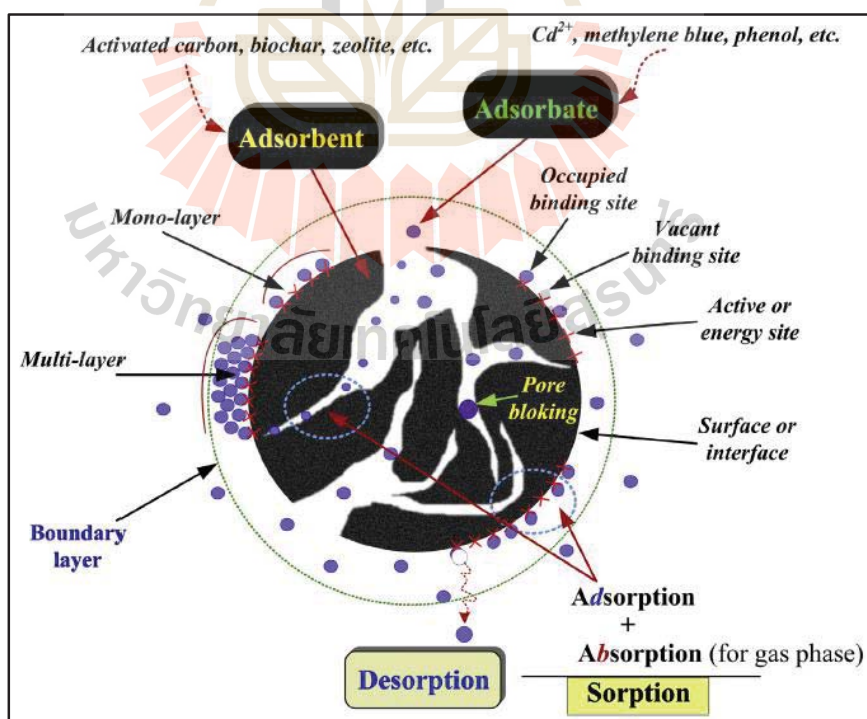
Figure 2.6 The processes with some basic terms in adsorption science (Tran et al., 2017)

most cases, accompanied with formation of a multilayer of the adsorbate on the adsorbent surface, likely to polarize the adsorbate, and absent of transfer of electrons between adsorbate and adsorbent (Sarkar and Paul, 2016; Yagub et al., 2014). Factors that influence the adsorption efficiency include properties of adsorbent, contact time or exposure time, initial adsorbate concentration, adsorbent dose, solution pH, temperature, and the presence of other chemical species (Ali, 2012; Sarkar and Paul, 2016).

Adsorption seems to rely much on the surface area of the adsorbent. Other important properties of adsorbents include morphology, crystalline structure, elemental composition, surface chemistry, physicochemical properties…etc. Numerous analytical methods can be used to characterize an adsorbent (Figure 2.7).
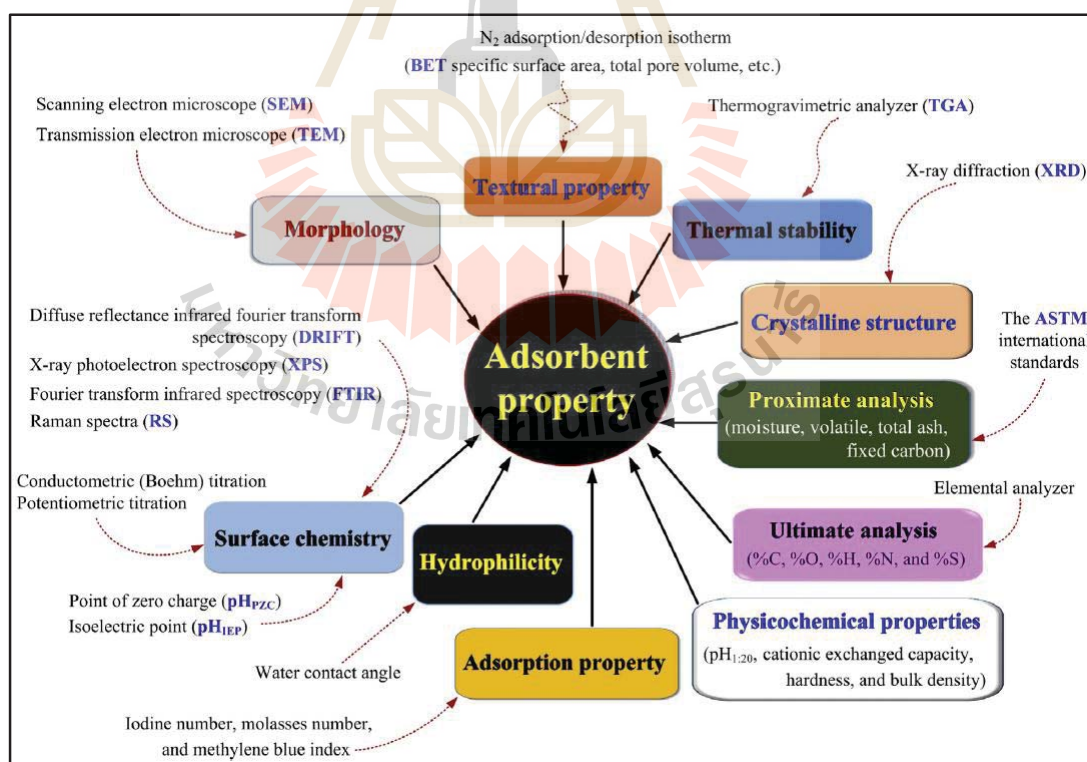
Figure 2.7   Basic properties of an adsorbent determined by various techniques (Tran et al., 2017)

2.4 Clay-based adsorbents

2.4.1 Clays and clay minerals

Clay can contain a fraction of soils, sediments, rocks, mixtures of clay minerals and other minerals such as quartz, carbonate, and metal oxides (Bhattacharyya and Gupta, 2008). Clay mineral is formed by layers of one or two tetrahedral silicate (Si-O) sheets and one octahedral metal oxide or hydroxide (M-O or M-OH) sheet (Figure 2.8) (Murray, 2006). A clay mineral with one tetrahedral silicate sheet and one octahedral metal oxide or hydroxide sheet is called a 1:1 type, i.e., kaolinite, halloysite and serpentine.
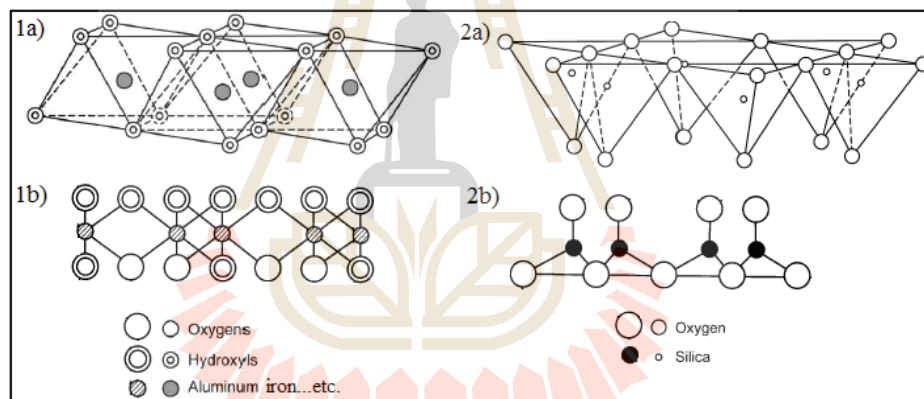
Figure 2.8 Diagrammatic sketch of the octahedral sheet in 3D (1a) and 2D (1b) and the tetrahedral sheet in 3D (2a) and 2D (2b) (Murray, 2006)

A clay mineral with an octahedral sheet sandwiched between two tetrahedral silicate sheets is called a 2:1 type, i.e., talc, vermiculite, montmorillonite, saponite, and sepiolite (Figure 2.9) (Zhou and Keeling, 2013).
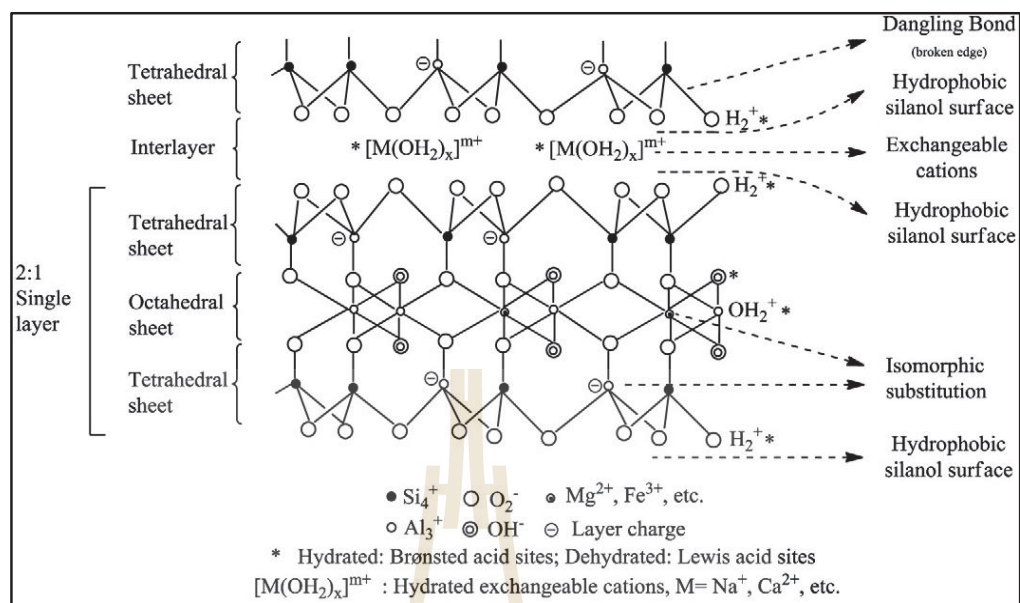
Figure 2.9 Schematic drawing of 2:1-type clay mineral (Zhou and Keeling, 2013)

Some clay minerals tend to express low adsorption capacity for some anionic metals due to predominant negative charges on their surface (Ren et al., 2014). To improve the adsorption efficiency, clay minerals are modified with following methods: adsorbing with active solutions, exchanging ions with inorganic cations or cationic complexes, binding to inorganic or organic anion (mainly at the edges), grafting with organic compounds, reacting with acid solutions, pillaring by different types of poly cations, and applying calcination (Bergaya and Lagaly, 2001).

2.4.2 Clays and modified clay adsorbents for arsenic removal

Clays and clay minerals are considered as natural contaminant scavengers in the environment and used as effective adsorbents for toxic metal removal from aqueous solutions (Srinivasan, 2011). Many researches have used clays or clay minerals and their modified forms for As(III) and/or As(V) removal from water.

Mohapatra et al. (2007) investigated the As(V) adsorption onto kaolinite, montmorillonite and illite from aqueous solution. The results showed that the As(V)

adsorption were pH dependent with the maximum efficiency in the pH range of 2.0-5.0. The Langmuir isotherm was the best model to fit the adsorption data, and the maximum adsorption capacities were 0.86, 0.64, and 0.52 mg/g for kaolinite, montmorillonite and illite, respectively. Plus, the study also suggested that kaolinite was a successful adsorbent for arsenic removal from two contaminated groundwater with arsenic in the range of 1.36-1.41 mg/L.

Rivera-Hernandez and Green-Ruiz (2014) used red clay as adsorbent for As(III) adsorption from aqueous solution in batch experiments. The red clay consists of quartz, albite, illite and kaolinite. The adsorption data were well fitted the pseudo-second order model, suggesting that the adsorption process were in a multistep. The Langmuir model was a better fit model to the experimental data, suggesting the process was carried out on a homogenous surface. The maximum As(III) adsorption capacity of the adsorbent was found to be 0.292 mg/g.

Bentahar et al. (2016) studied on As(V) adsorption behavior onto clayey materials from Morocco in a batch mode. The effect of the pH on the adsorption indicated that the arsenic adsorption was most favorable in the acidic pH range. The Langmuir model provided the best fit with the experimental adsorption data. The Freundlich model could describe the data well for some cases. The most effective clay adsorbent provided a maximum adsorption capacity of 1.076 mg/g.

Ramesh et al. (2007) modified montmorillonite with a combination of aluminum and ferric solutions for As(III) and As(V) adsorption. The results indicated that the maximum adsorption of polymeric Al/Fe modified montmorillonite was observed in the pH ranges of 3.0-6.0 and 7.0-9.0 for As(V) and As(III), respectively. The adsorption data were well correlated with the pseudo-second order kinetic model and Freundlich isotherm model, suggesting the adsorption process was in a multi-stage and heterogeneous

distribution of active sites. The adsorption process was endothermic and spontaneous in nature based on the results of thermodynamic studies.

Dousova et al. (2009) conducted a study on using modified kaolin and bentonite with irons, aluminum and manganese salts to remove As(III) from anoxic groundwater. Synthetic groundwater with As(III) was prepared to obtain the composition of 6.0 ppm of Fe^{2+}, 0.8 ppm of Mn^{2+}, 500.0 ppm of HCO_3^-, and 130.0 ppm of SO_4^{2-}, and 10 ppm of AsO_3^{3-}. The As(III) adsorption capacities of kaolin modified with Fe^{II}, Fe^{III}, Al^{III} and Mn^{II} were 1.4, 3.8, 0.8, and 1.3 mg/g, respectively, whereas the adsorption capacities of bentonite modified with Fe^{II}, Fe^{III}, Al^{III} and Mn^{II} were 4.3, 7.3, 1.3, and 3.0 mg/g, respectively. This suggested that the iron modified adsorbents expressed high As(III) adsorption capacities for synthetic groundwater.

Na et al. (2010) used Ti-pillared montmorillonite to adsorb As(V) and As(III) from aqueous solution. The results indicated that pH has little effect on the As(III) adsorption, whereas the As(V) adsorption was more favorable under acidic condition. The pseudo-second order kinetic reaction model well fitted to the adsorption data of both As(III) and As(V). Adsorption isotherms of both As(III) and As(V) were well fitted both the Freundlich and Langmuir models. The maximum As(III) and As(V) adsorption capacities were 14.72 and 12.503 mg/g, respectively. The As(III) adsorption decreased with an increase of temperature, and the As(V) adsorption decreases in the temperature range of 25-35°C and increases in the temperature range of 45-65°C. The presence of phosphate significantly decreased the As(V) adsorption.

Zhao et al. (2012) modified montmorillonite with hydroxyl Al modifiers for removing As(V). The adsorption data were better correlated with the pseudo-second order kinetic, Freundlich and Redlich-Peterson isotherm models. The maximum adsorption capacity from the Langmuir model was in the range of 1.530-5.008 mg/g with regression

coefficients in the range of 0.9154-0.9947. The As(V) adsorption had changed from physisorption to chemisorption after the modification.

Ren et al. (2014) investigated the arsenic adsorptive behavior on modified montmorillonite with Fe polycations (Fe-M) and cetyltrimethylammonium bromide (C-Fe-M). The adsorption reactions reached equilibrium within 20 min and the adsorption data were well fitted the pseudo-second order kinetic and Langmuir adsorption models. The maximum adsorption capacities of Fe-M and C-Fe-M were 8.85 and 15.15 mg/g for As(V), respectively, and 13.89 and 16.13 mg/g for As(III), respectively. The adsorption was efficient in the pH range of 4-10.

Mishra and Mahato (2016) synthesized iron and manganese oxide pillared clays as adsorbents towards As(III) and As(V) removal from water. For both As(III) and As(V) adsorption, the adsorption capacity of the modified adsorbents increased approximately 4-6 times in comparison to the raw clay. The modified adsorbents performed much better when subjected to actual contaminated water. No leaching of arsenic was observed after the adsorption.

In a short summary of those mentioned previous researches, different types of raw clays and clay minerals have an ability to adsorb arsenic from water in a batch technique. The maximum arsenic adsorption capacities of those raw materials are in a range of 0.292-1.076 mg/g. Many active materials or compounds have been used as modifiers on raw clays and clay minerals to improve the arsenic adsorption capacity. The modified adsorbents can uptake arsenic at the maximum uptake rate of 1.3-16.13 mg/g. The adsorption process is favorable with acidic or neutral pH conditions. Kinetic data are well described with a pseudo-second-order kinetic model. The Langmuir and Freundlich models perform well to fit the isotherm data. The presence of phosphate in water provides greatly adverse effects on the adsorption efficiency.

2.4.3 Clay-iron oxides/zero valent iron adsorbents for arsenic removal

Iron oxides and zero valent iron (iron powder) are widely used in the remediation of water pollutants. However, their applications have been limited by the facts that they tend to aggregate in the solution to become larger particles that make their surface area lower and the adsorption capacity greatly decreased, they are inapplicable in fixed-beds or other flow-through systems due to the excessive pressure drop resulting from poor mechanical strength, and they are difficult to be separated from aqueous systems after treatments (Ezzatahmadi et al., 2017; Hua et al., 2012). To overcome their restriction, they are impregnated into porous materials or supported by binder materials to be composite adsorbents. Many researchers have used clays or clay minerals as supporters or binders of iron oxides or zero valent iron for As(III) and/or As(V) adsorption from aqueous solutions.

Chen et al. (2012) developed a novel tablet ceramic adsorbent (TCA) with mixing prepared powders of Akadama mud, wheat starch and Fe_2O_3 at a ratio of 56%:24%:20% for As(V) adsorption from aqueous solution. TCA is a typical mesoporous material, and possesses a specific surface area of 38.19 m^2/g, an iron content of 27.23%, and a point of zero charge (pH_{pzc}) of 6.4. Batch adsorption experiments demonstrated that the adsorption capacity of TCA was 5.32 mg/g estimated by the Langmuir-Freundlich model.

Shafiquzzam et al. (2013) developed a porous adsorbent by heating the mixture of clay, rice bran and Fe(0) powder at 600˚C to adsorb arsenic from synthetic groundwater under batch experiments. The adsorption was pH dependent and most efficient for both As(III) and As(V) at pH 5-7. The adsorption followed the pseudo-second order kinetics and well fitted both the Freundlich and Langmuir isotherm models. The maximum adsorption capacities were 4.0 and 4.5 mg/g for As(III) and As(V), respectively. Phosphorous showed an adverse effect on both As(III) and As(V) adsorption.

Bhowmick et al. (2014) prepared montmorillonite-supported nZVI (Mt-nZVI) composite adsorbent to remove arsenic from aqueous solution in batch experiments. The results indicated that adsorption kinetics followed the pseudo-second-order model, high adsorption efficiencies for both As(V) and As(III) were obtained at pH values in the range of 4.0-8.0, and the efficiencies were significantly decreased at pH>9. Form the Langmuir adsorption isotherm, the maximum adsorption capacities for As(V) and As(III) at pH 7 were 45.5 and 59.9 mg/g, respectively. Moreover, the results suggested that an increase in the PO_4^{3-} concentration would decreased the arsenic adsorption, while the other co-present oxy-anions such as nitrate, sulfate, and bicarbonate had an insignificant effect on arsenic adsorption.

Yin et al. (2017) prepared a low-cost arsenic adsorbent through loading hydrate iron oxide into porous charred granulated attapulgite clay. Batch studies indicated that As(III) and As(V) fitted well with the Langmuir model as the maximum adsorption capacities were 3.25 and 5.09 mg/g, respectively. The kinetic data followed the pseudo-second-model. The iron modified adsorbent performed well with a pH range of 5-9. The presence of ions SO_4^{2-}, HCO_3^- and PO_4^{3-} provided inhibition effects on the adsorption process.

In a short note, iron oxides or zero valent iron plays important roles to improve the adsorption capacity of clay-based adsorbents for arsenic removal from aqueous solution. The arsenic maximum adsorption capacity was in the range of 3.25-59.9 mg/g and 4.5-45.5 mg/g for As(III) and As(V), respectively. The improvement is approximately 3 to 60 folds in comparison to that of the raw clay adsorbents. The adsorbents works efficiently in a wide pH range. The Langmuir and the pseudo-second-order models described well for isotherm and kinetic data, respectively. The adsorbent seems to be resistant to the presence of some coexisting anions, but phosphate.

2.4.4 Mechanisms of arsenic uptake with clay-based adsorbents

Figure 2.10 illustrates the possible mechanisms of the minerals/solution interface in the adsorption process. Ions up-take from aqueous solution by minerals consists of two main mechanisms: a surface adsorption and structural incorporation.
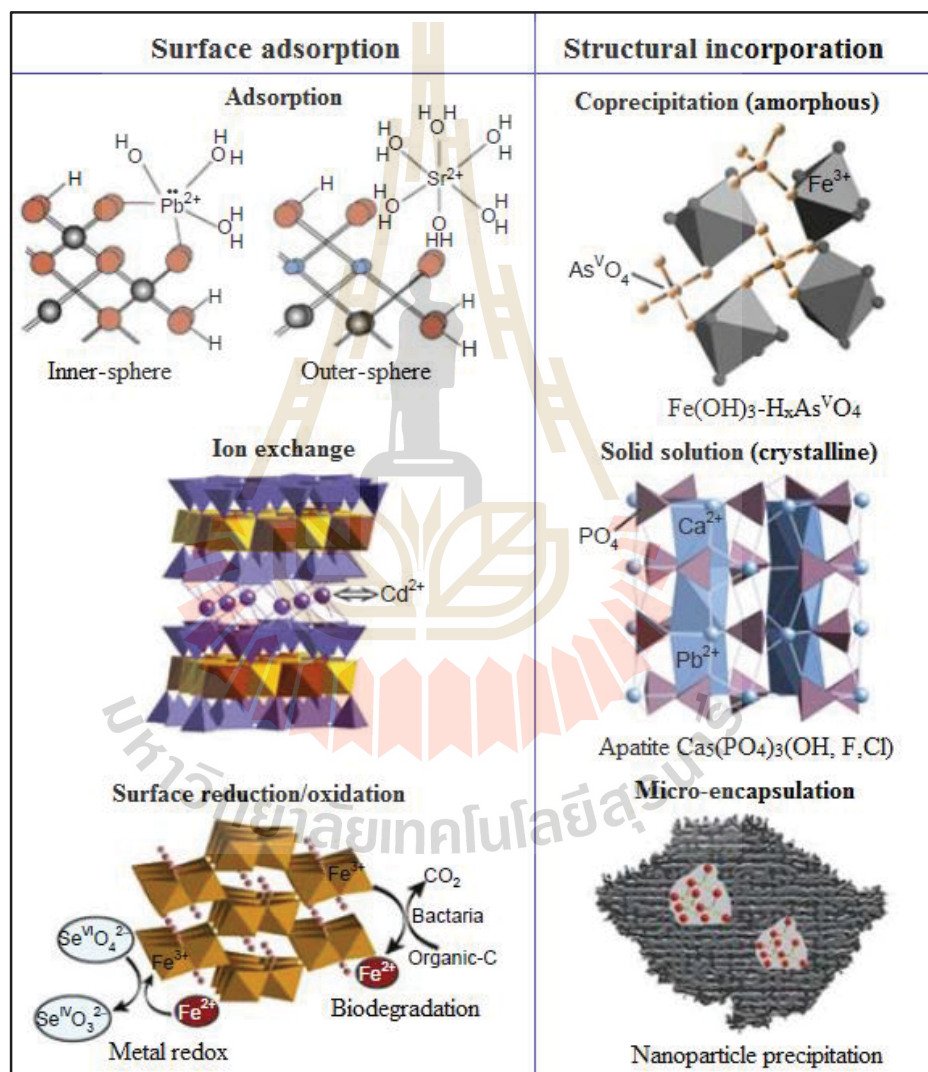
Figure 2.10 Conceptual models of metal ion uptake by minerals (O'Day and Vlassopoulos, 2010)

The surface adsorption includes processes such as adsorption (inner or outer sphere complexation), ion exchange, and surface reduction/oxidation, and the structural incorporation involves co-precipitation, solid solution (crystallization), and micro-encapsulation.

Many researches have proposed at least one of the suggested processes in the arsenic removal by clays or clay minerals.

Churchman et al. (2006) suggested that the uptake of heavy metal ions by clay minerals is possibly performed through surface complexation (either inner-sphere or outer-sphere), simple ion exchange, and surface precipitation. Inner-sphere complexation results from direct bonding of an ion to atoms on the mineral surface, whereas outer-sphere complexation indicates the presence of water or hydroxyl ligands between the metal center and the surface (O'Day and Vlassopoulos, 2010). On their surface, clays contain variety of cations and anions that can be easily exchangeable with other ions without affecting the structure of the clay. The most commonly found cations and anions on the clay surface include Ca^{2+}, Mg^{2+}, H^+, K^+, NH_4^+, Na^+, and SO_4^{2-}, Cl^-, PO_4^{3-}, NO_3^-, respectively (Bhattacharyya and Gupta, 2008).

Mohapatra et al. (2007) suggested that the surface charge of the clay minerals is responsible for a better or worse As(V) adsorption. At lower pH, more positive charge formation occurs on the surface of clay minerals due to the interaction of water with oxygen atoms on the clay surface in the acidic medium, resulting in higher As(V) adsorption. At higher pH, the clay surface becomes more and more negatively charged, resulting in lower As(V) adsorption. The formations can be represented as follows:

$$- MO + H–OH \longrightarrow M–OH_2^+ + OH^- \qquad \text{(Low pH)}$$

$$- MOH + OH^- \longrightarrow -MO^- + H_2O \qquad \text{(High pH)}$$

$$M–OH_2^+ + As(V) \longrightarrow M–OH_2^{\cdots}As(V)$$
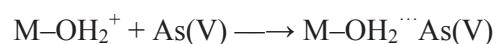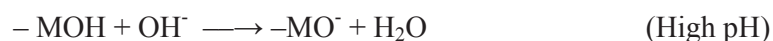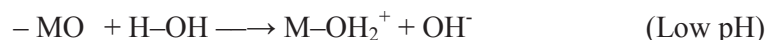
This implies that mechanisms of As(V) adsorption onto clay minerals under their studies is surface complexation.

Na et al. (2010) also suggested that the adsorption of arsenic onto Ti-pillared montmorillonite occurs through both inner and outer surface complexation. The complexation reactions of arsenite are as follows:

$$XOH_{(s)} + H^+_{(aq)} \leftrightarrow XOH_{2(s)}^+$$

$$XOH_{(s)} \leftrightarrow XO^-_{(s)} + H^+_{(aq)}$$

$$XOH_{(s)} + H_3AsO_{3(aq)} \leftrightarrow XH_2AsO_{3(s)} + H_2O_{(aq)}$$

$$XOH_{(s)} + H_3AsO_{3(aq)} \leftrightarrow XHAsO_3^-_{(s)} + H^+_{(aq)} + H_2O_{(aq)}$$
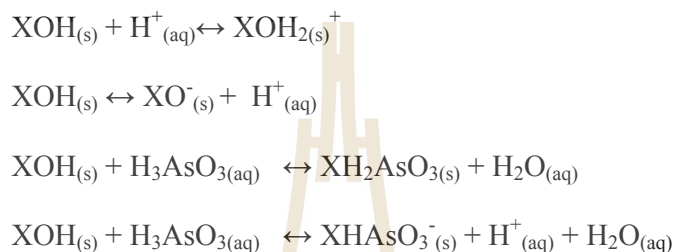
The complexation reactions of arsenate are as follows:

$$XOH_{(s)} + H^+ \leftrightarrow XOH_{2(s)}^+$$

$$XOH_{(s)} \leftrightarrow XO^-_{(s)} + H^+_{(aq)}$$

$$XOH_{(s)} + H_2AsO_4^-_{(aq)} \leftrightarrow XHAsO_4^-_{(s)} + H_2O_{(aq)}$$

$$XOH_{(s)} + H_2AsO_4^-_{(aq)} \leftrightarrow XHAsO_4^{2-}_{(s)} + H^+_{(aq)} + H_2O_{(aq)}$$

$$XOH_{(s)} + H_2AsO_4^-_{(aq)} \leftrightarrow XOH_{2(s)}\text{-}H_2AsO_4^-_{(s)}$$
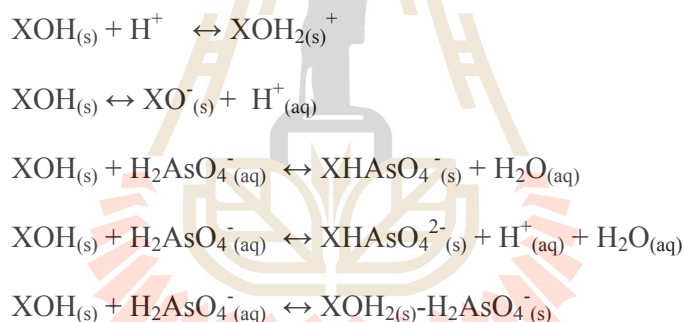
In the reactions above, $XOH_{(s)}$ represent a hydroxyl group of the Ti-pillared montmorillonite, $H^+_{(aq)}$ is the H^+ in the solution, $XH_2AsO_{3(s)}$ and $XHAsO_{3(s)}$ are the inner complexes of arsenite, $XHAsO_{4(s)}$ and $XAsO_{4(s)}$ are the inner complex of arsenate, and XOH_2^+ - $H_2AsO_{4(s)}$ is the outer complex of arsenate.

Similar suggestions have been proposed by Dousova et al. (2009) and Ren et al. (2014). Therefore, the arsenic adsorption form aqueous solutions onto clay-based adsorbents occur mainly through a surface complexation process by forming both inner and outer complexes of the adsorbent surfaces.

2.4.5 Mechanisms of arsenic uptake with iron oxide/zero valent iron

The surface of clay-based adsorbents is predominated with iron oxides or zero valent iron if those iron species are applied, and the interaction between arsenic species

and those iron species will occur during the adsorption process. Therefore, mechanisms of arsenic uptake onto iron oxides or zero valent iron should be mentioned or understood.

Goldberg and Johnston (2001) suggested that arsenate forms inner-sphere surface complexes on iron oxides while arsenite forms both inner-and outer surface complexes. Inner-sphere surface complexes can either form with 1:1 stoichiometry (forming monodentate complex), or with 1:2 stoichiometry (forming bidentate complex), as illustrated in Figure 2.11.
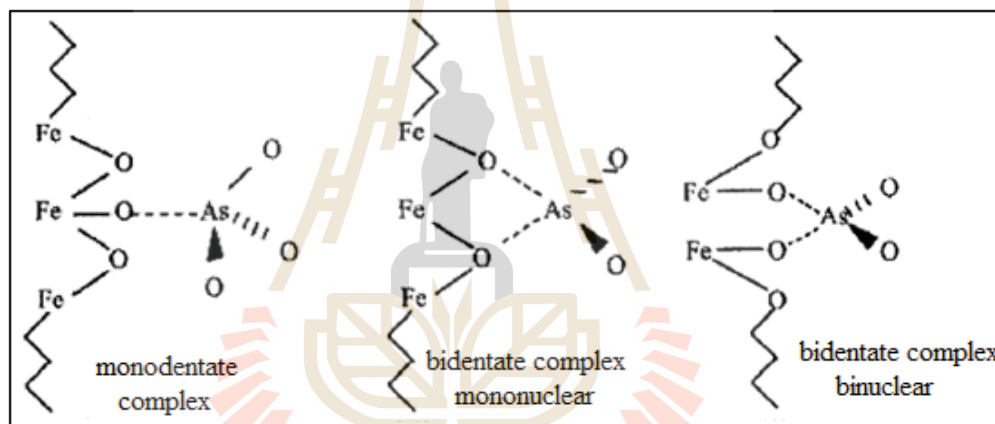
Figure 2.11 Schematic representation of arsenate complexes formed on iron oxide surfaces (Gallegos-Garcia et al., 2012)

Grossl et al. (1997) proposed that the mechanisms for As adsorption on goethite follows two-step processes (Figure 2.12). First, a reaction of oxyanions like $H_2AsO_4^-$ in the aqueous with goethite occurs, forming an inner-sphere monodentate surface complex. Then, the succeeding step involves a second ligand exchange reaction, resulting in the formation of an inner-sphere bidentate surface complex.
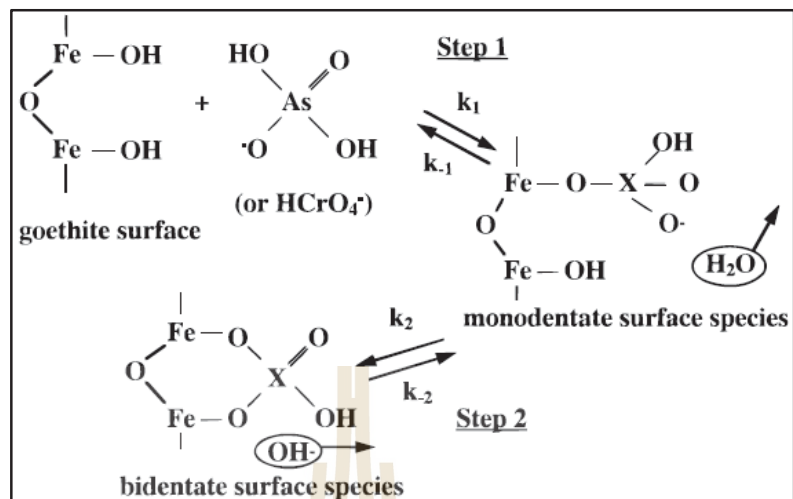
Figure 2.12 Proposed mechanism for oxyanion adsorption/desorption on goethite. The X represents either As(V) or Cr(VI) (Grossl et al., 1997)

Li et al. (2017) presented the summary of the major mechanisms of heavy metals removal by zero valent iron, as shown in Figure 2.13. Zero valent iron contains a metallic iron core and an amorphous oxide shell. Oxyanions like arsenate (AsO_4^{3-}) could be reduced by a reducing or electron-donating power of a metallic iron. This chemical reduction followed by sorption is likely one of the most important mechanism responsible for contaminant immobilization.
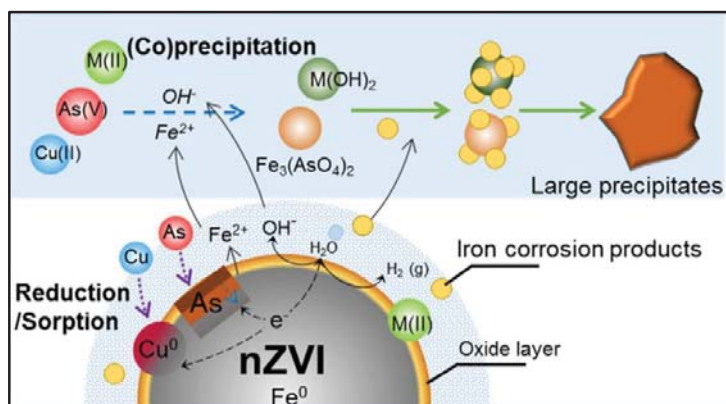
Figure 2.13 Schematic removal of heavy metals using zero valent iron (Li et al., 2017)

Moreover, arsenic could be precipitate with Fe(II), a derivative ions from ZVI. This precipitation process is significant in removing concentrated arsenic at near neutral pH. The iron oxide shell of ZVI and its corrosion products offer the coordinative and electrostatic functions to attract and adsorb charged ion.

2.5   Experimental mixture design for optimization

An experimental mixture design is used to study the effects of mixture components on the response variable. If 'q' represents the number of constituents in the system under a study and 'x_i' represents the proportions of ith constituent in the mixture, then:

$$\sum_{i=1}^{q} x_i = x_1 + x_2 + \cdots + x_q = 1; \quad x_i > 0; \, i = 1, 2, 3, \ldots, q \tag{2.1}$$

In a mixture problem, the purpose of the experiment is to model the blending with some forms of mathematical equations so that predictions of the response for any mixture or combination of the constituents can be made empirically, and a measure of the influence on the response from a single component and a combination of components can be drawn (Rao and Baral, 2011).

Scheffe (1963) firstly introduced the models and designs, known as Simplex Lattice Designs and Simplex Centroid Designs, for a mixture experiment where the mean response is assumed to depend only on the relative proportions of the ingredients or components (Mandal et al., 2008).

In a simplex-centroid design, with the exception of the overall centroid point, all the design points are on the boundaries of the simplex. Points on the vertices represent pure mixtures, points on the edges represent binary blends and any other point with in the region is a ternary blend (Scheffe, 1963). In a q-component simplex-centroid design, the number of distinct points is $2^q - 1$. These points correspond to q permutations of (1, 0, 0,…,0) or q

single-component blends, the $\binom{q}{2}$ permutations of (1/2, 1/2, 0, …,0) or all binary mixtures,

the $\binom{q}{3}$ permutations of (1/3, 1/3, 1/3, 0, …, 0), …, and so on, with the overall centroid

point (1/q, 1/q …, 1/q). Figure 2.14 presents the three-component and four-component simplex-centroid designs (Cornell, 2011).
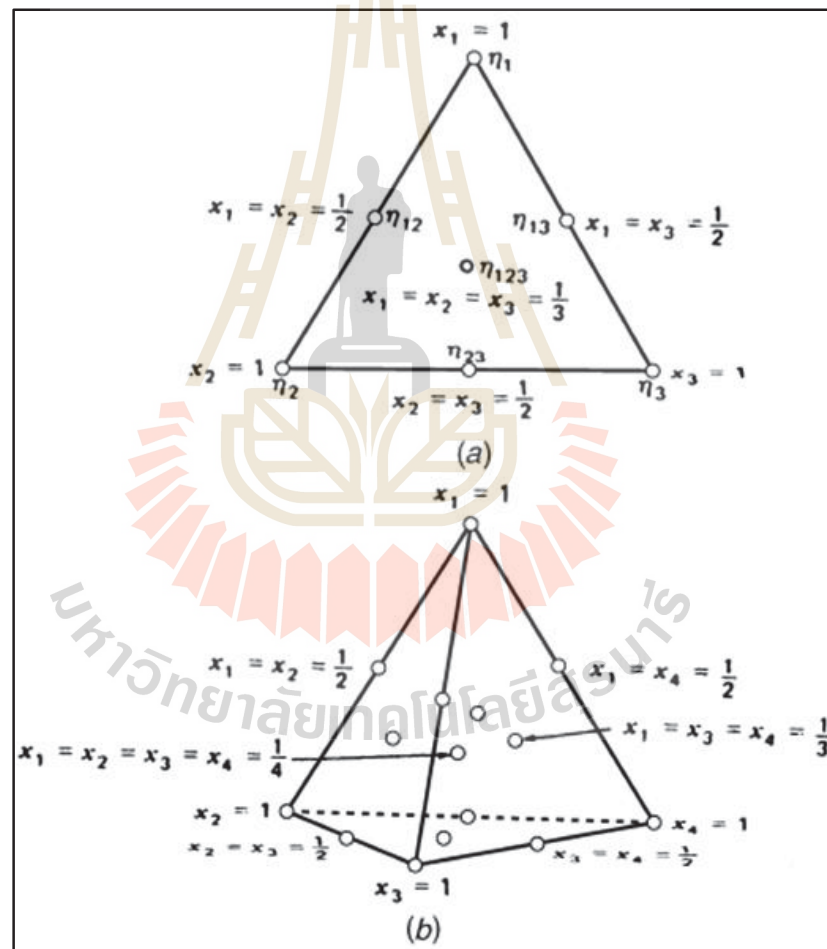
Figure 2.14   Simplex-centroid designs for (a) 3 components and (b) 4 components

At the design points of the simplex-centroid design, data on the response are collected, and the polynomial equation to be developed for modeling is given as follow:

$$\eta = \sum_{i=1}^{q} \beta_i x_i + \sum \sum_{i<j}^{q} \beta_{ij} x_i x_j + \sum \sum \sum_{i<j<k}^{q} \beta_{ijk} x_i x_j x_k + \cdots + \beta_{12\ldots q} x_1 x_2 \cdots x_q \qquad (2.2)$$

where β_i represents the coefficient of the expected response to the pure component i, and β_{ij} is the coefficient subjected to components i and j. The other β_{ijk} parameters are defined similarly. To make a better prediction of a complete mixture, it would be highly desirable to have more runs in the interior of the simplex. This can be done by augmenting the usual simplex designs. The augmented simplex centroid design (ASCD) is superior for studying the response of complete mixtures because it can detect and model curvature in the interior. Figure 2.15 illustrates the design points in the augmented simplex centroid design for three components.

Some mixture designs normally have constraints on the component proportions, and the components with the upper and lower bound constraints can be expressed as follow:

$$L_i \le x_i \le U_i, \quad i = 1, 2, \ldots, q \qquad (2.3)$$

where L_i is the lower bound for the ith component and U_i is the upper bound for the ith component. The transformed region is still a simplex design, so it is possible to define a new set of components that take on the values from 0 to 1, which the regression polynomial of the simplex-centroid design model can be constructed and fitted with. These new components (x_i') are called pseudo components and are defined using the following formula:

$$x_i' = \frac{x_i - L_i}{1 - L} \qquad (2.4)$$

where $L = \sum_{i=1}^{q} L_i < 1$, denoting the sum of all the lower bounds. Rearranging the above given equation, the original components of the mixtures can be derived from the following shown equation:

$$x_i = L_i + (1 - L)x_i' \qquad (2.5)$$
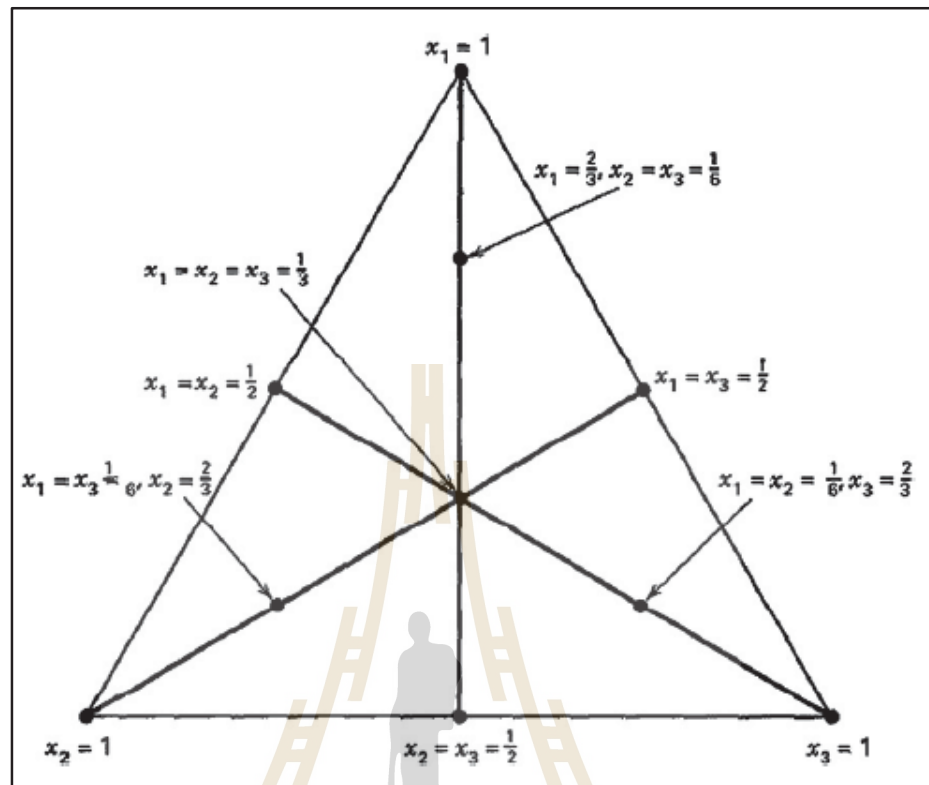
Figure 2.15 The augmented simplex centroid design for three components (Rao and Baral, 2011)

For example, using this equation, the coordinate $(x_1^{'}, x_2^{'}, x_3^{'}) = (1,0,0); (0,1,0); (0,0,1)$ of the pseudo setting components correspond to the coordinates $(x_1, x_2, x_3) = (1 - L_2 - L_3 , L_2, L_3)$; $(L_1, 1 - L_1 - L_3, L_3)$; $(L_1, L_2, 1 - L_1 - L_2)$ of the real setting components, respectively.

2.6   Adsorption concepts in a fixed-bed column study

Adsorption in a fixed bed column depends on a time and distance passing through the adsorbent. The process of the adsorbent particle accumulating adsorbate from the introduced influent to reach equilibrium takes place in the mass transfer zone (MTZ) or adsorption zone. Three different zones within the adsorbent bed in the column can be observed for a single-solute adsorption at a given time (Worch, 2012) (Figure 2.16)
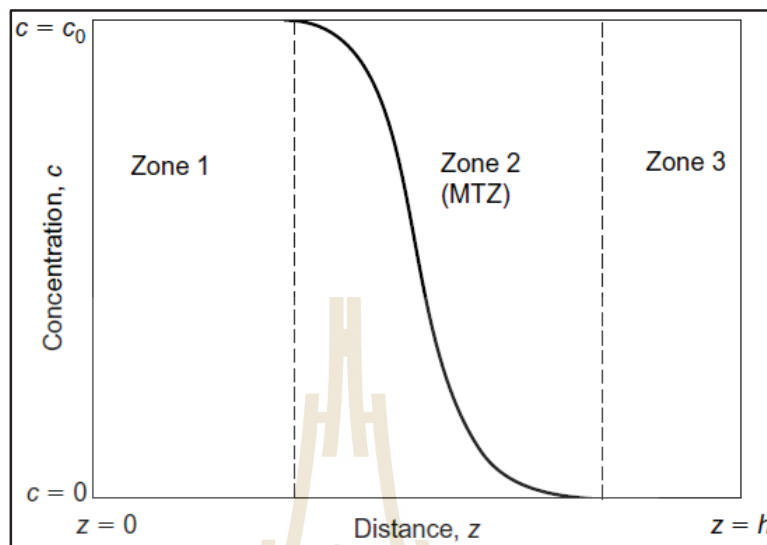
Figure 2.16 Concentration profile during single-solute adsorption in a fixed-bed column of adsorbent height h (Worch, 2012)

In zone 1, the adsorbent is already fully loaded with the adsorbate from the influent. No more mass transfer from the liquid phase to the adsorbent particles occurs in this zone. In zone 2, the interaction between adsorbate from the solution and the surface of the adsorbent just takes place. The adsorbate concentration in this zone decreases from the initial value to zero. For zone 3, the surface of adsorbent is still fully available for adsorption because the adsorbate in this zone is zero.

During the adsorption process in a fixed-bed column, more or less height of MTZ travels through the adsorbent bed to the outlet. When the MTZ has not reached the column outlet, the effluent concentration is supposed to be zero. The presence of adsorbate in the effluent is observed for the first time when the MTZ reaches the end of the column. The corresponding time to the first appearance of adsorbate is referred to as breakthrough time (t_b). When the entire MTZ has left the column, the effluent concentration would be equal the influent concentration and no more adsorption occurs at this point. The corresponding

time to this event is referred to as saturation time (t_s). The plot of the effluent-influent ratio versus service time or treated volume is referred to as the breakthrough curve (BTC). The movement of the MTZ and the development of the BTC are related, as presented in Figure 2.17 (Worch, 2012).
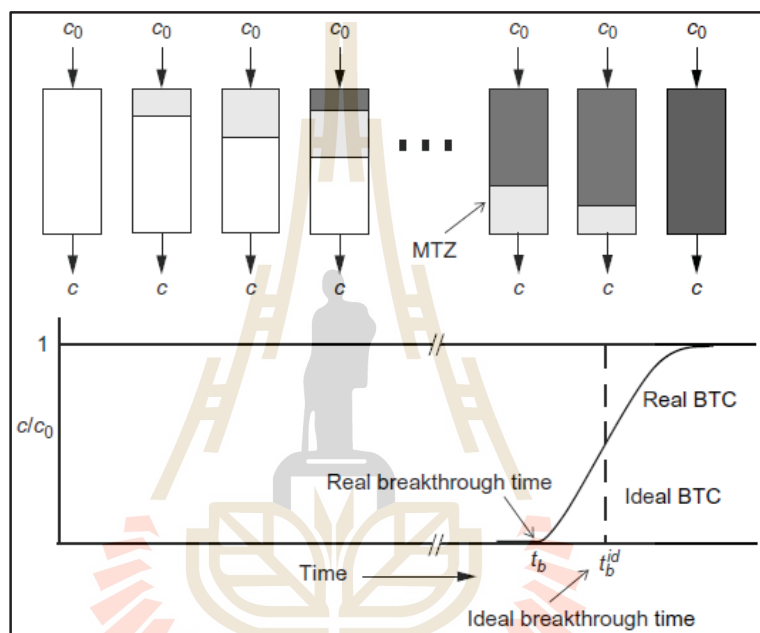
Figure 2.17   Traveling of the MTZ through the adsorbent bed and development of the breakthrough curve (BTC) (Worch, 2012)

Afroze et al. (2015) provided an example of an ideal BTC for a completely utilized capacity of the column (Figure 2.18). At the breakthrough point, the effluent concentration is arbitrarily chosen at C_b. The adsorbent is considered to be saturated when the effluent concentration (C_t) reaches approximately 99.5% of the influent concentration (C_o). At this point, the adsorption in the fixed-bed column can be stopped.

The parameters for column data analysis can be calculated as follow (Lin et al., 2017):

Time equivalent to total or Stoichimoetric capacity is:

$$t_t = \int_{t=0}^{t=\infty} \left(1 - \frac{C_t}{C_o}\right) dt = A_1 + A_2 \tag{2.6}$$

Time equivalent to usable capacity is:

$$t_b = \int_{t=0}^{t_b} \left(1 - \frac{C_t}{C_o}\right) dt = A_1 \tag{2.7}$$

Areas under the breakthrough curve (A1 and A2) can be determined either graphically or by numerical integration.
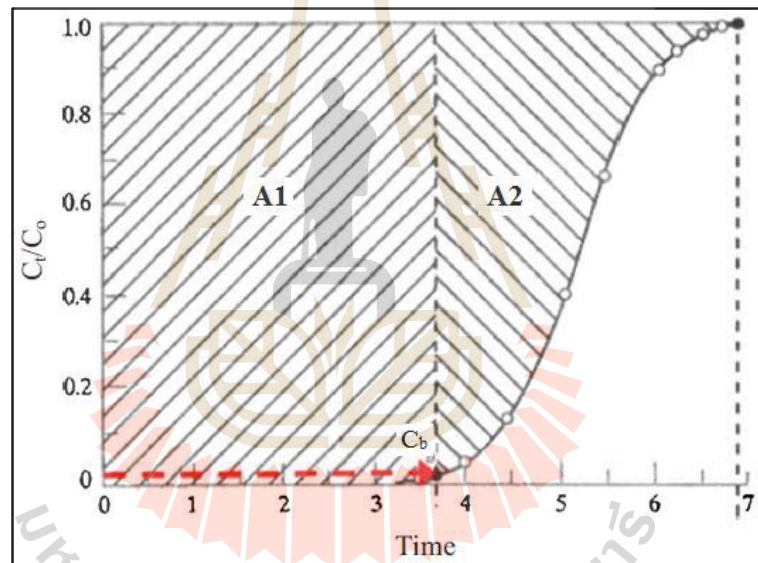
Figure 2.18   An example of an ideal breakthrough curve (Afroze et al., 2015)

Worch (2012) suggested that a fixed-bed column experiment should be initially conducted in a laboratory to determine the BTC, and the column data could be used to verify a chosen adsorption model to predict the adsorption behavior of a full-size column. The laboratory-scale fixed-bed column should have the ratio of column diameter and adsorbent particle diameter greater than 10 to eliminate wall effects, and the influent should be introduced from the bottom to the top of the column to ensure a uniform streaming and avoid channeling.

2.7   Rationale for the Study

The application of adsorption process for removing contaminants from water is extensively carried out due to its exclusive benefits over other remediation techniques. Currently, the development of a low-cost and effective adsorbent with natural materials is still a challenge and gains much attention for a reason that it reduces an operational cost and more plausible for a real application. Although clays and clay minerals are popularly used as adsorbents for water or wastewater treatment, using natural clays as main materials to develop clay-based adsorbents for arsenic adsorption from water is few reported.

Natural clays collected from Dan Kwian, Nakhon Ratchasima, Thailand would be used as a main raw material to develop modified natural clay adsorbents for arsenic removal from aqueous solution. Previous studies indicate that raw clays or clay minerals expressed low adsorption capacities toward arsenic in comparison to modified ones. During a preliminary investigation, Te et al. (2015) observed that natural and modified clays in powdery forms (<75 μm) were difficult to separate from the liquid solution after adsorption, and natural clays with initial bigger particle sizes tended to break down and became plastic when they were mixed with water. On the other hand, natural clays calcined at a high temperature (500-600°C) appeared to be stable in particle size, even in water. Enchancing the surface of the calcined natural clays by treating with ferrous and ferric iron solutions follwed by heating at a moderate temperature is a simple impregnating and cost effective technique.

The average pore size of calcined natural clay and its modified forms is in the range of 4-6 nm, whereas ferric-coated porous clay ceramic filter has pore size of 25.9 nm (Te et al., 2017a; Te et al., 2016). When pore sizes are small for adsorbate ions passing through, pore blocking takes place, resulting in less available active sites and low adsorption efficiency (Tran et al., 2017). Therefore, natural clays, iron oxide, iron powder and rice bran

are mixed to develop iron mixed porous clay pellet adsorbents for improving arsenic removal from water. On the other hand, the proportion selection of constituent materials for composite adsorbents is generally equalized, i.e., 1/2:1/2 for two materials, 1/3:1/3:1/3 for three materials, and 1/4:1/4:1/4:1/4 for four materials. A mixture design approach allows for determining the best proportions of constituent materials to obtain a final product in accordance with the target (BahramParvar et al., 2015). In this case, the optimum proportion of natural clay, iron oxide and iron powder can be obtained to produce high adsorption efficiencies for both arsenite and arsenate removal.

The iron mixed porous clay pellet adsorbent is applied for arsenic adsorption from aqueous solution in both batch mode and dynamic fixed-bed column systems. The batch experiments are mainly performed in laboratory to determine adsorption capacity of adsorbents for designing a particular water treatment system. Contact time, initial solution pH, adsorbent dosage, and initial adsorbate concentration are the main operational parameters that can be optimized using a response surface methodology (RSM). On the other hand, a fixed-bed adsorption is normally conducted to obtain the breakthrough data for providing an accurate full scale design of the column system. Plus, the dynamic system is easily scaled up, simple to operate, cost effective and practical in a real situation.

Additionally, a lightweight bio-sand filter is embedded with iron mixed porous clay pellet adsorbent for treating a real arsenic contaminated groundwater in Cambodia to make ensure that the adsorbent is practical.

CHAPTER III

GENERAL PROCEDURES

3.1   General research processes

The overall research processes can be summarized in the following flowchart diagram (Figure 3.1).
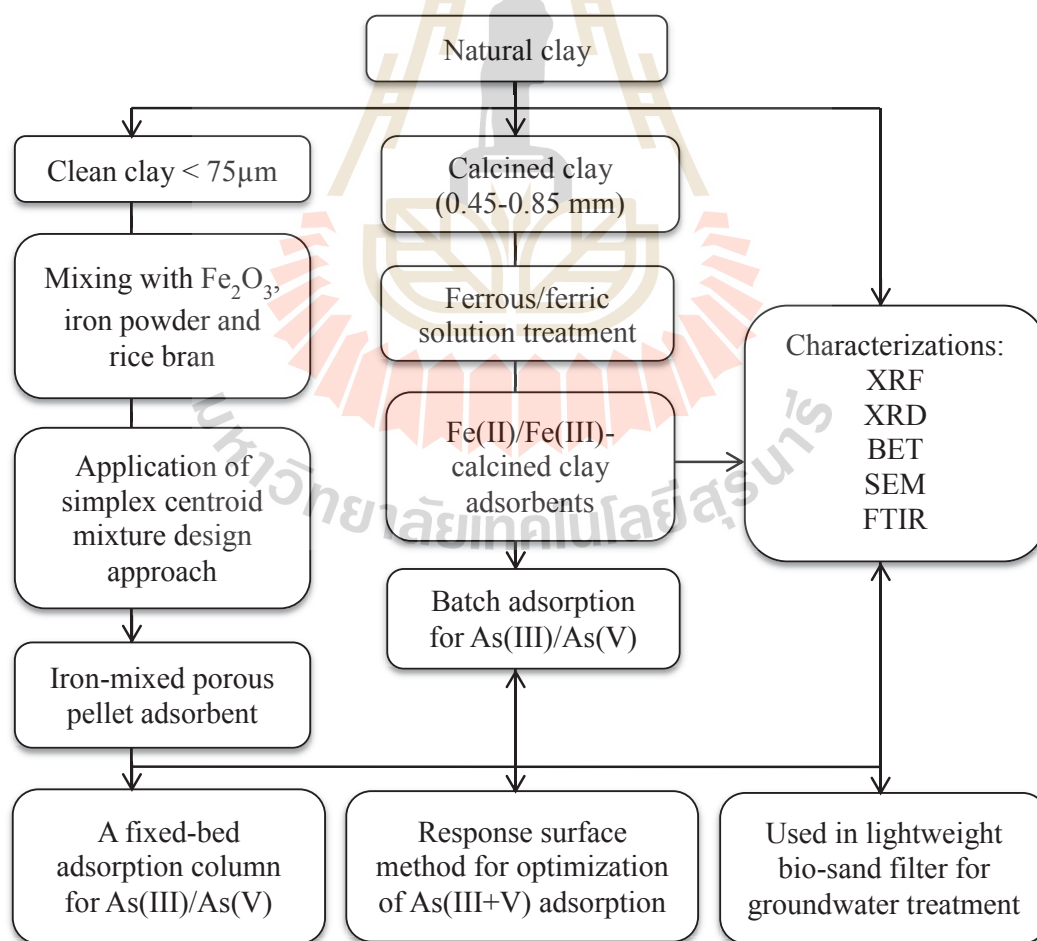
Figure 3.1   Flowchart diagram for the overall processes of the present study

The present research is conducted in five main stages as follows: arsenic adsorption from aqueous solution with modified calcined natural clay adsorbents, application of mixture design approach for a development of iron mixed porous pellet adsorbent, optimization of arsenic adsorption from water with response surface methodology, arsenic adsorption in a continuous fixed-bed column study, and the use of iron mixed clay adsorbent in bio-sand filter for treating arsenic contaminated groundwater.

3.2   Natural clay material

Natural clay as a raw material for the present study was collected from a ceramic production village located in Dan Kwian sub-district, Chok Chai district, Nakhonratchasima province, Thailand. This village is famous for pottery products made from the local natural clays. It is believed that the uniqueness of the Dan Kwian clay lies on the possession of small particle sizes, high plasticity, and high durability and toughness after firing (Srilomsak et al., 2014). The materials were taken from piles of clays stored for molding into pottery shape products, and no chemical additives or preservatives were added. The clays were broken down into small pieces, dried under the sun, and stored for further usages in the study. The main chemical compositions of the natural clay samples consist of Al_2O_3 (25.26%), SiO_2 (66.86%), K_2O (1.48%), CaO (0.52%), TiO_2 (1.04%), MnO_2 (0.05%), and Fe_2O_3 (5.29%). The BET surface area, total pore volume, and mean pore diameter are 52.45 m^2/g, 0.075 cm^3/g, and 5.76 nm, respectively. The point of zero charge (pH_{pzc}) is approximately 5.90 (Te et al., 2015).

CHAPTER IV

MODIFIED CALCINED NATURAL CLAY ADSORBENTS

FOR ARSENIC REMOVAL FROM AQUEOUS SOLUTION

4.1   Introduction

One of the highly potential toxic and carcinogenic elements is arsenic. Elevated arsenic concentration found in natural water is ranged from <100µg/L to 5000µg/L, i.e., an average of 552µg/L in groundwater in Cambodia (Te et al., 2017a). The major arsenic forms in natural water are arsenate, As(V), and arsenite, As(III). The most suitable arsenic remediation method is the adsorption technique due to its simple operation, high removal efficiency and cost-effectiveness (Mahmood et al., 2012). Many low cost materials such as natural materials, agricultural wastes, and industrial wastes have increasingly gained interest to be used as adsorbents for arsenic removal from water (Baig et al., 2015). Natural clay has been interestingly used as adsorbents to uptake various pollutants due to its widely availability and low cost (Srinivasan, 2011; Zehhaf et al., 2015).

Typically, the adsorption capacity of natural adsorbents is low, so a modification process is applied. Among several modification techniques, iron impregnation seems to be simple, cost-effective, and removal efficiency-improved. This was proved by several studies such as modified porous ceramic adsorbents (Chen et al., 2012a), iron-impregnated chitosan (Gang et al., 2010), iron-modified bamboo charcoal (Liu et al., 2012), iron oxide-coated pumice and sepiolite (Öztel et al., 2015), and magnetic nanoparticle-coated sand (Kango and Kumar, 2016).

A preliminary investigation suggested that natural and modified clays used as a fine powder form were difficult to completely separate after adsorption. Plus, natural clays with initially bigger size tended to break down when mixing with water, while natural clays calcined at high temperature appeared to be stable in particle size. Furthermore, so far of our knowledge, research on using modified calcined natural clays for As(III) and As(V) removal from water is still limited. Hence, in this study, it aims to modify the natural clay heated at high temperature through a simple impregnation method to remove As(III) and As(V) from aqueous solution.

4.2   Materials and methods

4.2.1   Chemical reagents

All chemicals in the experiments were of analytical grade and used without further purification. Arsenite and arsenate stock solutions (100 mg/L) were prepared by dissolving $NaAsO_2$ and $Na_2HAsO_4 \cdot 7H_2O$ (Sigma Aldrich, USA), respectively in deionized (DI) water. $FeSO_4 \cdot 7H_2O$ and $FeCl_3 \cdot 6H_2O$ were used for ferrous and ferric solutions, respectively. NaOH and HCl were used for pH adjustment. NaCl, $NaNO_3$, $NaHCO_3$, Na_2CO_3, Na_2SO_4, and Na_3PO_4 were for anion solutions.

4.2.2   Preparation of adsorbents

Natural clay collected from Dan Kwian area, Nakhonratchasima, Thailand, was manually cleaned and ground for particle sizes of 0.45-0.85 mm. The natural clay was calcined at 550°C for 4 to 5 h in a muffle furnace. The calcined clay was labeled as MC. The modification process was conducted with ferrous or ferric solutions. Twenty gram (20 g) of MC was added to 100 mL of 0.25M $FeCl_3 \cdot 6H_2O$ (pH 1.28) or 0.25M $FeSO_4 \cdot 7H_2O$ (pH 3.08). The mixture was magnetically stirred on a hot plate with temperature of 60°C under agitation speed of 250 rpm for 24 h. The suspension was dried at 105°C for 24 h and

then further heated at 350°C for 3 h to ensure higher effective affinity of iron. The product was washed with DI water and labeled as MC-FeIII and MC-FeII, respectively.

4.2.3 Adsorption experiments

The adsorption was carried out in a series of batch experiments at room temperature (25±1°C). The contact time was conducted by mixing 10g/L of the adsorbents with 25mL of the 500 μg/L arsenite or arsenate solution (pH=7 ± 0.1) from 0 to 72h. The effect of initial solution pH was investigated in the pH range of 3-11. Isotherm study was carried out by varying As(III) or As(V) concentrations from 100 to 10000μg/L. The effect of co-exisiting anions was investigated by adding a certain concentration of anions to 500 μg/L As(III) or As(V) solutions. Each experiment was conducted in duplicate and the average was reported. The adsorption efficiency and capacity were calculated with the following equations:

$$R(\%) = \frac{(C_o\text{-}C_e)}{C_o} \times 100 \tag{4.1}$$

$$Q_t = \frac{(C_o\text{-}C_t) \times V}{M} \tag{4.2}$$

$$Q_e = \frac{(C_o\text{-}C_e) \times V}{M} \tag{4.3}$$

where R (%) is either As(III) or As(V) adsorption efficiency; Q_t and Q_e (μg/g) are the adsorption capacity at a certain contact time and at an equilibrium time, respectively; C_o, C_t and C_e (μg/L) are the As(III) or As(V) concentration at initial, a certain time and an equilibrium, respectively; V (L) is the adsorbate volume; M (g) is the mass of adsorbents.

4.2.4 Analytical methods

A(III) or As(V) concentration was measured using Inductively Coupled Plasma-optimal Emission Spectrometry (ICP-OES, Optima 8000, PerkinElmer, USA) with a wavelength of 193.7 nm. The Energy Dispersive X-ray Fluorescence (XRF, HORIBA

Ltd., Japan) was used for the elemental composition analysis. The mineralogical phases were analyzed by X-ray diffraction method with the Bruker XRD (D2-PHASER). The surface morphology were examined by a scanning electron microscope (SEM, JSM-6010LV, JEOL, Japan) coupled with Energy-dispersive X-ray spectroscopy (EDX). The surface area, pore volume, and average pore diameter were calculated from nitrogen adsorption-desorption isotherm data at 77 K by the Brunauer-Emmett-Teller (BET) method using the BET analyzer (BELSORP Mini II, BEL Inc., Japan). The samples were outgassed at 60°C for 24 h under N_2 flow by BELPREP-vacII (BEL Inc., Japan). The point of zero charge (pH_{pzc}) was evaluated by plotting the initial pH as a function of the equilibrium pH (0.01M NaCl as background electrolyte with the equilibrium time of 72h) (Su et al., 2011).

4.3   Results and discussion

4.3.1   Characterization of adsorbents

The characteristic analysis of the physico-chemical properties of the adsorbents is illustrated in Table 4.1.

Table 4.1   Physical-chemical properties of adsorbents

Properties	MC	MC-FeII	MC-FeIII
SiO_2 (wt.%)	71.25	68.34	68.63
Al_2O_3 (wt.%)	20.51	20.07	16.55
Fe_2O_3 (wt.%)	5.585	8.361	11.77
Surface area (m^2/g)	41.69	55.41	55.99
Total pore volume (cm^3/g)	0.059	0.067	0.068
Mean pore diameter (nm)	5.712	4.807	4.799
pH_{pzc}	6.3	5.9	5.1

The main chemical constituents of all the adsorbents were silicate (SiO_2), alumina (Al_2O_3) and iron oxide (Fe_2O_3). The percentage of silica and alumina of MC-FeII and MC-FeIII were observed to be lower than those of MC. However, an increase of iron oxide content was observed for modified adsorbents compared to that of MC (roughly 1.5 and 2 times for MC-FeII and MC-FeIII, respectively). This indicated that the applied iron impregnation technique in this study successfully improved iron content.

The surface area of MC, MC-FeII and MC-FeIII were $41.69m^2/g$, $55.41m^2/g$ and $55.99m^2/g$, respectively. The improvement of surface area after iron treatment could result from the presence of open spaces on the surface of modified adsorbents. It could be due to the hydrolysis changes of the solid surface from a long hydratation in the course of iron adsorption processes, and the exhibition of corrosive effect from the iron solutions (Dousova et al., 2006; Chen et al., 2012a). The two effects did not destroy the structure of pore, but made the surface coarse, and it was supported by the calculation of the total pore volume and SEM images. It was observed that there was an increase of total pore volume for modified adsorbents. All adsorbents exhibited the mean pore size within 2 to 50 nm, indicating that the materials are relatively mesoporous according to the pore classification recommendation of the International Union of Pure and Applied Chemistry (IUPAC) (Kuila and Prasad, 2013).

XRD pattern analysis of the adsorbents is presented in Figure 4.1. The pattern of all adsorbents was almost identical. However, the intensity to develop peaks for the modified adsorbents increased and the development of new peaks was observed for MC-FeIII. This may be contributed to the increase in the amount of iron oxide on the surface. The main composting minerals for the adsorbents include quartz, illite-montmorillonite, kaolinite and hematite.
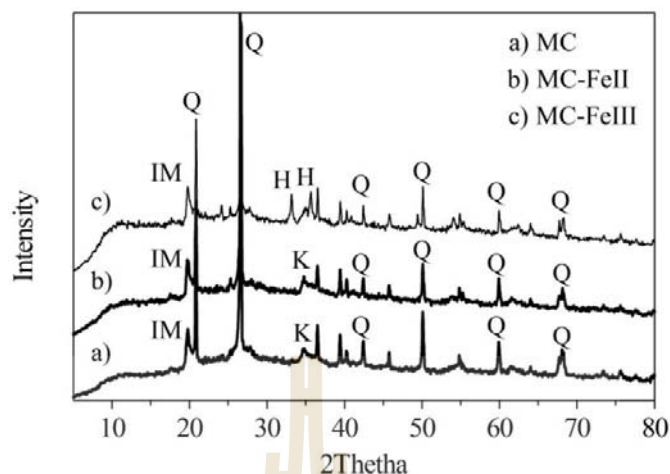
Figure 4.1 XRD patterns of the adsorbents: Q (Quartz), K (Kaolinite), IM (Illite-montmorillonite), and H (Hematite)

Figure 4.2 shows the surface morphological feature of MC, MC-FeII and MC-FeIII analyzed by SEM. A pretty smooth with few rough particle attachments was observed on the surface of MC, which could be a result of exposure of silica to high temperature. Surface features of MC-FeII and MC-FeIII were similar with the occurrence of several concave shapes and many small pores. This was strongly supportive to the occurrence of the corrosive effect from treating acidic iron solutions.

The EDX analysis (Figure 4.2d, 4.2e and 4.2f) showed that there are some iron peaks, confirming the presence of iron element on the surface of the adsorbents.
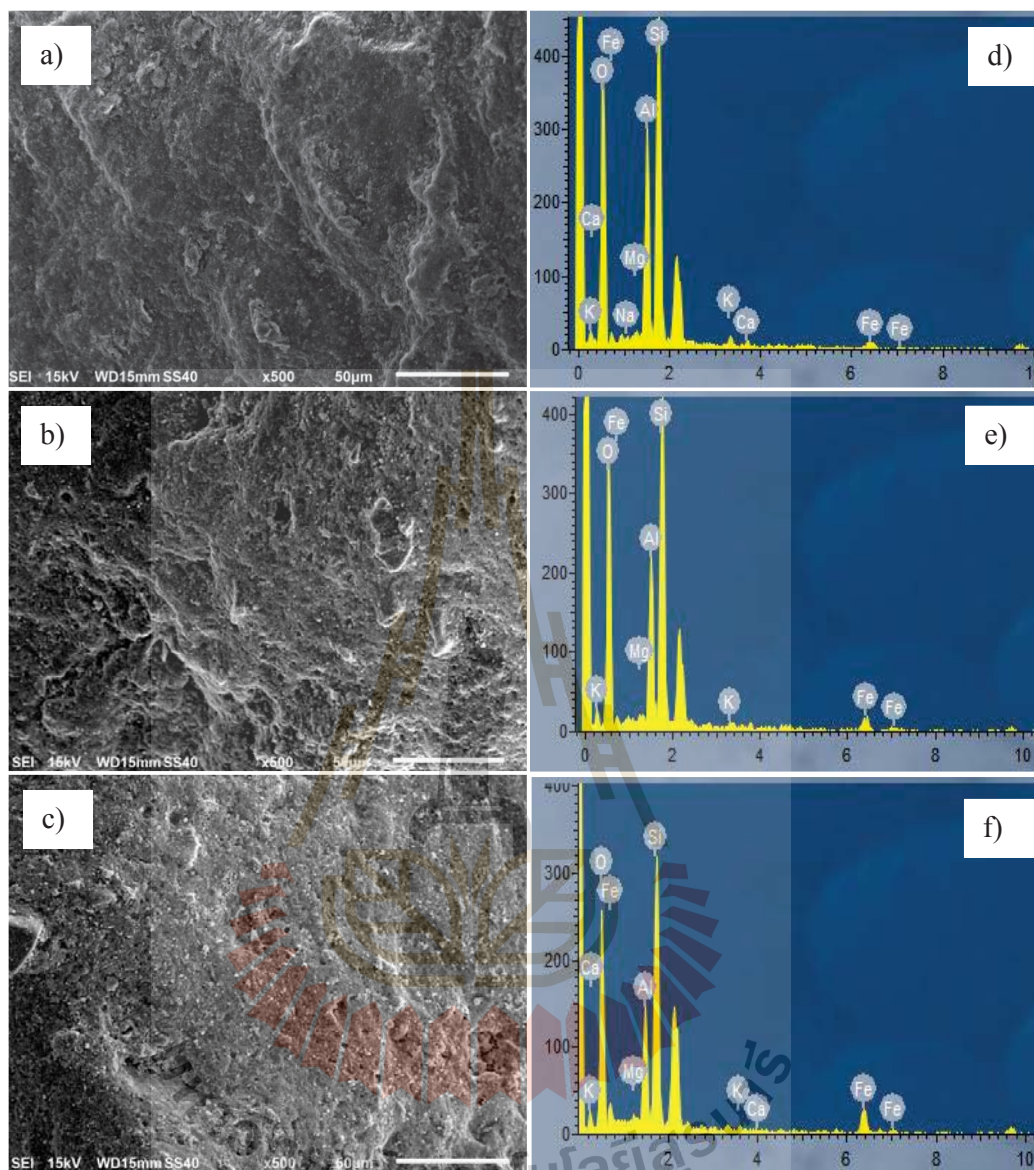
Figure 4.2 SEM analysis of (a) MC, (b) MC-FeII, (c) MC-FeIII, and EDX results: (d) EDX-MC, (e) EDX-MC-FeII, and (f) EDX-MC-FeIII

4.3.2 Kinetic studies

Figure 4.3 shows the effect of time dependent for As(III) and As(V) adsorption onto MC, MC-Fe(II), and MC-Fe(III). For As(III) adsorption, the removal process occurred similarly for both modified adsorbents.
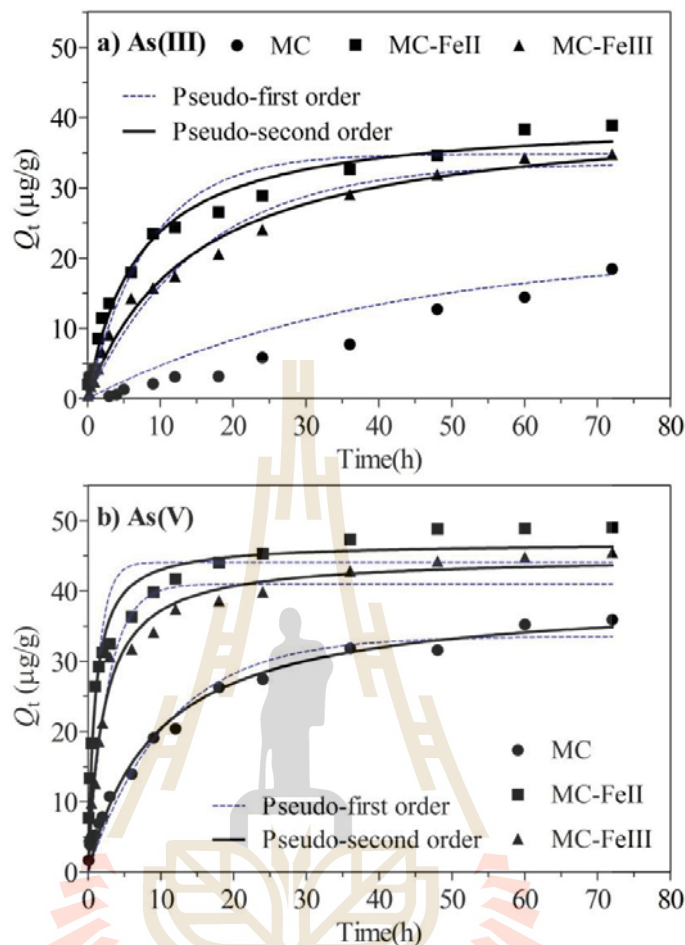
Figure 4.3   Effect of contact time and its fitting models for arsenic adsorption on the adsorbents: a) A(III) and b) As(V)

The first 12 h indicated a fast uptake and then slowed down with a gradual increase of adsorption capacity in the following 60 h. No significant adsorption improvement was observed up to 72 h, which was considered to be an equilibrium time. This equilibrium time was also used for MC. For As(V) adsorption, within the first 18h, all adsorbents expressed fast adsorption toward arsenate in the aqueous solution. Later, the uptake rate was insignificantly improved and reached the equilibrium with 72h. For both As(III) and As(V) adsorption cases, the initial fast adsorption process can be explained by an initial wide availability of active sites of adsorbents, particularly the external surface. The decrease of

active surface area and diffusion to inner sites of adsorbents most probably occur in a gradually slowing down phase.

The kinetic data were fitted with pseudo-first-order and pseudo-second-order kinetic models with the none-linearized equation forms expressed as follows:

Pseudo-first-order: $$Q_t = Q_e(1 - e^{-k_1 t}) \tag{4.4}$$

Pseudo-second-order: $$Q_t = \frac{Q_e^2 k_2 t}{1 + Q_e k_2 t} \tag{4.5}$$

where t(h) is the time; k_1(1/h) and k_2(g/μg/h) are the rate constants of the pseudo-first-order and pseudo-second-order models, respectively. To determine whether the adsorption process involves a single or multiple binding process, Weber Morris intra-particle diffusion model was deployed and its equation is given by Pillewan et al. (2011):

$$Q_t = k_{id} t^{0.5} \tag{4.6}$$

where k_{id} (μg/g/h$^{0.5}$) is the intra-particle diffusion rate constant. The intra-particle diffusion plots for As(III) and As(V) adsorption on the adsorbents are illustrated in Figure 4.4.

The evaluation of kinetic parameters for both As(III) and As(V) adsorption onto the adsorbents is presented in Table 4.2. The high values of correlation coefficient (R^2) and closeness of the values of the calculated equilibrium uptake ($Q_{e,cal}$) to the experimental equilibrium uptake ($Q_{e,exp}$) indicate that the model well fits to the experimental data. For As(III) adsorption, the pseudo-second-order model was a better fitted model to the kinetic data of the adsorption onto the adsorbents, MC-FeII ($R^2 = 0.989$) and MC-FeIII ($R^2 = 0.986$). The suitability of the kinetic data to the pseudo-second-order model suggests that the adsorbate and adsorbents exchange or share electron and the surface properties of adsorbents and adsorbate concentration play significant roles in controlling the adsorption rate (Li et al., 2015).
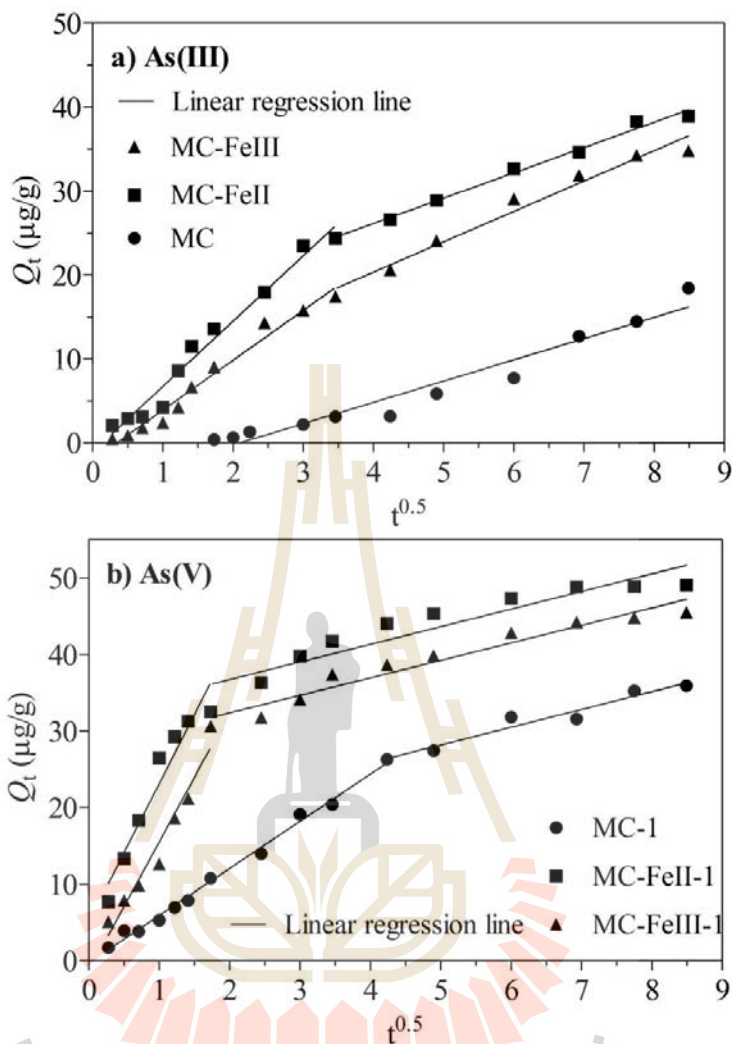
Figure 4.4 Intra-particle diffusion model for a) As(III) and b) As(V) adsorption by the adsorbents

However, the As(III) adsorption onto the adsorbent MC followed the pseudo-first-order model with $R^2 = 0.947$. In case of As(V) adsorption, for all adsorbents, the correlation coefficients (R^2) of the pseudo-second order model were higher than those of the pseudo-first order model. Plus, the arsenate adsorption capacity obtained from pseudo-second order model ($Q_{e,cal.}$) was comparable to the arsenate adsorption capacity from the experiment ($Q_{e,exp.}$). Thus, the kinetic data were well described by the pseudo-second order model.

Table 4.2   Kinetic parameters for As(III) and As(V) adsorption by the adsorbents

Models	As(III)			As(V)		
	MC	MC-FeII	MC-FeIII	MC	MC-FeII	MC-FeIII
$Q_{e,exp}$ (µg/g)	18.45	38.92	34.80	36.00	49.05	45.51
Pseudo-first-order model						
$Q_{e,cal}$ (µg/g)	21.02	33.51	41.01	33.54	44.08	41.00
k_1 (1/h)	0.025	0.056	0.052	0.092	0.763	0.378
R^2	0.947	0.934	0.959	0.972	0.883	0.945
Pseudo-second-order model						
$Q_{e,cal}$ (µg/g)	-	40.83	37.38	38.09	49.77	46.34
k_2 (g/µg/h)	-	0.004	0.002	0.004	0.014	0.009
R^2	0.2265	0.989	0.986	0.986	0.999	0.998
Intra-particle diffusion						
$k_{id\text{-}1}$ (µg/g/h$^{0.5}$)	2.534	7.788	5.938	6.158	18.044	16.880
R^2	0.948	0.9748	0.9755	0.993	0.933	0.953
$k_{id\text{-}2}$ (µg/g/h$^{0.5}$)	-	3.014	3.619	2.323	2.301	2.285
R^2	-	0.9908	0.9717	0.951	0.874	0.945

From Figure 4.4 and Table 4.2, Weber Morris intra-particle diffusion model provided high values of R^2 for As(III) and As(V) adsorption, and it can be clearly observed that two linear regression lines occurred for all adsorbents, except for As(III) removal onto MC adsorbent. This implies that the adsorption processes occurring on all adsorbents, but MC for As(III) adsorption, involved multiple binding steps. The rate constants for the first linear section of each adsorbent were higher than those of the other section, implying a fast uptake initially and then later gradually slowing down. It is consistent with the data of

As(III) and As(V) adsorption capacities against time (shown in Figure 4.3). All plots of the model did not pass through the origin, suggesting that intra-particle diffusion was not rate limiting step and the adsorption process onto the adsorbents possibly involves surface adsorption, film diffusion and intra-particle diffusion (Fufa et al., 2014; Hamayun et al., 2014).

4.3.3 Effect of initial solution pH

Figure 4.5 presents the effect of initial solution pH for As(III) and As(V) adsorption onto MC, MC-Fe(II), and MC-Fe(III). In case of As(III) adsorption, the adsorption efficiency of MC-FeII gradually increased over a pH range of 3-7, and significantly improved when pH was increased to 9. Both MC and MC-FeIII expressed a slightly change on the adsorption efficiency over a pH range of 3-9. Apparently, all adsorbents exhibited the dramatically decreased adsorption efficiencies for pH more than 9. The results are comparable with some previous reports on arsenite adsorption by mixed-oxide-coated sand (Vaishya and Gupta, 2010), iron-modified bamboo charcoal (Liu et al., 2012), iron and titanium co-pillared montmorillonite (Li et al., 2015), and iron-impregnated chitosan (Gang et al., 2010). In case of As(V) adsorption, all the adsorbents shared a similar pattern of the adsorption efficiency over the studied pH range. The arsenate adsorption efficiency gradually decreased for pH from 3 to 7. When pH was beyond 7, a significant decrease was observed and a great decline was observed for pH 11.

The results can be explained through the properties of the surface of adsorbents and the arsenic speciation at various pH values. Iron-coated adsorbents are enriched in hydrated metal particles possibly being protonated or deprotonated to dominate with a positive or negative surface charge depending on pH value (Dousova et al., 2009; Šiljeg et al., 2012). The surface of the adsorbents was more positively charged for pH lower than point of zero charge (pH_{pzc}) and predominated with the negative charge for $pH>pH_{pzc}$ (Chang et al., 2010).
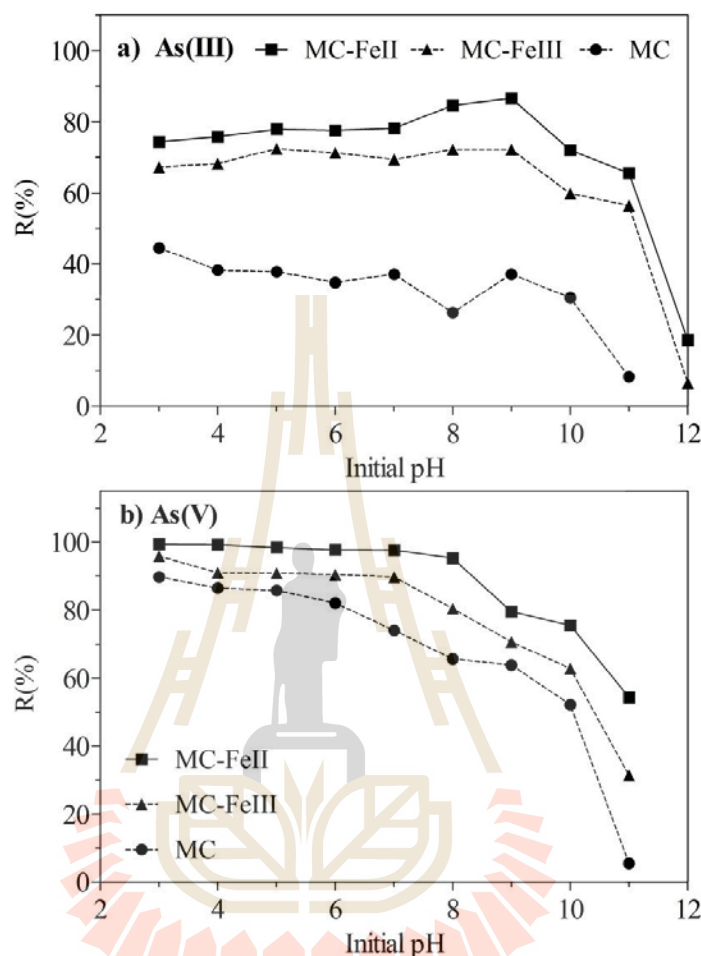
Figure 4.5 Effect of initial solution pH for adsorbing: a) As(III) and b) As(V)

The proposed active surface site of the adsorbents can be expressed as follows:

$$M \cdot Fe\text{-}OH_{(s)} + H^+ \leftrightarrow M \cdot Fe\text{-}OH_{2(s)}^+ \qquad (pH < pH_{pzc})$$

$$M \cdot Fe\text{-}OH_{(s)} \leftrightarrow M \cdot Fe\text{-}O_{(s)}^- + H_{(aq)}^+ \qquad (pH > pH_{pzc})$$

Generally, in natural water, arsenite species occur as: H_3AsO_3 (pH<9.2), $H_2AsO_3^-$ (9<pH<12), $HAsO_3^{2-}$ (12<pH<13), and AsO_3^{3-} (pH>13), and arsenate mainly exists in water as H_3AsO_4 at pH less than 2.2, $H_2AsO_4^-$ at pH between 2.2 and 6.98, $HAsO_4^{2-}$ at pH between 6.98 and 11.5, and AsO_4^{3-} at pH above 11.5 (Mohan and Pittman, 2007). The point

of zero charge (pH$_{pzc}$) for MC, MC-FeII and MC-FeIII were 6.3, 5.9 and 5.1, respectively (Table 4.1). Obviously, the unfavorable electrostatic interaction or the electrical repulsion between the adsorbents and the adsorbate resulted in less adsorption capacity at pH>9. The arsenite sorption onto MC-FeII and MC-FeIII at pH<9 could be attributed to ligand exchange or electrostatic forces. The proposed adsorption mechanism for either As(III) or As(V) onto the iron modified clay adsorbents could be expressed according to the following formulas:

For As(III) adsorption:

$$M \cdot Fe\text{-}OH_{(s)} + H_3AsO_{3(aq)} \leftrightarrow M \cdot Fe\text{-}H_2AsO_{3(s)} + H_2O \qquad \text{(mondentate)}$$

$$2M \cdot Fe\text{-}OH_{(s)} + H_3AsO_{3(aq)} \leftrightarrow M \cdot Fe_2\text{-}HAsO_{3(s)} + 2H_2O \qquad \text{(bidentate)}$$

For As(V) adsorption:

$$M \cdot Fe\text{-}OH_{(s)} + H_2AsO_{4(aq)}^- \leftrightarrow M \cdot Fe\text{-}HAsO_{4(s)}^- + H_2O \qquad \text{(mondentate)}$$

$$2M \cdot Fe\text{-}OH_{(s)} + H_2AsO_{4(aq)}^- \leftrightarrow M \cdot Fe_2\text{-}H_2AsO_{4(s)}^- \qquad \text{(bidentate)}$$

These ligand exchanged reactions may occur at both internal and external surfaces for modified calcined clay.

4.3.4 Isotherm studies

Results from the effect of different initial As(III) or As(V) concentrations for the adsorption onto the adsorbents, MC, MC-Fe(II), and MC-Fe(III), can be used for the study of isotherm. Langmuir and Freundlich models were used to fit the isotherm data and their non-linear forms are expressed in equation 4.7 and 4.8, respectively.

$$Q_e = \frac{K_L Q_m C_e}{1 + K_L C_e} \qquad (4.7)$$

$$Q_e = K_F C_e^{1/n} \qquad (4.8)$$

where Q$_m$ (µg/g) is the maximum adsorption capacity based on the Langmuir equation, K_L (L/µg) is the Langmuir constant; K_F and n are the Freundlich's adsorption coefficients.

Figure 4.6 and 4.7 show the effect of As(III) and As(V) adsorption onto the adsorbents with various initial concentrations and the fitting isotherm models, respectively. For both As(III) and As(V) adsorption cases, the adsorption capacity of all adsorbents significantly increased at the lower adsorbate concentrations, but gradually declined with an increase of initial adsorbate concentrations. The proportion of active sites on the surface of the adsorbents to the presence of arsenic ions probably attributes to the reason for this (Kango and Kumar, 2016). The calculated isotherm parameters are presented in Table 4.3.
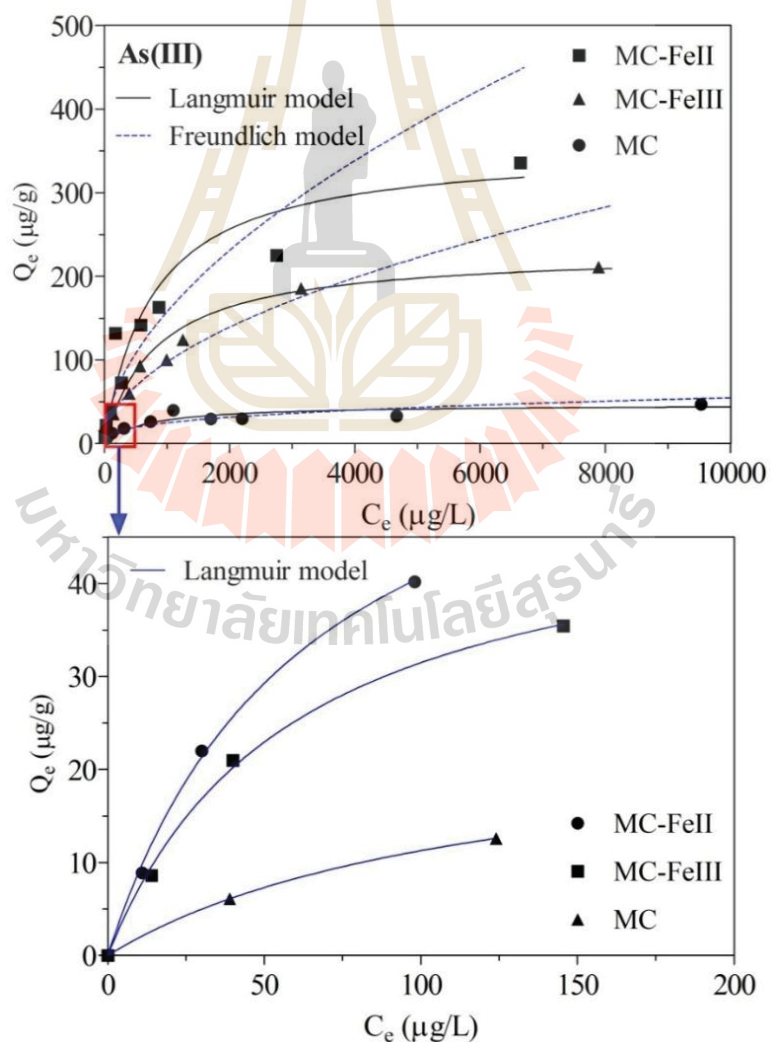
Figure 4.6 Effect of initial As(III) concentration and isotherm fitting models for the adsorption onto the adsorbent
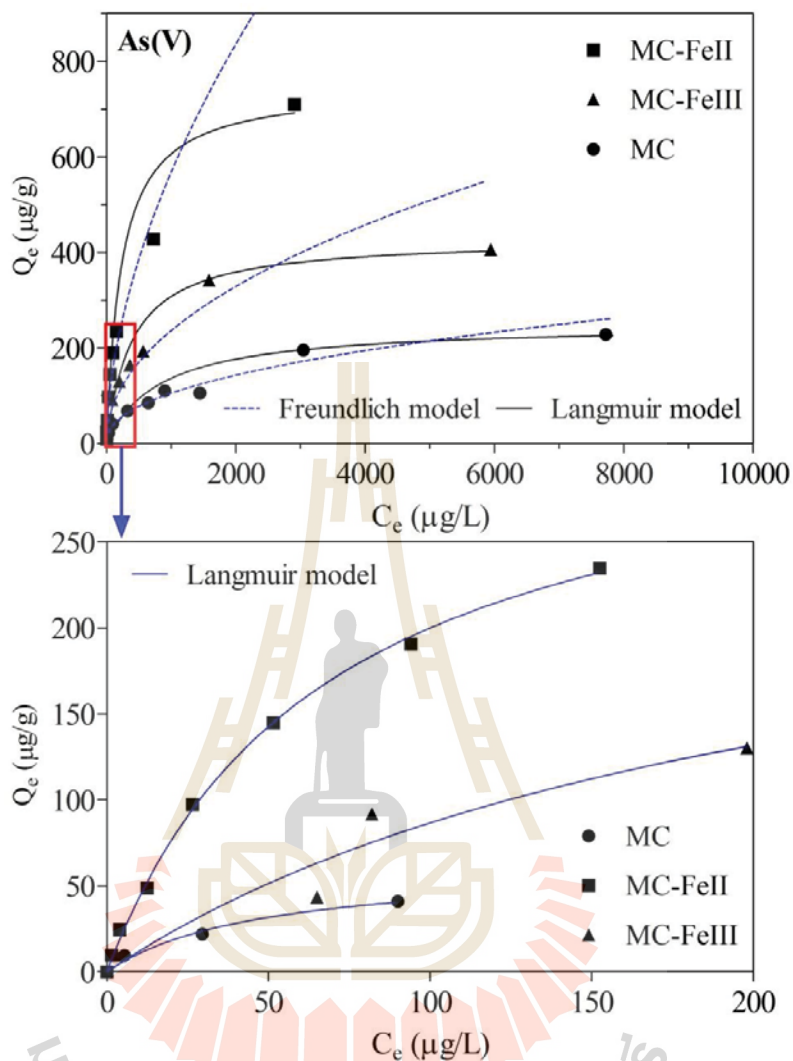
Figure 4.7 Effect of initial As(V) concentration and isotherm fitting models for the adsorption onto the adsorbent

For As(III) adsorption case, the Langmuir model exhibited higher correlation coefficients for all adsorbents in a comparison to the values obtained for the Freundlich model. The calculated maximum adsorption capacities ($Q_{m,cal}$ = 46.729, 354.99 and 230.47µg/g for MC, MC-FeII and MC-FeIII, respectively) were comparable to the experimental maximum adsorption capacities ($Q_{m,exp}$ = 47.095, 335.70 and 210.85µg/g for MC, MC-FeII and MC-FeIII, respectively).

Table 4.3   Isotherm parameters for As(III) and As(V) adsorption by the adsorbents

Models	As(III)			As(V)		
	MC	MC-FeII	MC-FeIII	MC	MC-FeII	MC-FeIII
$Q_{m,exp}$	47.095	335.70	210.85	227.95	709.50	405.85
Freundlich model						
$1/n$	0.3432	0.5514	0.5115	0.4427	0.5584	0.4765
K_F	2.3173	3.4900	2.8500	4.9413	11.989	8.7845
R^2	0.8773	0.9190	0.9730	0.9887	0.9619	0.9438
Langmuir model						
Q_m	46.729	354.99	230.47	250.00	747.38	429.74
K_L	0.0015	0.0013	0.0012	0.0012	0.0043	0.0025
R_L	0.06-0.87	0.07-0.88	0.08-0.89	0.07-0.89	0.02-0.67	0.04-0.79
R^2	0.9614	0.9650	0.9850	0.9556	0.9801	0.9883

This implies that the Langmuir model was a better one to describe the isotherm data, indicating the adsorption process expresses a monolayer on the homogeneous surface of the adsorbent without having any interaction between adsorbed adsorbate (Ouadjenia-Marouf et al., 2013).

For As(V) adsorption case, the results indicated that MC-FeII and MC-FeIII were better fitted to the Langmuir model due to the higher values of correlation coefficient (R^2). However, MC was well described by the Freundlich model. This implied that MC possessed a heterogeneous surface with multi layers adsorption for As(V). The improvement of iron contents of MC-FeII and MC-FeIII seems to overpass the uptake capacity of other parallel existing minerals on the surface of calcined clay and provided a

monolayer arsenate adsorption on the their homogeneous surface. The maximum As(V) adsorption capacities from the Langmuir model were 250μg/g, 747.38μg/g and 429.74μg/g for MC, MC-FeII and MC-FeIII, respectively.

Generally, the performance of isotherm study at high arsenic concentration is for calculating the maximum adsorption capacity of a used adsorbent. However, it is also necessary to evaluate the adsorption capacity of arsenic at low equilibrium arsenic concentration since the targeted arsenic concentration in drinking water must be below 10 μg/L. The isotherm experimental data of equilibrium As(III) or As(V) lower than 200 μg/L were fitted by the Langmuir model, as shown in Figure 4.6 and 4.7, respectively, and the obtained adsorption capacities of As(III) and As(V) on the adsorbents at the equilibrium arsenic concentration of 10 μg/L based the developed model are presented in Table 4.4.

From Table 4.4, at the equilibrium arsenic concentration of 10 μg/L, the adsorption capacities for As(III) was about 1.92 μg/L on MC adsorbent, 9.05 μg/L on MC-FeII adsorbent, and 7.24 μg/L on MC-FeII adsorbent. The adsorption capacities of As(V) on MC, MC-FeII, and MC-FeIII adsorbents were 10.76, 43.23, 12.07 μg/L, respectively. Apparently, the performance of MC-FeII for both As(III) and As(V) adsorption was better compared to that of MC-FeIII. This may be explained by the presence of more potential available active sites on the surface of MC-FeII compared to MC-FeIII. Ferric species tends to gather into bigger ferric(hydr)odixe particles. Such a phenomenon may decrease the availability of this ion species to the inner porosity of the calcined clay by blocking some pores, hence limiting the homogeneity of the impregnating. On the other hand, ferrous species may diffuse inside the inner porosity of the calcined clay that can lead to a homogenous dispersion on the surface of hosting materials (Munis et al., 2009). Munis et al. (2009) also suggested that more and smaller iron species using in an impregnating protocol would lead to the highest arsenic uptakes for the resultant impregnated adsorbent.

Table 4.4   Langmuir isotherm parameters for As(III) or As(V) adsorption onto the adsorbents at low arsenic concentration (<200 μg/L)

Parameters	As(III)			As(V)		
	MC	MC-FeII	MC-FeIII	MC	MC-FeII	MC-FeIII
$Q_{e,10ppb}$	1.92	9.05	7.24	10.76	43.23	12.07
$Q_{m,<200ppb}$	24.65	66.52	50.15	61.84	334.73	275.73
K_L	0.0084	0.0157	0.0169	0.0211	0.0148	0.0046
R^2	0.9998	0.9986	0.9977	0.9165	0.9871	0.9984

A dimensionless constant separation factor or equilibrium parameter (R_L) is an essential feature of a Langmuir isotherm that is used to predict if an adsorption system is "favorable" or "unfavorable", and it can be defined by:

$$R_L = \frac{1}{1 + K_L C_o} \tag{4.9}$$

The adsorption process is irreversible ($R_L=0$), favorable ($0<R_L<1$), linear ($R_L=1$) and unfavorable ($R_L>1$) (Khan and Khan, 2015).

For initial adsorbate concentrations in the range of 100-10000μg/L, the R_L values for MC, MC-FeII, and MC-FeIII were in the range of 0.06-0.87, 0.07-0.88 and 0.08-0.89, respectively, for As(III) adsorption, and 0.07-0.89, 0.02-0.67 and 0.04-0.79, respectively, for As(V) adsorption. This suggested that all adsorbents uptake As(III) and As(V) from aqueous solution favorably. It is also consistent with the results for $1/n$ values for all adsorbents. The adsorption is favorable when $0<1/n<1$, irreversible when $1/n=1$ and unfavorable when $1/n>1$ (Fufa et al., 2014). For all adsorbents in both cases, $1/n$ values were within 0 and 1.

4.3.5 Effect of coexisting anions

Figure 4.8 shows the results of As(III) and As(V) adsorption efficiency onto the adsorbents in the presence of individual anion. The effect of common existing anions in water such as Cl^-, NO_3^-, HCO_3^-, CO_3^{2-}, SO_4^{2-}, and PO_4^{3-} (representing univalent, bivalent, and trivalent anions) was separately investigated by adding 0.1mM of each anion to 500µg/L of either As(III) or As(V) solution. In case of As(III) adsorption, the anions expressed the influence on the adsorption efficiency similarly for both iron modified adsorbents.
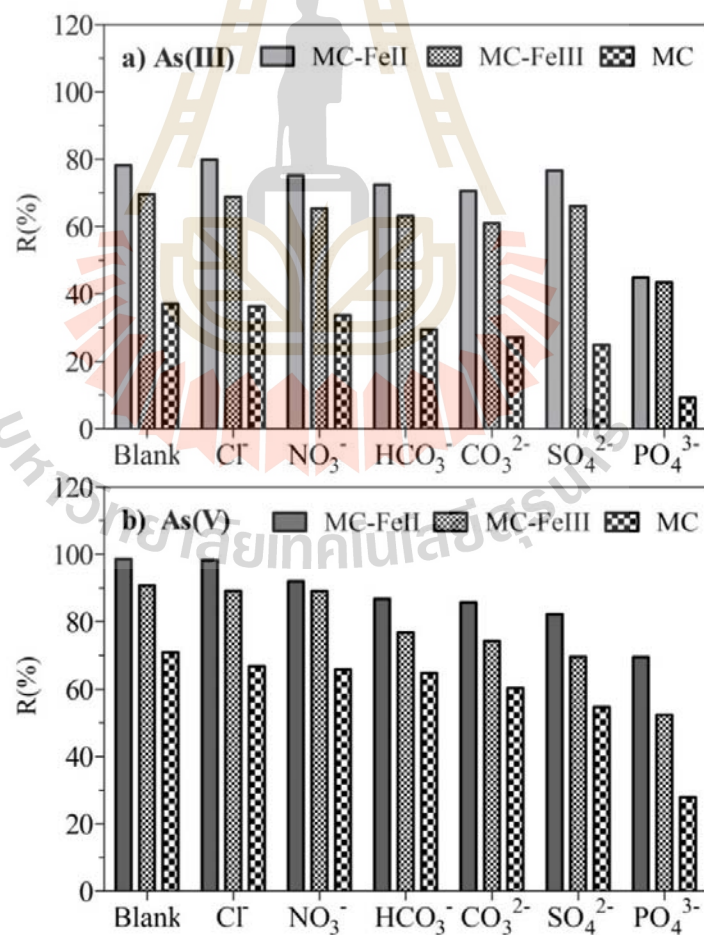
Figure 4.8   Effect of coexisting anions on a) As(III) and b) As(V) adsorption

The presence of Cl^-, NO_3^-, and SO_4^{2-} showed an insignificant reduction of As(III) adsorption efficiency, whereas HCO_3^- and CO_3^{2-} anions exhibited a slightly decrease. The most adverse effect was observed in the presence of PO_4^{3-}. For MC adsorbent, each anion significantly reduced the As(III) removal efficiency, particularly PO_4^{3-}. In case of As(V) adsorption, the results showed that a similar trend of influence on the As(V) efficiency was observed for all adsorbents. The presence of univalent anions showed less reduction in the As(V) adsorption efficiency. A further reduction of adsorption efficiency was observed when bivalent anions were added. Trivalent anion (PO_4^{3-}) significantly decreased the As(V) adsorption efficiency. For both As(III) and As(V) uptake, the significant reduction in the removal efficiency for all adsorbents in the presence of introduced coexisting anions, especially phosphate, can be explained by the competition for active sites on the surface of the adsorbents. Phosphate and arsenic are in the same group, and have similarities in chemical properties (Maliyekkal et al., 2009). Plus, phosphate easily forms an inner-sphere complex and strongly attaches to iron(oxy)hydroxides than arsenic (Hsu et al., 2008; Su and Puls, 2001).

4.4 Conclusion

Natural clay could be stabilized the particle size by calcination. Iron impregnation on MC successfully improved the iron oxide content for MC-FeII and MC-FeIII, as well as their adsorption efficiencies. For As(III) adsorption, the kinetic data were well described by the pseudo-second order, except for MC. All adsorbents expressed a slightly change of the adsorption efficiency over a wide range of pH, and a significant decline of the uptake efficiency at pH>9. The isotherm data were well fitted to the Langmuir model for all adsorbents. The presence of introduced coexisting anions (except for phosphate) insignificantly affected on the adsorption efficiency by the modified adsorbents, but the

reduction of removal efficiency was observed for MC. In case of As(V) adsorption, the pseudo-second order model was more suitable for fitting the kinetic data for all adsorbents. All adsorbents exhibited high arsenate adsorption efficiency at lower initial solution pH and a significant reduction occurred at high pH value. The introduced coexisting anions influenced on the arsenate adsorption efficiency of all adsorbents in the following order: trivalent> bivalent> univalent anions.
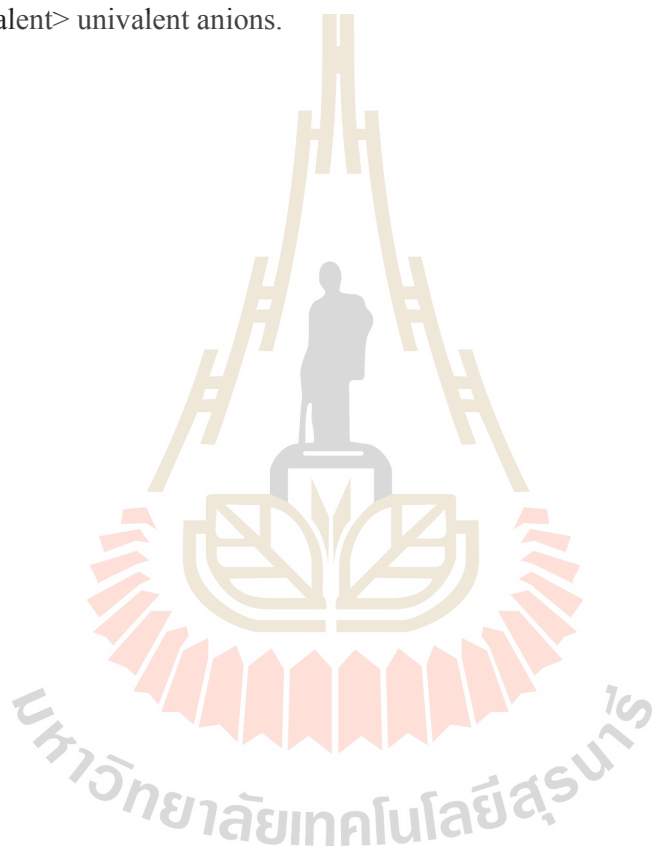
CHAPTER V

DEVELOPING IRON MIXED POROUS PELLET

ADSORBENT BY MIXTURE DESIGN APPROACH FOR

ARSENITE AND ARSENATE ADSORPTION FROM WATER

5.1 Introduction

Toxic pollutant is one of the major sources of contamination and amongst of the most highly toxic and carcinogenic elements is arsenic (As). Drinking arsenic contaminated water is a main pathway for the toxin to enter the human body since arsenic lacks taste, color and odor (Mondal et al., 2013; Sharma et al., 2014). Normally, arsenite (As(III)) and arsenate (As(V)) are the common forms in natural water. Arsenic removal efficiency through adsorption significantly depends on the nature and characteristic of an adsorbent that can be either natural or synthetic materials such as commercial and synthetic activated carbons, agricultural products or by-products, industrial by-products or wastes, and metal oxides (Mohan and Pittman, 2007). Currently, developing a low-cost and effective adsorbent with natural materials has gained more attention because of the cost reduction and plausibility of a real application.

Clay supported metal oxides has been proved to remove some pollutants through various studies such as Pb(II) and Zn(II) removal by ceramisite produced from bentonite, iron powder and activated carbon (Yuan and Liu, 2013); As(V) adsorption on adsorbents made from clay, iron oxide and starch (Chen et al., 2010); Cr(VI) and As(V) removal by zero-valent iron and iron oxide-coated sand adsorbent (Mak et al., 2011); As(III) and As(V)

removal by montmorillonite-supported zero valent iron (Bhowmick et al., 2014); and As removal by iron mixed ceramic pellet (Shafiquzzam et al., 2013). However, application of a systematic method to determine optimal proportion of each material for developing more effective adsorbent to remove both As(III) and As(V) is still limited.

The present study mainly aimed to develop porous pellets produced from natural clay to support iron oxide and iron powder to be a low-cost and effective adsorbent for both As(III) and As(V) removal from water.

5.2   Materials and Methods

5.2.1   Materials and chemical reagents

Natural clay used in this study was collected from Dankwian District, Nakhon Ratchasima, Thailand. The clay was cleaned with deionized (DI) water to remove debris and large particles, dried at $104 \pm 1°C$ for 24h, crushed and sieved to achieve the particle size passing through a 200-mesh ($<75 \mu m$) sieve. Iron oxide powder ($Fe_2O_3 > 95\%$, Himedia, India) was supplied by Italmar chemical supply company (Thailand). Iron powder ($Fe > 96\%$) was purchased from a local supply store. Rice bran powder (chemical composition: P_2O_5 53.744wt.%, K_2O 17.316wt.%, SO_3 12.828wt.%, MgO 7.569wt.%, SiO_2 5.362wt.% and CaO 2.237wt.%) was obtained from a local grinding mill. As(V) and As(III) stock solutions (100 mg/L) were prepared by dissolving appropriate amount of $Na_2HAsO_4 \cdot 7H_2O$ and $NaAsO_2$ (Sigma Aldrich), respectively. NaCl, $NaNO_3$, $NaHCO_3$, Na_2CO_3, Na_2SO_4 and NaH_2PO_4 were used to prepare for anion solutions of chloride (Cl^-), nitrate (NO_3^-), bicarbonate (HCO_3^-), carbonate (CO_3^{2-}), sulfate (SO_4^{2-}) and phosphate (PO_4^{3-}), respectively. Moreover, NaOH and HCl were used for solution pH adjustment.

5.2.2 Adsorbent development

The porous pellet adsorbent was developed from mixing natural clay (NC), iron oxide powder (Fe_2O_3), iron powder (IP) and rice bran powder (RB) at a specific mass proportion with DI water. The ratios of NC:Fe_2O_3:IP were selected by the mixture design method and the mass proportion of RB was constantly kept at 15% of the total mass. The prepared powders were uniformly mixed with addition of water to form a paste. The paste was continually stirred and pressed into long cylindrical shape with 1-1.5 mm in diameter by a plastic syringe. The long pellet was cut into 1-2 mm in length, placed in clean crucibles, dried at 60˚C for 24 h, and further heated at 600˚C for 1 h in a muffle furnace to carbonize and produce pores. After cooling down, the finished product was kept in a dry and clean container for further experiments.

5.2.3 Mixture design and statistical analysis

Mixture design approach is a type of experimental design used for analyzing the relationships between mixture components and responses, and for determining the best proportions of mixture components to obtain a final product in accordance with the target (BahramParvar et al., 2015). The proportion of a component in the mixture must be between 0 and 1 and the sum of the proportion of all mixture components is equal to 1 (Rosales et al., 2015). In this study, a three component augmented simplex-centroid mixture design was used to formulate different mixtures of independent variables i.e., NC (X_1, wt.%), Fe_2O_3 (X_2, wt.%) and IP (X_3, wt.%), and to assess the relationship of the mixtures to the responses, As(V) and As(III) adsorption efficiency (Y_1 and Y_2, respectively). For the aspect of economy and being a binder, the amount of NC should be used more than others i.e., Fe_2O_3 and IP serving as active site providers to the adsorbent. Therefore, constraints on individual component were applied and selected to be 50%<X_1<90%, 5%<X_2<45%, and 5%<X_3<45% in the form of $X_1+X_2+X_3$=100%. Totally, ten different mixture design points were obtained and illustrated in Figure 5.1.

The general polynomial function of the mixture models is represented by the following equation (Scheffe, 1963):

$$Y_i = \sum_{i=1}^{q} a_i X_i + \sum \sum_{i<j}^{q} a_{ij} X_i X_j + \sum \sum_{i<j<k}^{q} \sum a_{ijk} X_i X_j X_k \qquad (5.1)$$

where Y_i represents the predicted responses; q is the number of components in the mixtures; X_i, X_j, X_k are the represented independent variables; and a_i, a_{ij}, a_{ijk} are the coefficient of regression models for the linear, binary and ternary mixture systems, respectively.
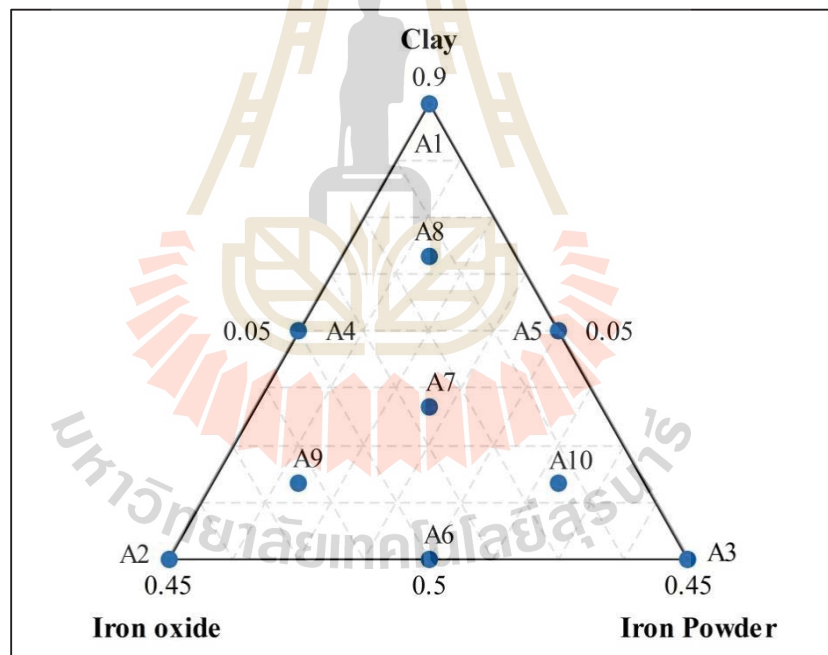
Figure 5.1 The overall design points based on the three-component augmented simplex-centroid design

Minitab statistical software (version 16.0, Minitab Inc., State College, PA) was used for designing the mixtures, analyzing the data, fitting the models and optimizing constituent proportions.

5.2.4 Batch adsorption study

Batch mode was employed to conduct adsorption experiments that were carried out at room temperature ($25 \pm 1°C$) in acid washed 60 mL polyethylene bottles with an agitation speed of 150 rpm on a horizontal mechanical shaker (New Brunswick Scientific, Canada). For kinetic study, a series of adsorption between 10 g/L of adsorbent and 10 mg/L of either As(V) or As(III) solution (pH = 7±0.1) was prepared and shaken for 0 to 72 h. While shaking, samples were taken at preset time intervals. Isotherm experiments were performed with As(V) or As(III) concentration ranging from 0.5 to 100 mg/L. Effect of solution pH was conducted by varying pH from 3 to 11. Effect of coexisting anions were investigated using 10 g/L of adsorbent and 10 mg/L As(V) or As(III) solution (pH = 7±0.1) containing 0.1, 1 and 10mM of Cl^-, NO_3^-, HCO_3^-, CO_3^{2-}, SO_4^{2-} and PO_4^{3-}. The samples were filtered through 0.22 μm syringe filters and the filtrates were acidified with 1%v/v concentrated HNO_3, kept at 4°C and analyzed for As(V) or As(III) concentration within 24 h. The adsorption capacity and efficiency (Q_e(mg/g) and R(%), respectively) were determined by equations defined as (Chutia et al., 2009):

$$Q_e = \frac{(C_o - C_e)}{M} \times V \tag{5.2}$$

$$R(\%) = \frac{(C_o - C_e)}{C_o} \times 100 \tag{5.3}$$

where C_o and C_e are the initial and equilibrium As(V) or As(III) concentration, respectively (mg/L), V is the volume of As(V) or As(III) solution (L), and M is the mass of adsorbent (g).

5.2.5 Adsorbent regeneration and arsenic leaching test

In order to observe the potential reuse of the adsorbent, three consecutive regeneration cycles were conducted. The adsorbed adsorbent of 10 g/L was dispersed in 25 mL of 1M NaOH and shaken for 24 h. The desorbed adsorbent was washed several times

with DI water and then reused to remove 10mg/L of As(V) or As(III). Leaching of either As(V) or As(III) from the adsorbed adsorbent was examined using the US EPA Toxicity Characteristic Leaching Procedure (TCLP). The adsorbed adsorbent was mixed with the TCLP extraction fluid (5.7 mL of glacial acetic acid added to 500 mL of DI water and diluted to 1L, pH 2.91) at a ratio of 1:20 and shaken with a mechanical shaker for 18 ± 2 h. The samples were filtered with 0.22 μm syringe filters and the filtrates were acidified and analyzed for As (V) or As(III) concentration.

5.2.6   Analytical methods

As(V) or As(III) concentration was measured by ICP-OES (Optima 8000DV, PerkinElmer) using a wavelength of 193.7 nm. Elemental composition analysis was carried out with Energy Dispersive X-ray Fluorescence (ED-XRF, XGT-5200 X-ray Analytical Microscope, HORIBA Ltd., Japan). The surface area, total pore volume and average pore diameter were obtained from the Brunauer-Emmett-Teller (BET) method using the BET analyzer (BELSORP Mini II, BEL Inc., Japan). X-ray diffraction (XRD) for mineralogical phases was performed using the Bruker XRD (D2 PHASER). The morphological features of adsorbent before and after adsorption were examined by a scanning electron microscope (SEM, JSM-6010LV, JEOL, Japan) and the Fourier transform infrared spectra (4000-400 cm^{-1} at a resolution of 4 cm^{-1}) was recorded using a PerkinElmer spectrum GX spectrophotometer (FT-IR) instrument. The point of zero charge (pH_{pzc}) was evaluated by the equilibrium method (Su et al., 2011).

5.3   Results and Discussion

5.3.1   Model fitting and analysis of variance

The detail of the experimental mixture design points and the experimental results of the responses are presented in Table 5.1. Each response was measured into two

sets, Measurement 1 (M1) and Measurement 2 (M2) to minimize variance and improve the simulation for obtaining a better model.

Table 5.1 Experimental design points and obtained responses, R(%)-As(V) and R(%)-As(III) measured in two sets (M_1 and M_2), for the corresponding mixtures

Mixture	Natural Clay (X_1)	Iron Oxide (X_2)	Iron Powder (X_3)	R(%)-As(V) (Y_1)		R(%)-As(III) (Y_2)	
				M1	M2	M1	M2
A1	0.9	0.05	0.05	32.99	33.71	15.40	15.29
A2	0.5	0.45	0.05	67.73	67.86	84.26	82.43
A3	0.5	0.05	0.45	93.02	93.17	93.07	92.13
A4	0.7	0.25	0.05	53.14	51.46	47.89	43.54
A5	0.7	0.05	0.25	85.99	83.10	85.80	84.98
A6	0.5	0.25	0.25	91.26	91.73	92.63	92.66
A7	0.633	0.183	0.183	65.21	67.19	65.40	68.47
A8	0.766	0.116	0.116	58.20	59.59	51.90	54.69
A9	0.566	0.316	0.116	72.77	72.98	81.03	81.15
A10	0.566	0.116	0.316	94.33	94.50	94.13	93.01

Models with linear, quadratic and special cubic degrees were applied to predict the independent variables and the responses. Run by the Minitab software, statistical parameters such as standard deviation (S), predicted sum of squares (PRESS), and predicted regression coefficient (R^2) were obtained for linear (S=7.224, PRESS=1333.0, R^2=0.8145), quadratic (S=4.466, PRESS=437.3, R^2=0.9391), and special cubic models (S=3.221,

PRESS=249.9, R^2=0.9652) in case of the As(V) response, and for linear (S=9.907, PRESS=2424.9, R^2=0.7973), quadratic (S=4.331, PRESS=389.7, R^2=0.9674), and special cubic models (S=3.831, PRESS=358.5, R^2=0.9700) in case of the As(III) response. The model with lower standard deviation and predicted sum of squares and higher predicted regression coefficient is a better one to predict the response data (Abdullah and Chin, 2010; Rao and Baral, 2011). Thus, special cubic model was the most suitable to fit the experimental data of both responses.

The analysis of variance (ANOVA) for the responses was evaluated based on 95% confidence level and p value was used to determine the significance of each component or the combination effect (Table 5.2). The special cubic model containing linear, two-component and three-component interactions is statistically significant for both responses (p <0.001). In case of As(V) response, all terms were significant (p <0.05). The interactions of components: X_1X_2, X_1X_3, X_2X_3 and $X_1X_2X_3$ (p value of 0.027, <0.001, 0.001 and 0.003, respectively) had a significant effect. The interaction of X_1X_3 provided the highest significant effect due to its lowest p value. In case of As(III) response, component interaction X_1X_2, X_1X_3, X_2X_3 and $X_1X_2X_3$ influenced the response with p value of 0.534, <0.001, 0.045, and 0.045, respectively. Thus, X_1X_2 showed an insignificant effect and X_1X_3 provided the most significant influence on the As(III) removal efficiency.

The polynomial equations of the selected models for both responses can be expressed as follow:

$$Y_1 = 2X_1 - 18X_2 - 202X_3 + 264X_1X_2 + 762X_1X_3 + 2422X_2X_3 - 4258X_1X_2X_3$$

with $R^2 = 0.9652$ (5.4)

$$Y_2 = -24X_1 + 145X_2 - 266X_3 + 944X_1X_3 + 1637X_2X_3 - 3005X_1X_2X_3$$

with $R^2 = 0.9700$ (5.5)

Table 5.2   Analysis of variance for all responses

Response	Source	DF	Seq SS	Adj SS	Adj MS	F	p value
As(V)	Regression	6	7050.42	7050.416	1175.069	113.22	<0.001
	Linear	2	6298.05	218.571	109.285	10.53	0.002
	Quadratic	3	608.03	637.744	212.581	20.48	<0.001
	X_1X_2	1	8.67	64.158	64.158	6.18	0.027
	X_1X_3	1	508.00	534.229	534.229	51.48	<0.001
	X_2X_3	1	91.35	167.741	167.741	16.16	0.001
	Special cubic	1	144.34	144.336	144.336	13.91	0.003
	$X_1X_2X_3$	1	144.34	144.336	144.336	13.91	0.003
	Residual error	13	134.92	134.919	10.378		
	Total	19	7185.34				
As(III)	Regression	6	11774.9	11774.89	1962.482	133.71	<0.001
	Linear	2	10297.0	737.51	368.754	25.12	<0.001
	Quadratic	3	1406.0	1442.18	480.727	32.75	<0.001
	X_1X_2	1	57.1	5.99	5.993	0.41	0.534
	X_1X_3	1	1339.6	819.58	819.579	55.84	<0.001
	X_2X_3	1	9.3	76.58	76.578	5.22	0.040
	Special cubic	1	71.9	71.86	71.863	4.90	0.045
	$X_1X_2X_3$	1	71.9	71.86	71.863	4.90	0.045
	Residual error	13	190.8	190.80	14.677		
	Total	19	11965.7				

5.3.2   Residual graphs

The residual values are used to construct normal probability plots for evaluating the normal distribution of the data. The data are considered as normal distribution when the plotted points are close to the fitted straight line (Rostamiyan et al., 2014). Apparently, the plotted points for both cases seem closer to the distribution line, indicating the data were normally distributed (Figure 5.2).
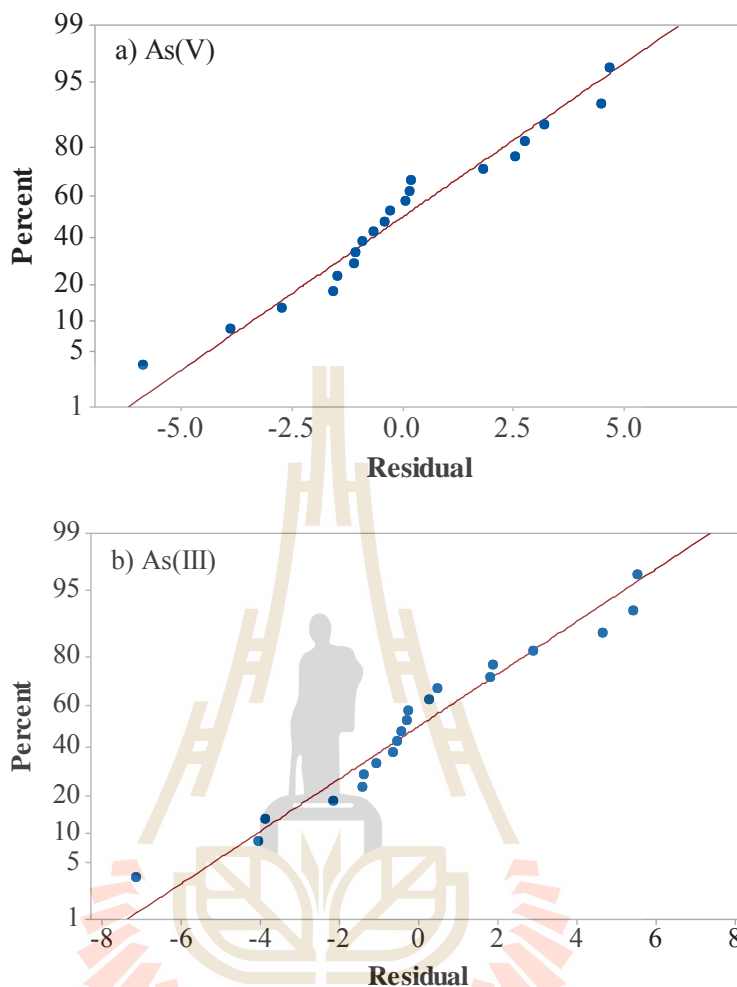
Figure 5.2   Normal probability plots for a) As(V) response and b) As(III) response

5.3.3   Contour plots of the responses

Figure 5.3 illustrates the mixture contour plots of As(V) and As(III) responses resulting from the effect of the component interactions. A contour plot shows a detail effect on a certain response value by various establishing interactions of the mixture components in a two-dimensional view. The different desirable values of the responses were obtained and varied by changing in color. The darker color of the regions represents higher adsorption efficiency of the responses.
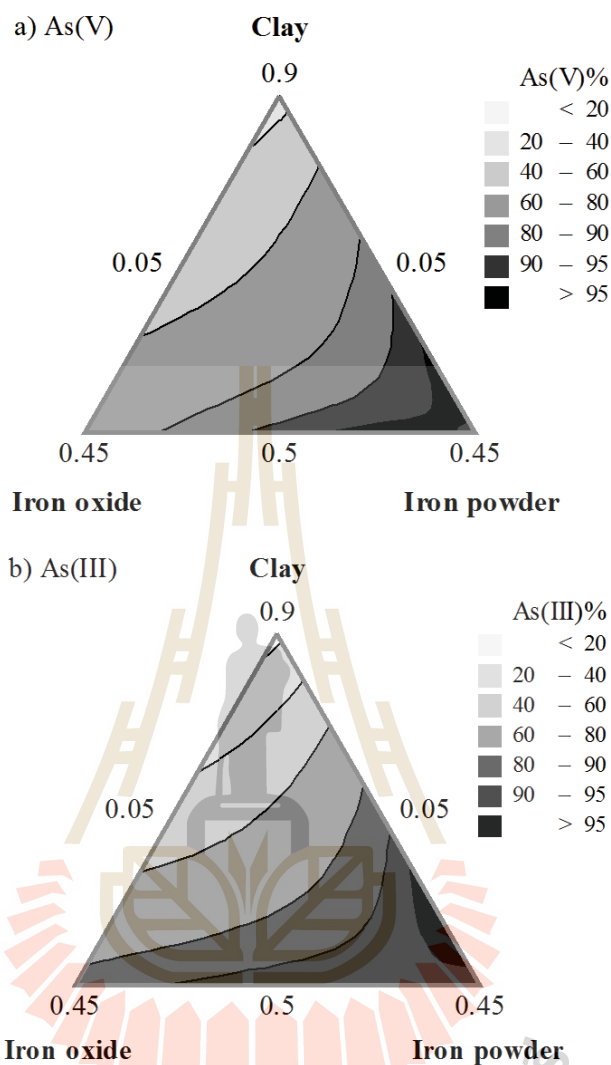
Figure 5.3   The mixture contour plots of the responses: a) As(V) and b) As(III)

For both responses, the maximum removal efficiency occurred toward the edge of Fe_2O_3 and IP with IP as vertex. This implies that adding Fe_2O_3 and IP proportion into the mixture improved both As(V) and As(III) adsorption efficiency to certain level.

5.3.4 Mixture proportion optimization and model validation

Response optimization involves defining independent variable settings that collaboratively produce optimized responses, and its satisfactory is measured by the composite desirability (Rao and Baral, 2011). The desirability is scaled from 0.0 (undesirable) to 1.0 (very desirable) (Shahamirifard et al., 2016). In the present study, the

response optimization was processed using Response Optimizer of Minitab that identifies a combination of independent variables (NC, Fe_2O_3 and IP) to jointly optimize adsorption efficiency of As(V) and As(III). Figure 5.4 presents the optimization plot of independent variables affecting the predicted As(V) and As(III) adsorption efficiency. Independent variable settings on the plot could be adjusted by moving the vertical red line to obtain more desirable predicted responses. To obtain high composite desirability with a high comparable adsorption efficiency of both As(V) (91.3217%) and As(III) (91.8716%) by using less amount of iron oxide or iron powder as possible, the ideal mixture proportion of the materials is 0.5215 of NC, 0.1922 of Fe_2O_3 and 0.2863 of IP. The predicted As(III) desirability, As(V) desirability and composite desirability were found to be d = 0.93048, d = 0.91826 and D = 0.9243, respectively, which were close to 1, indicating that the selected mixture ratio has a significant positive effect on maximizing the As(V) and As(III) adsorption efficiency (Rao and Baral, 2011).
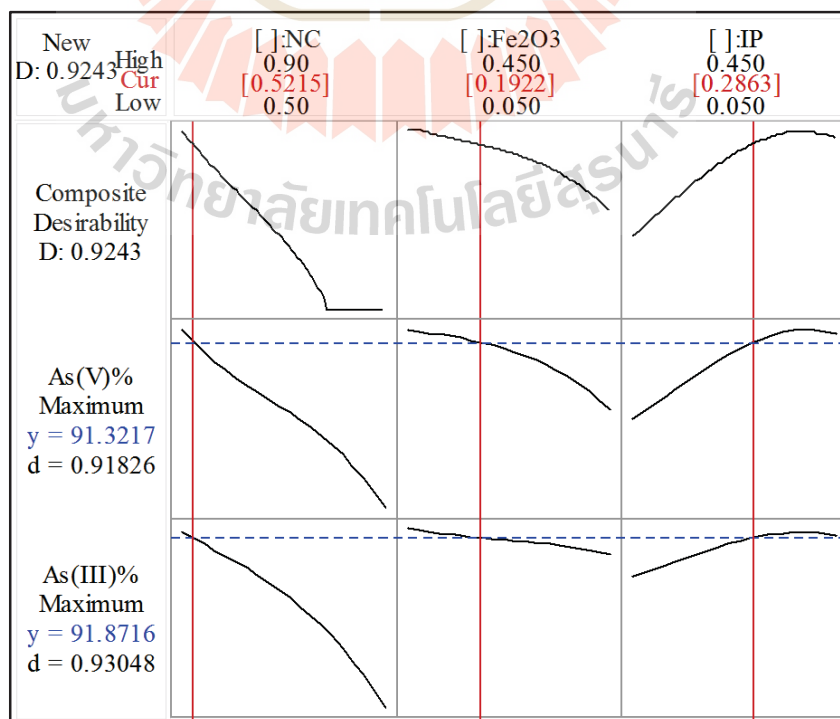
Figure 5.4   The mixture optimization plot for As(V) and As(III) responses

The optimum components were used to develop the porous pellet adsorbent for the As(V) or As(III) adsorption to validate the model. The results indicated that the As(V) and As(III) removal efficiency were 91.40% and 92.57%, respectively, comparable enough to the predicted values, suggesting that the predicted models were valid and adequate.

5.3.5 Characterization of the developed adsorbent

The BET surface area, total pore volume and mean pore diameter of the porous pellet adsorbent were 18.267 m^2/g, 0.0916 cm^3/g and 20.063 nm, respectively. The mean pore diameter within 2 to 50 nm suggested that the adsorbent is mesoporous according to the pore classification of the International Union of Pure and Applied Chemistry (Kuila and Prasad, 2013). Regardless the presence of oxygen, elemental composition analyzed by XRF indicated that the main constituent elements of porous pellet adsorbent were Si (21.829%), Al (7.251%), and Fe (25.780%) (Table 5.3). Apparently, the amount of iron element of the porous adsorbent has dramatically increased approximately 7 times compared to that of natural clay.

Table 5.3 Chemical composition (wt.%) of natural clay and porous pellet adsorbent analyzed by XRF

Composition (wt.%)	Si	Al	Fe	K	Ca	Ti	O
Natural clay	31.254	13.366	3.696	1.232	0.373	0.624	49.835
Porous pellet	21.829	7.251	25.780	0.626	0.308	0.342	43.246

Figure 5.5 shows the XRD pattern of the porous pellet adsorbent. The mineral constituents mainly consisted of quartz and hematite, as well as illite-montmorillonite and iron. The

main crystalline phases of quartz and hematite were contributed by natural clay and iron oxide, respectively.
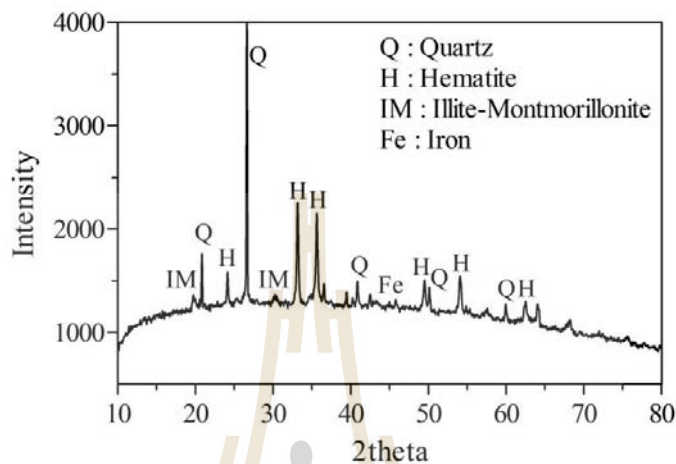
Figure 5.5 XRD pattern of the iron mixed porous pellet adsorbent

Figure 5.6 shows the surface morphological features of the adsorbent before and after adsorption. The porous pellet adsorbent has a cylinder shape with numerous pores surrounding the surface, developed by carbonization of rice bran (Figure 5.6a). The scattered rough surface structure was observed before adsorption (Figure 5.6b). This indicated the spreading of iron oxide and iron powders to form heterogeneity on the surface. After adsorption of As(V) and As(III) (Figure 5.6c and 5.6d, respectively), similar morphology of the surface were observed. The surface became smoother, consisted of small pores and seemed to be layered by various sizes of flat sheet. This is probably due to the binding between arsenic and iron species on the layer-structure of clay.
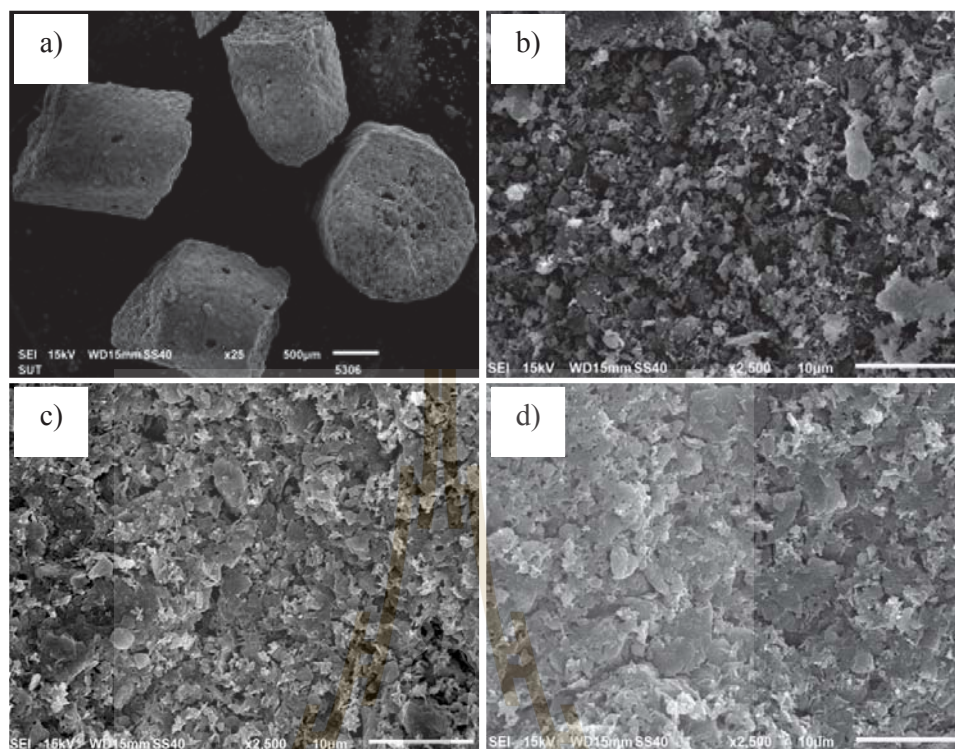
Figure 5.6   SEM images of a) shape of porous pellet (x25), b) surface of porous pellet before adsorption, and porous pellet after adsorption c) As(V) and d) As(III)

The FTIR spectra of the adsorbent before and after As(V) and As(III) adsorption showed that the major peak bands were observed in the wavenumber range from 400 to 1200 cm^{-1} (Figure 5.7). The peak band of 1029.94 cm^{-1} and 800.42cm^{-1} was assignable to the stretching vibration of Si-O-Si group and Si-O deformation (Nayak and Singh, 2007; Petala et al., 2013; Tandon et al., 2013). The band of 692.41cm^{-1} corresponds to the spectrum for iron oxide (Fe_2O_3) (Li et al., 2010). The peak bands of 524.62 and 437.82 cm^{-1} could be assigned to the vibration of Si-O-Al and Fe-O groups, respectively (Chen et al., 2011; Li et al., 2016). After As(V) and As(III) adsorption, reduction of stretching the peak bands, increase of transmittance percent of corresponding bands, and no presence of new peak bands were observed. This could be reasoned by As(V) and As(III) in the solution mostly adsorbed on the surface of the adsorbent (Chen et al., 2011).
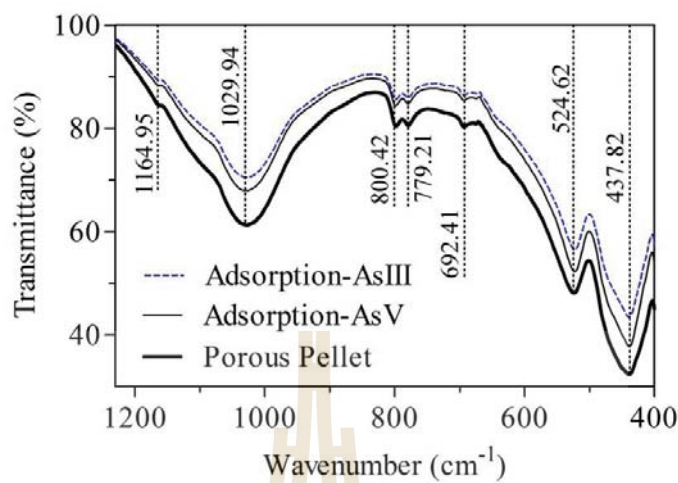
Figure 5.7 FTIR spectrum of porous pellet before and after As(V) and As(III) adsorption

5.3.6 Adsorption kinetics

Kinetic study illustrates the chemical rate of adsorption process between adsorbate and adsorbent by observing the speed of a chemical reaction until reaching its equilibrium in a particular amount of time (Sen Gupta and Bhattacharyya, 2011). Adsorption performance of As(III) and As(V) onto porous pellet adsorbent dependent on time along with the fitting kinetic models showed a similar trend, which an initial wide availability of active sites provides a rapid uptake first and the filling up of active sites slows down and stabilizes the adsorption process within 72 h (Figure 5.8).

Kinetic experimental data were fitted to the pseudo-first order and pseudo-second order models defined as (Far et al., 2012; Salameh et al., 2010):

Pseudo-first order: $\quad Q_t = Q_e \left(1 - e^{-k_1 t}\right)$ $\qquad$ (5.6)

Pseudo-second order: $\quad Q_t = \dfrac{k_2 Q_e^2 t}{1 + k_2 Q_e t}$ $\qquad$ (5.7)
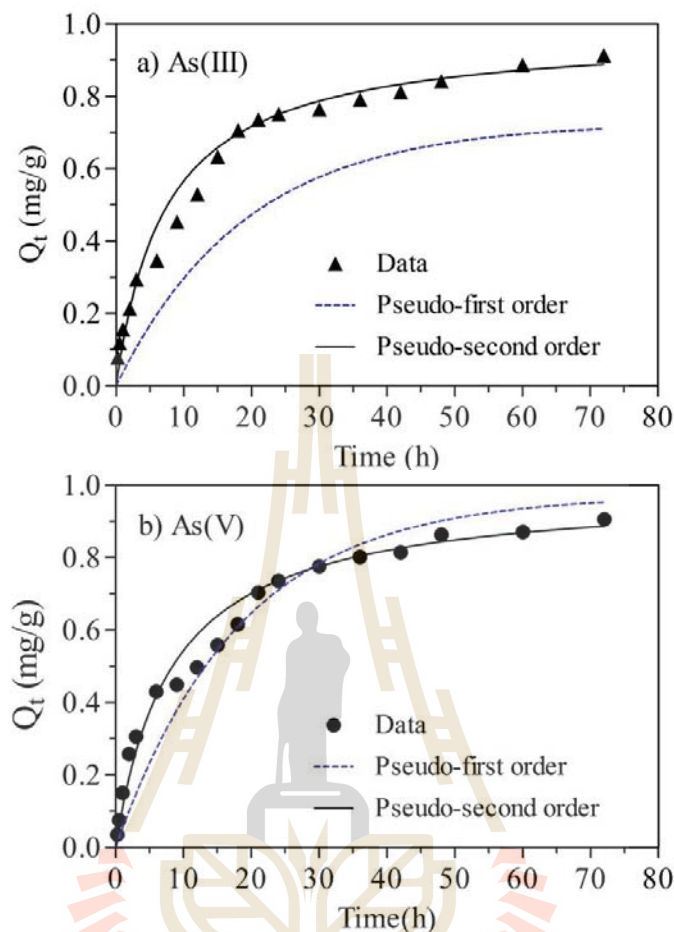
Figure 5.8   Time dependent for a) As(III) and b) As(V) adsorption onto the adsorbent

where Q_t (mg/g) is the amount of As(V) or As(III) adsorbed at time t; Q_e (mg/g) is the amount of As(V) or As(III) adsorbed at equilibrium time; k_1 (h^{-1}) is the rate constant of the pseudo-first order model; k_2 (g/mg.h^{-1}) is the rate constant of the pseudo-second order model.

The correlation coefficients (R^2) of the pseudo-second order model (As(V): $R^2 = 0.9919$; As(III): $R^2 = 0.9901$) were higher than those of the pseudo-first order model (As(V): $R^2 = 0.9706$; As(III): $R^2 = 0.9824$) and the calculated equilibrium adsorption capacity (As(V): 0.987 mg/g; As(III): 0.977 mg/g) was comparable enough to the experimental adsorption capacity (As(III): 0.914 mg/g; As(V): 0.906 mg/g) (Table 5.4).

Table 5.4   Kinetic parameters of As(III) and As(V) uptake onto the adsorbent

As	$Q_{e,exp}$ (mg/g)	Pseudo-first order			Pseudo-second order		
		Q_e(mg/g)	k_1(h^{-1})	R^2	Q_e(mg/g)	k_2(g/mg.h^{-1})	R^2
As(III)	0.914	0.727	0.0526	0.9706	0.977	0.1408	0.9901
As(V)	0.906	0.972	0.0548	0.9824	0.987	0.1242	0.9919

Therefore, it is concluded that the adsorption kinetics for both As(V) and As(III) could be better described by the pseudo-second order rate model. This implied that the both As(III) and As(V) adsorption onto the adsorbent could be a chemisorption (Qi et al., 2015). From the pseudo-second order model, the initial adsorption rate (h) calculated by h = k_2 Q_e^2 for As(V) and As(III) were 0.134 mg/g.h^{-1} and 0.121 mg/g.h^{-1}, respectively, indicating that the adsorbent removed As(III) faster than As(V).

5.3.7   Effect of initial solution pH

As(V) adsorption capacity gradually decreased with the pH range from 3 to 7 and significantly decreased when pH was more than 7 (Figure 5.9). For As(III) adsorption, the removal capacity was not remarkably changed over the pH range from 3 to 9. Both As(V) and As(III) adsorption dramatically declined as pH raised above 9. Arsenic speciation and the characteristic of adsorbent surface importantly influence the adsorption capacity over various solution pH. In water, As(V) mainly exists in the form of H_3AsO_4 at pH less than 2.2, $H_2AsO_4^-$ at pH between 2.2 and 6.98, $HAsO_4^{2-}$ at pH between 6.98 and 11.5, and AsO_4^{3-} at pH above 11.5 (Chang et al., 2010). As(III) species occur as: H_3AsO_3 (pH<9.2), $H_2AsO_3^-$ (9<pH<12), $HAsO_3^{2-}$ (12<pH<13), and AsO_3^{3-} (pH>13) (Mohan and Pittman, 2007). The surface of the adsorbent was more positively charged for pH<pH$_{pzc}$ and predominated the negative charge for pH>pH$_{pzc}$ (Chang et al., 2010). The porous pellet adsorbent exhibited the point of zero charge (pH$_{pzc}$) of 7.50.
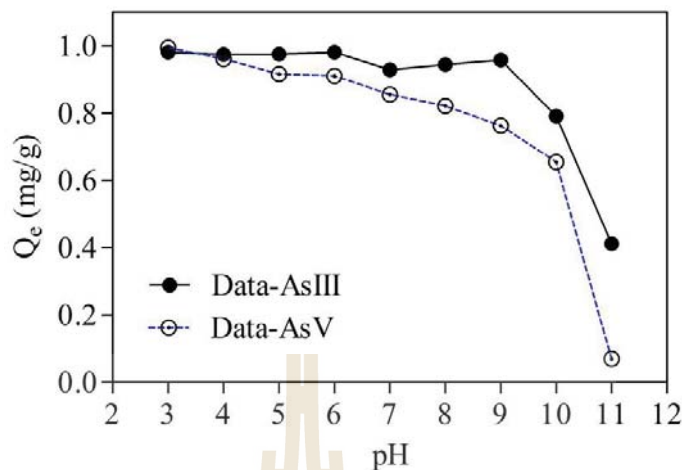
Figure 5.9   Effect of initial solution pH for As(III) and As(V) adsorption

This indicated that the unfavorable electrostatic interaction or the electrical repulsion between the adsorbent and the adsorbate could result in low As(V) and As(III) adsorption capacity at pH>9.

5.3.8 Isotherm studies

Isotherm study was conducted to determine the characteristic of the adsorption and the maximum adsorption capacity of the adsorbent. The isotherm models such as the Langmuir, Freundlich, and Sips models were applied to predict the equilibrium isotherm data. The isotherm models were expressed as follow (Foo and Hameed, 2010; Jung and Ahn, 2016):

Freundlich:
$$Q_e = K_F C_e^{1/n} \tag{5.8}$$

Langmuir:
$$Q_e = \frac{Q_{max} K_L C_e}{1 + K_L C_e} \tag{5.9}$$

Sips:
$$Q_e = \frac{Q_m K_{L-F} C_e^{1/n}}{1 + K_{L-F} C_e^{1/n}} \tag{5.10}$$

where C_e (mg/L) is the As(V) or As(III) concentration at equilibrium; Q_e (mg/g) is the amount of As(V) or As(III) adsorbed at equilibrium per unit mass of the adsorbent; Q_{max}

(mg/g) and Q_m(mg/g) are the maximum adsorption capacity based on the Langmuir and Sips models, respectively; K_L (L/mg), K_F ($mg^{1-1/n}L^{1/n}$/g), K_{L-F} (L/mg) are the Langmuir constant, Freundlich constant, and Langmuir-Freundlich constant, respectively. 1/n is the heterogeneity factor. Sips model or Langmuir-Freundlich model is a combination of Langmuir (assuming a monolayer adsorption onto a homogenous surface) and Freundlich (assuming a multilayer adsorption onto a heterogeneous surface) (Jung and Ahn, 2016; Ouadjenia-Marouf et al., 2013). Experimental isotherm data and the fitting models are illustrated in Figure 5.10.
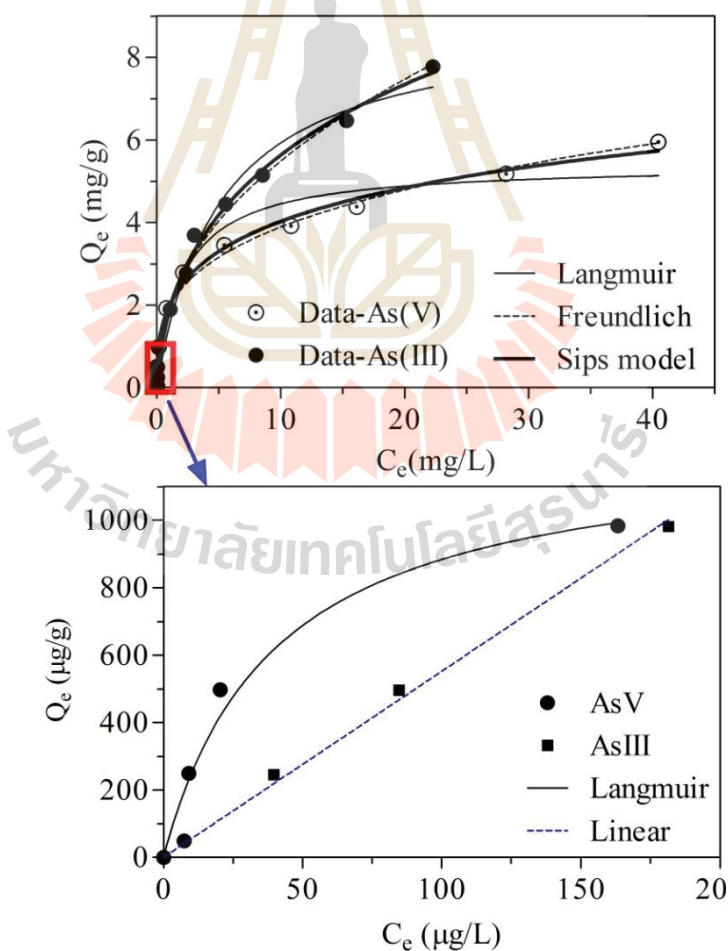
Figure 5.10   Isotherm study of As(III) and As(V) adsorption onto the adsorbent

Isotherm parameters such as the maximum adsorption capacity, constants of the fitting models, and correlation coefficient (R^2) were calculated from non-linear forms of isotherm models (Table 5.5).

Table 5.5 Isotherm parameters of As(III) and As(V) uptake onto the adsorbent

As	Freundlich			Langmuir			Sips (Langmuir-Freundlich)			
	1/n	K_F	R^2	Q_{max} (mg/g)	K_L	R^2	Q_m (mg/g)	K_{L-F}	1/n	R^2
As(III)	0.446	1.963	0.989	8.944	0.196	0.978	19.06	0.110	0.579	0.992
As(V)	0.302	1.940	0.989	5.403	0.467	0.948	13.33	0.173	0.398	0.993

The correlation coefficient (R^2) of the Sips model was higher than that of the Langmuir and Freundlich for both As(V) and As(III) adsorption. This implied that the isotherm experimental data fit well to the Langmuir-Freundlich or Sips model, suggesting that As(V) or As(III) adsorption occurred as a monolayer on heterogeneous surface of the adsorbent (Chen et al., 2012b). Obtained from the Sips model, the saturated removal capacities of As(V) and As(III) were 13.33 mg/g and 19.06 mg/g, respectively. On the other hand, the experimental isotherm data at low equilibrium concentration (<200 µg/L), as shown in Figure 5.10, was used to evaluate the adsorption capacity at low arsenic concentration. The Langmuir and linear models were used to fit the data of As(V) and As(III), respectively. And, the obtained model equations could be expressed as follow:

For As(V):
$$Q_e = \frac{31.05 \cdot C_e}{1 + 0.0251 \cdot C_e} \qquad R^2 = 0.9567 \qquad (5.10)$$

For As(III):
$$Q_e = 5.519 \cdot C_e \qquad R^2 = 0.9962 \qquad (5.11)$$

Thus, the adsorption capacities of As(V) and As(III) at equilibrium concentration of 10 µg/L were 248.20 µg/L and 55.19 µg/L, respectively.

The characteristic of the adsorption can be determined through either the value of a dimensionless constant separation factor (R_L) or the Freundlich constant ($1/n$). The separation factor was calculated by $R_L = 1/(1+K_LC_o)$, where C_o (mg/L) is the initial As(V) or As(III) concentration. The adsorption process is irreversible ($R_L=0$), favorable ($0<R_L<1$), linear ($R_L=1$) and unfavorable ($R_L>1$) (Khan and Khan, 2015). Similarly, the magnitude of the adsorption intensity, $1/n$, can suggest the type of isotherm from the Freundlich model. The adsorption is favorable when $0<1/n<1$, irreversible when $1/n=1$ and unfavorable when $1/n>1$ (Fufa et al., 2014). The values of $1/n$ for As(III) and As(V) were 0.446 and 0.302, respectively. Plus, for the studied initial concentration range, the R_L values for As(III) and As(V) adsorption were in the range of 0.05-0.91 and 0.02-0.81 (within 0 to 1). This showed that the adsorbent expressed a favorable adsorption toward As(V) or As(III). Noticeably, higher initial arsenic concentration tends to lead the adsorption to an irreversible isotherm and the adsorption approaches a linear isotherm at lower initial arsenic concentration.

5.3.9 Effect of coexisting anions

A similar trend of the influence of inorganic anions introduced separately and jointly on As(III) and As(V) adsorption was observed (Figure 5.11). The presence of Cl^- over the studied concentration range showed no significant effect on the adsorption. The anions NO_3^- and SO_4^{2-} at higher concentrations could decrease the efficiency to 82.76% and 80.46%, respectively for As(III) and 78.31% and 77.64%, respectively for As(V). Increasing the concentration of CO_3^{2-} and HCO_3^- could reduce the adsorption efficiency to 69.01% and 35.08%, respectively for As(III) and 64.24% and 31.12%, respectively for As(V). It was also observed that the presence of PO_4^{3-} strongly inhibited the removal of As(III) and As(V). The As(III) and As(V) efficiency decreased to 73.9% and 71.33%, respectively for 0.1mM PO_4^{3-} and it could be sharply reduced to 13.35% and 10.41%, respectively for 10mM PO_4^{3-}.
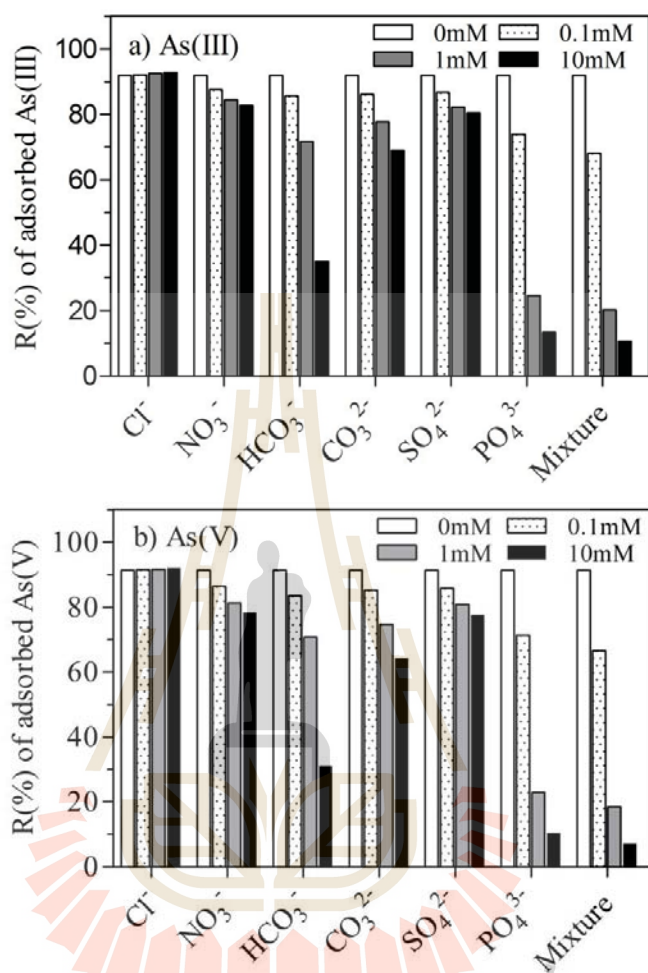
Figure 5.11   Effect of coexisting anions on the removal of a) As(III) and b) As(V)

The decrease observed for the mixture (combining all anions in the same solution) and for the presence of PO_4^{3-} was slightly different, which could be due to the capacity of PO_4^{3-} to surpass the buffering abilities of the other anions (Fufa et al., 2014). The reduction of adsorption efficiency when introducing the coexisting anions could be caused by the competition for active sites on the surface of the adsorbent. The remarkably negative influence of PO_4^{3-} could be explained by the reason that phosphate has similar chemical properties to arsenic and easily attaches to iron species by forming an inner-sphere complex compared to arsenic (Maliyekkal et al., 2009; Hsu et al., 2008).

5.3.10 Adsorbent regeneration and arsenic and iron leaching test

The ability of the adsorbent to be regenerated and reused for As(III) and As(V) adsorption is presented in Figure 5.12.
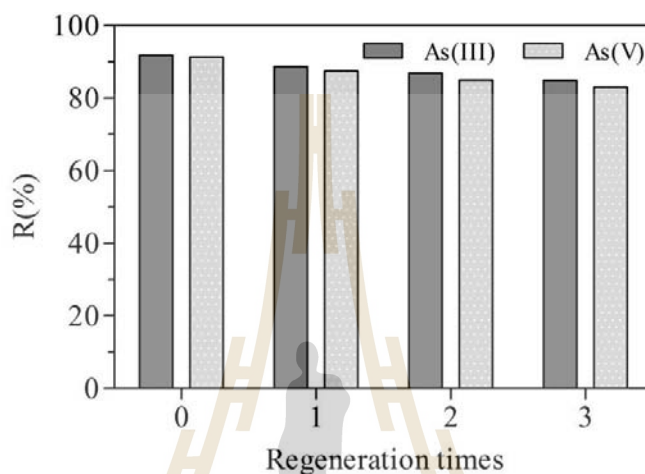
Figure 5.12   Reuse of the adsorbent for As(III) and As(V) removal

Apparently, the adsorption efficiency of As(III) and As(V) gradually decreased when the number of regeneration cycle increases. However, after the third regeneration time, the adsorbent could still maintain its well adsorption performance by being able to remove 84.94% and 83.06% for As(III) and As(V), respectively. In addition, the adsorbent expressed insignificant loss or no physical crush of the particle size. Thus, the adsorbent could be reused effectively for several times through desorption of NaOH treatment.

The toxicity characterization leaching procedure was applied to categorize the adsorbed adsorbent as either hazardous or non-hazardous material to be disposed. The US EPA recommends the permissible limit of 5mg/L for the arsenic concentration in the leachate. The result indicated that As(III) and As(V) concentrations in the leachate were 0.54mg/L and 0.73mg/L, respectively, which were much lower than that of the limit.

Therefore, the spent adsorbent was non-hazardous material and could be safely disposed as a solid waste.

There is a possibility of the leaching of iron from the adsorbent matrix during the adsorption. The concentration of iron in the solution (pH = 7 ± 0.1) was found to be 0.16 mg/L, which is within the permissible limit (0.3 mg/L) prescribed for drinking water. Therefore, it can be concluded that it is safe to use the iron-mixed clay pellet as adsorbent without the risk of iron contamination.

5.4   Conclusion

Widely available natural clay could be easily used to bind iron oxide and iron powder to be the effective adsorbent for efficiently removing arsenate and arsenite from water. The augmented simplex-centroid mixture design method was a successful and useful tool to optimize the proportion of the constituent materials of the adsorbent. In the batch adsorption, the optimized adsorbent expressed a favorable adsorption toward both arsenate and arsenite even though the certain extent reduction of the efficiency occurred in the presence of some anions, especially phosphate. The adsorbent maintained high adsorption efficiency after several times of regeneration, was easily separated from the aqueous solution, and was non-hazardous solid waste after adsorption. In addition, regarded the low cost and availability of raw materials, the adsorbent could be cost-effective for arsenic removal from water.

CHAPTER VI

COEXISTING ARSENATE AND ARSENITE ADSORPTION FROM WATER USING IRON MIXED CLAY PELLET: OPTIMIZATION BY RESPONSE SURFACE METHODOLOGY

6.1   Introduction

Arsenic is a global well-known problematic contaminant and considered as a highly toxic and carcinogenic element by some international agencies, i.e., IARC and USEPA (Bhatia et al., 2014). Generally, a pretreatment is applied for converting As(III) to As(V) before elevated As-polluted water is treated to a safe or permissible level. However, the application of pretreatment has some drawbacks in term of time consuming, cost-addition and possibility of generating toxic by-products. Therefore, it is significant to use a proper removal technique that can simultaneously remove As(III) and As(V). The study of treating the aqueous solution with coexisting arsenate and arsenite, As(III+V), is still limited.

The main operational parameters affecting the adsorption efficiency in a batch experiment include contact time, adsorbent dosage, initial pH, and initial concentration. The interaction and optimization of those variables are normally investigated by a statistical technique like response surface methodology (RSM). RSM is considered as one of the most efficient statistical tools applied to design an experiment and simulate a model to evaluate the interactive influences of multiple factors and optimize the conditions (Roosta et al., 2014).

The present study aims to use porous pellet adsorbent to investigate the optimization process of batch adsorption parameters for removing arsenate and arsenite coexisting in aqueous solutions. The main characteristics of the adsorbent were evaluated by various methods. Central composite design (CCD) under RSM was used as a main technique for this optimization process. The Pareto analysis was applied to obtain the variable effects on the adsorption efficiency in term of percentage.

6.2   Materials and Methods

6.2.1   Preparation and characterization of adsorbent

Porous pellet adsorbent was developed by mixing natural clay, iron oxide, iron powder and rice bran. Natural clay (NC) with particle size of <75 μm was collected from Dankwian, Thailand. Iron oxide powder (Fe_2O_3, analytical grade, Himedia, India) was supplied by a chemical company. Iron powder (IP, industrial grade) and rice bran powder (RB) were purchased from a local supply store. The mixture was carried out at a ratio of 52.15% (NC):19.22% (Fe_2O_3):28.63% (IP), and 15% of RB was added for pore development. The detail procedure to define the optimal proportion is mentioned in another work (Te et al., 2017b). The mixture was homogeneously mixed by adding deionized water slowly to produce a paste form. The paste was strongly stirred by hand for about 5-10min and dried at 104±1°C for 24 h, and further heated at 600°C for 2-3 h in a muffle furnace to carbonize the rice bran. After cooling down, the product was prepared for desired particle size of 0.6-1.12mm, and stored properly in a plastic container for further experiments.

Brunauer-Emmett-Teller (BET) method was employed to determine surface area, total pore volume, and mean pore size of the adsorbent using N_2 adsorption-desorption isotherm data at 77 K (BELSORP Mini II, BEL Inc., Japan). Prior to the analysis, the adsorbent sample was outgassed under presence of N_2 at 60°C for 24 h. Surface

morphological features were obtained from a scanning electron microscope (SEM, JSM-6010LV, JEOL, Japan). SEM was coupled with Energy Dispersive X-ray (EDX) to perform elemental composition analysis.

6.2.2 Adsorption experiments

The 200 mg/L stock solution [As(III+V), 50%+50%] was prepared from dissolving appropriate amount of $Na_2HAsO_4 \cdot 7H_2O$ and $NaAsO_2$ (Sigma Aldrich, USA) together into deionized water. Batch mode study was employed to conduct adsorption experiments. The experiments were carried out at room temperature ($25 \pm 1°C$) in acid washed 60 mL polyethylene bottles with an agitation speed of 150 rpm on a horizontal mechanical shaker (New Brunswick Scientific, Canada). The contact time, adsorbent dose and adsorbate initial concentration were varied from 24 to72h, 0 to 20g/L and 0.25 to 4.25mg/L, respectively. The initial solution pH was adjusted with 0.1M HCl or NaOH to vary from 3 to 11. All samples were filtered through 0.45 μm syringe filters, acidified with 1%v/v HNO_3 and kept at 4°C until the adsorbate analysis within 24 h. Total arsenic concentration was measured by inductively coupled plasma-optical emission spectrometry (ICP-OES) (Optima 8000, PerkinElmer, USA) using a wavelength of 193.7 nm. The adsorption efficiency (A%) was determined by the following equation:

$$A\% = \frac{(C_o - C_e)}{C_o} \times 100 \tag{6.1}$$

where C_o and C_e (mg/L) are the initial and equilibrium adsorbate concentration.

6.2.3 Experimental design and data analysis

Central composite design (CCD) under (RSM) was used for investigation the individual and interaction effect of four variables such as contact time, initial solution pH, adsorbent dose and initial adsorbate concentration. The number of experiments (N) to be carried out was obtained from:

$$N = 2^k + 2k + n_c \tag{6.2}$$

where k is the number of variable and n_c is the number of replicates in central points.

The adsorbate adsorption efficiency, as a response, is explained by the following quadratic model equation:

$$Y = a_o + \sum_{i=1}^{q} a_i X_i + \sum_{i=1}^{q} a_{ii} X_{ii}^2 + \sum a_{ij} X_i X_j \tag{6.3}$$

where Y represents the predicted responses; X_i and X_j represent the independent variables; a_0 is the constant coefficient; a_i is linear coefficients; a_{ii} is the interactive coefficients; and a_{ij} is quadratic coefficients. The statistical and mathematical software (Minitab version 17.0, Minitab Inc., State College, PA) was used for designing the experiments, analyzing the data, fitting the models and optimizing the experimental conditions.

6.3   Results and Discussion

6.3.1   Adsorbent characterization

The N_2 adsorption-desorption isotherm and Barrett-Joyner-Halenda (BJH) pore size distribution for the studied adsorbent is depicted in Figure 6.1. According to the International Union of Pure and Applied Chemistry (IUPAC) classification, the isotherm is a typical type IV and with the presence of hysteresis loop at high relative pressure, it demonstrates the mesoporous characteristic of the material. The graphical plot of BJH pore size distribution indicates that the material comprised of two main pore size ranges, the smaller mesopore of 2-10nm and larger mesopore of 10-30nm.
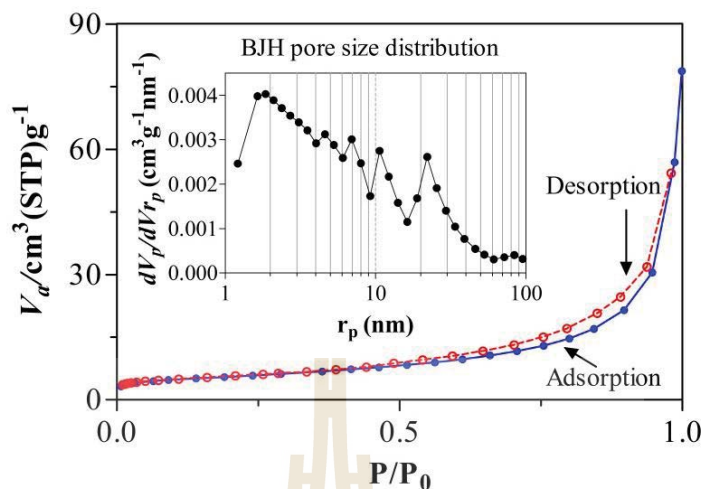
Figure 6.1   N$_2$ adsorption- desorption isotherm and BJH pore size distribution plots of

iron mixed porous clay pellet adsorbent

Totally, the adsorbent significantly presents the pore size distribution

between 2nm and 50nm, implying that it is a mesoporous adsorbent as defined by IUPAC

classification for pore size ranges (Kuila and Prasad, 2013). From the BET analysis, the

adsorbent exhibits a BET surface area of 19.393 m^2/g, total pore volume of 0.0978 cm^3/g

and mean pore size of 20.169 nm.

The surface morphology of the adsorbent before and after the adsorption

analyzed by SEM is illustrated in Figure 6.2a and 6.2b, respectively. The adsorbent before

the adsorption appears to have a rough surface structure with flat none unified shape

particles scattering around. After the adsorption reaction, the surface of the adsorbent forms

the concave morphology attached by spherical particles with various sizes. EDX analysis

showed that the major elemental composition of the adsorbent was silica (Si$_2$O$_4$, 71.5%),

alumina (Al$_2$O$_3$, 21.5%) and iron oxide (Fe$_2$O$_3$, 30.5%) (Figure 6.2c). Several peaks of

arsenic element were observed after the adsorption process (Figure 6.2d).
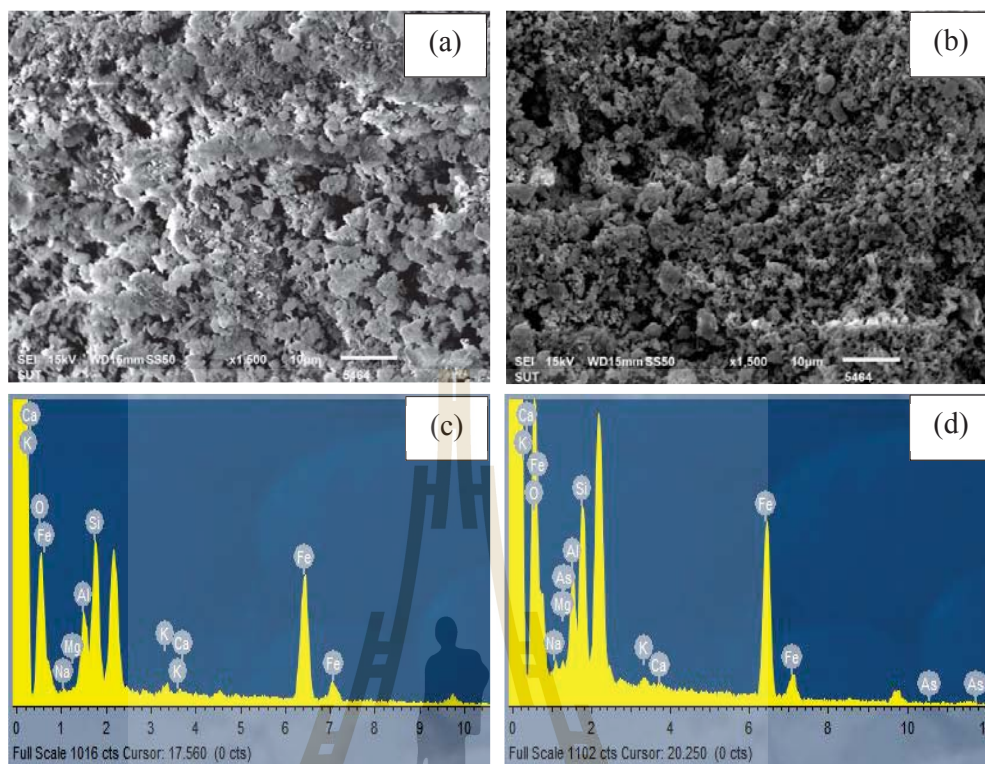
Figure 6.2 SEM images of pre-adsorption of mesoporous pellet adsorbent (a), post-adsorption of mesoporous pellet adsorbent (b), and EDX analysis of the adsorbent before and after adsorption (c) and (d), respectively

6.3.2 Model development and analysis

The optimization process with CCD under RSM involves the following steps: defining the problem and the objective, identifying the factors or variables and their levels, designing the experimental matrix, conducting the designed experiments, performing the analysis and evaluation of the mathematical model, determining the optimal levels for variables, and conducting confirmation experiments (Khataee et al., 2010; Massoudinejad et al., 2016). In this work, independent variables (contact time, solution pH, adsorbent dose and adsorbate concentration) were represented as X_1, X_2, X_3 and X_4, respectively, and their low and high levels were selected accordingly (Table 6.1).

Table 6.1   The experimental levels and representative codes of independent variables

Parameters	Codes	Level				
		$-\alpha$	-1	0	$+1$	$+\alpha$
Contact time (h)	X_1	24	36	48	60	72
Solution pH	X_2	3	5	7	9	11
Adsorbent dose (g/L)	X_3	0	5	10	15	20
Adsorbate concentration (mg/L)	X_4	0.25	1.25	2.25	3.25	4.25

According to the design of CCD under RSM based factors and their levels selected, a total number of 31 experiments (16 factorial points, 8 axial points ($\alpha = 2$) and 7 replicates at the center point) was established for response surface modeling. The experiments were designed at different combinations of the factors (variables) to obtain certain values of the response (the adsorbate adsorption efficiency) for further analysis. The experimental design matrix with the observed and predicted results for simultaneous adsorption of arsenate and arsenite is presented in Table 6.2.

Based on the experimental results, the empirical relationship between the adsorbate adsorption efficiency (Y) and independent parameters was established as the following mathematical expression:

$$Y = -75.9 + 1.523 X_1 + 22.31 X_2 + 12.20 X_3 - 19.67 X_4 - 0.00690 X_1 X_1 - 2.271 X_2 X_2 -$$
$$0.4033 X_3 X_3 + 1.545 X_4 X_4 + 0.0144 X_1 X_2 - 0.0527 X_1 X_3 + 0.0404 X_1 X_4$$
$$+ 0.2105 X_2 X_3 + 0.666 X_2 X_4 + 0.437 X_3 X_4 \qquad (6.4)$$

Table 6.2   Experimental design points and obtained responses for the interactions

Run	X_1 (h)	X_2	X_3 (g/L)	X_4 (mg/L)	A%	Predicted A%
1	36	9	5	1.25	34.704	32.263
2	60	5	15	1.25	99.830	103.56
3	48	7	10	2.25	90.393	90.394
4	48	7	10	2.25	90.382	90.394
5	60	5	5	3.25	70.394	68.298
6	36	9	5	3.25	30.069	26.094
7	48	7	10	2.25	90.408	90.394
8	60	9	15	3.25	87.897	89.554
9	60	5	5	1.25	80.472	77.855
10	72	7	10	2.25	99.623	99.027
11	36	5	5	1.25	62.480	60.585
12	48	11	10	2.25	32.206	33.301
13	48	7	10	2.25	90.367	90.394
14	36	9	15	3.25	78.416	81.610
15	36	5	15	3.25	94.182	96.184
16	48	7	10	2.25	90.372	90.394
17	48	7	10	0.25	99.368	100.07
18	60	9	15	1.25	83.908	85.043
19	60	5	15	3.25	99.724	102.75
20	48	7	20	2.25	99.332	90.676
21	48	7	10	4.25	93.966	93.081
22	48	3	10	2.25	76.079	74.815
23	48	7	10	2.25	90.258	90.394
24	48	7	0	2.25	0.0560	9.4530
25	36	5	15	1.25	97.389	98.940
26	36	5	5	3.25	49.646	49.089
27	48	7	10	2.25	90.393	90.394
28	60	9	5	1.25	53.166	50.915
29	60	9	5	3.25	47.669	46.686
30	36	9	15	1.25	77.197	79.038
31	24	7	10	2.25	73.402	73.812

To ensure the reliability of the predictive ability of the model for an adequate approximation of the real experiment, the chosen mathematical model has been validated before it used for prediction. A number of statistical parameters such as the Fisher test, P-

value, coefficient of determination (R^2) and adjusted coefficient of determination (R^2-adj) can be used to evaluate the adequacy of the model and the significance of the terms (Alidokht et al., 2011; Yaqubzadeh et al., 2016). The values of those statistical parameters were obtained from ANOVA analysis (Table 6.3). A mathematical model is a well predictive tool for the experiment results when F-value is large (the value is greater than that from the tabulated value of F-distribution for a certain number of degrees of freedom with a certain significance level) or P-value is small (the value is less than 0.05 for the 95% confidence level) (Alidokht et al., 2011; Kakavandi et al., 2016). The selected model is considered to be statistically significant or adequate for describing the experimental results because, at the 95% confidence level, the obtained P-value (<0.001) for the model is lower than 0.05 and the associated F-value was 84.58 obviously greater than the calculated tabulated F-value ($F_{0.05, 14, 16}$ = 2.68). (Nair et al., 2014) suggested that a model is suitable and has a good prediction efficiency if the value of R^2 is close to 1 and more comparable to the value of R^2-adj, and if R^2 and R^2-adj are largely different, a model may include statistically insignificant terms. From the ANOVA results, the values of R^2 and R^2-adj of the predicted model were 0.9867 and 0.9750, respectively, which is very close to 1 and comparable to each other. It implies that the model satisfactorily provides a goodness of fit to the experimental results and only 1.33% of the total variations for the adsorbate adsorption efficiency could not be explained by the empirical model.

Table 6.3   ANOVA table for response surface quadratic model

Source	Degree of freedom	Sum of squares	Adjusted mean square	F-value	P-value
Model	14	19048.8	1360.63	84.58	<0.001
X_1	1	955.3	955.32	59.38	<0.001
X_2	1	2580.0	2579.99	160.38	<0.001
X_3	1	9942.8	9942.81	618.05	<0.001
X_4	1	73.3	73.34	4.56	0.049
X_1X_1	1	27.1	27.09	1.68	0.213
X_2X_2	1	2350.3	2350.28	146.10	<0.001
X_3X_3	1	2962.3	2962.27	184.14	<0.001
X_4X_4	1	70.1	70.06	4.36	0.053
X_1X_2	1	1.9	1.91	0.12	0.735
X_1X_3	1	160.2	160.19	9.96	0.006
X_1X_4	1	3.8	3.77	0.23	0.635
X_2X_3	1	70.9	70.88	4.41	0.052
X_2X_4	1	28.4	28.36	1.76	0.203
X_3X_4	1	76.3	76.30	4.74	0.045
Residual	16	257.4	16.09		
Total	30	19306.2			

$R^2 = 0.9867$, $R^2\text{-adj} = 0.9750$

Figure 6.3 indicates the graphical plot representing the relationship between the predicted values and the actual values of the response.
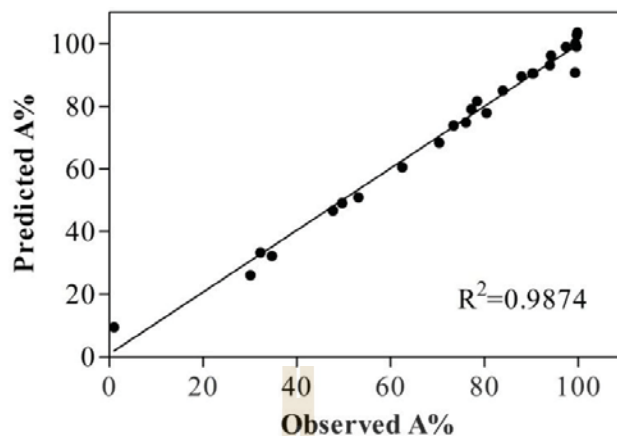
Figure 6.3   Correlation of the experimental and predicted results of the response

The recorded measurement of the adsorbate adsorption efficiency (the response) in the real batch experiments provides the actual data set. The measure of the adsorption efficiency generated through the chosen mathematical model was the predicted data set. The agreement degree of the two data sets is evaluated in accordance with the value of the coefficient of determination obtained from a linear regression. The R^2 of the correlation between the predicted and actual data was found to be 0.9874, implying that the predicted values match the experimental values reasonably well.

Graphical methods such as normal probability plot and residuals versus the predicted value plot were applied to observe the nature of residual data (the difference between experimental and predicted values) for evaluating the proportionality of the model. The model with high proportionality should have a normal distribution of residual. For normal probability plot, the data is considered as a normal distribution when the plotted points are close to the fitted straight line (Rostamiyan et al., 2014). As presented in Figure 6.4a, the plotted points were apparently closer to the distribution line, indicating the data

was normally distributed. On the other hand, the plotted points in the residuals versus predicted values scattered without obvious pattern, implying that the residuals were randomly distributed (Figure 6.4b).

The significance of each term of the model could be statistically checked using the P-value. At the 95% confidence level, the term is statistically significant if the P-value is lower than 0.05. From the ANOVA analysis (Table 6.3), all individual terms (X_1, X_2, X_3, and X_4) ($p < 0.05$) were significant to the response.
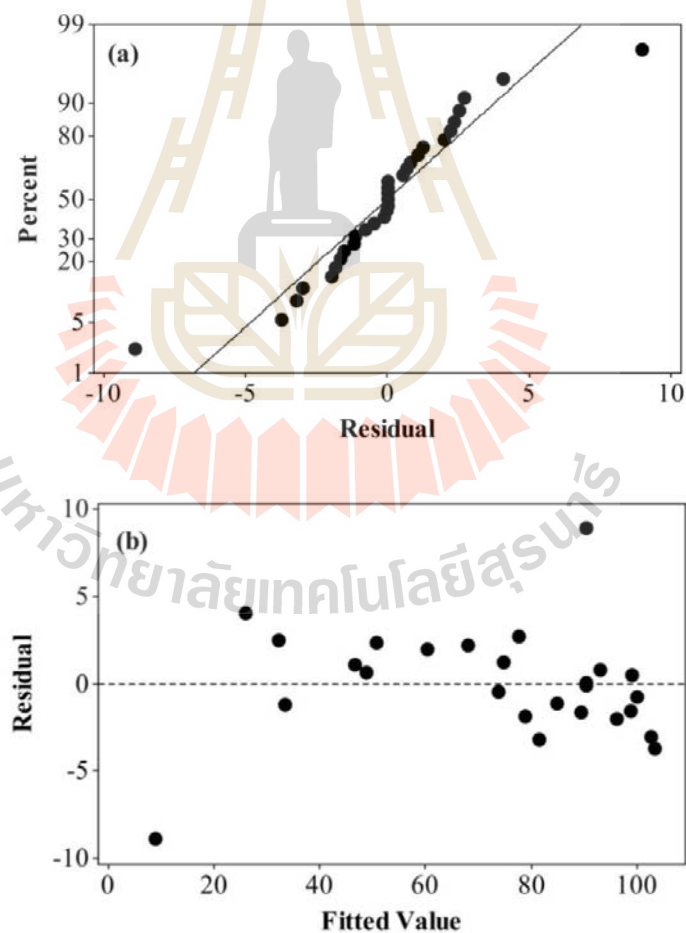
Figure 6.4   Residual plots for the response: normality plot (a) and residual versus fitted result (b)

For the quadratic or square terms, X_2X_2 and X_3X_3 were highly significant. The P-value of X_4X_4 was 0.053 (slightly greater than 0.05) implying very least insignificant and could be included in the model. For the interaction terms, X_1X_3 and X_3X_4 were significant for this response. It was also worth-noticing that X_2X_3 had P-value of 0.052, indicating less non-significant and possibly to be added. The developed model equation to be used as predictor for the response should be eliminated non-significant term.

The individual or interactive effect of parameters on the adsorbate adsorption efficiency using the new developed adsorbent in term of the numerical percentage effect can be measured using the Pareto analysis. The analysis is possibly to identify factors that have the greatest cumulative effect or the least effect on the response. The calculation is in accordance with the following equation:

$$P_i = (b_i)^2 / \sum (b_i)^2 \times 100 \quad (i \neq 0) \tag{6.5}$$

where b is the related regression coefficient of the parameter. The analysis results are illustrated in Figure 6.5. It clearly indicated that among the designed factors, solution pH (47.69%), initial concentration (37.07%), and adsorbent dose (14.26%) provide the highest effect on the response.
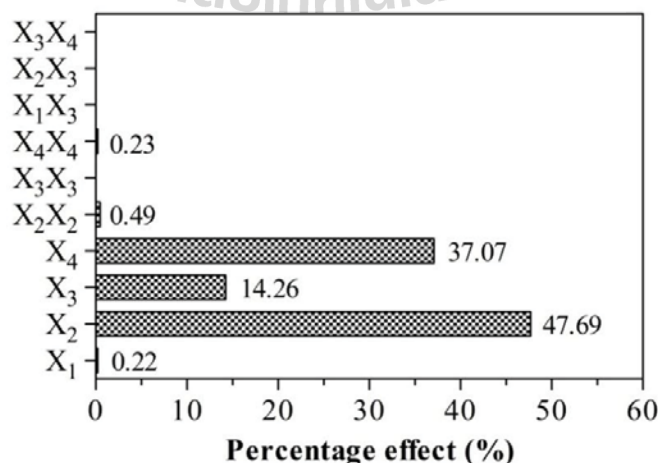
Figure 6.5 Pareto graphic analysis for the percentage effect of the investigated factors

6.3.3 Effect of variables

The three dimensional (3D) response surface and contour (2D) plots were developed based on the model equation in order to view interactive effects on the predicted response value by establishing various interactions of the investigated parameters. The plots were created by varying two variables within the designed range and keeping the other two constant. Figure 6.6a and 6.6b represents the 3D surface plot and associating 2D contour plot for the response in term of the interaction effect of solution pH and initial concentration, respectively. The high adsorption efficiency area represented by the darkest green color (> 95%) can be seen for the range pH of 3.5 to 7.5. The adsorption rate moved toward lower efficiency when increasing in pH values.

It is well known that the pH of the solution plays an important role in the adsorption of heavy metals because it controls the surface charge of the adsorbent and speciation of metallic species (Prakash et al., 2008; Srivastava et al., 2015). In water, As(V) mainly exists in the form of H_3AsO_4 at pH less than 2.2, $H_2AsO_4^-$ at pH between 2.2 and 6.98, $HAsO_4^{2-}$ at pH between 6.98 and 11.5, and AsO_4^{3-} at pH above 11.5 (Chang et al., 2010). As(III) species occur as: H_3AsO_3 (pH<9.2), $H_2AsO_3^-$ (9<pH<12), $HAsO_3^{2-}$ (12<pH<13), and AsO_3^{3-} (pH>13) (Mohan and Pittman, 2007). The surface of the adsorbent in this study was more positively charged for the acidic condition and predominated the negative charge for the alkaline pH (Te et al., 2017b).
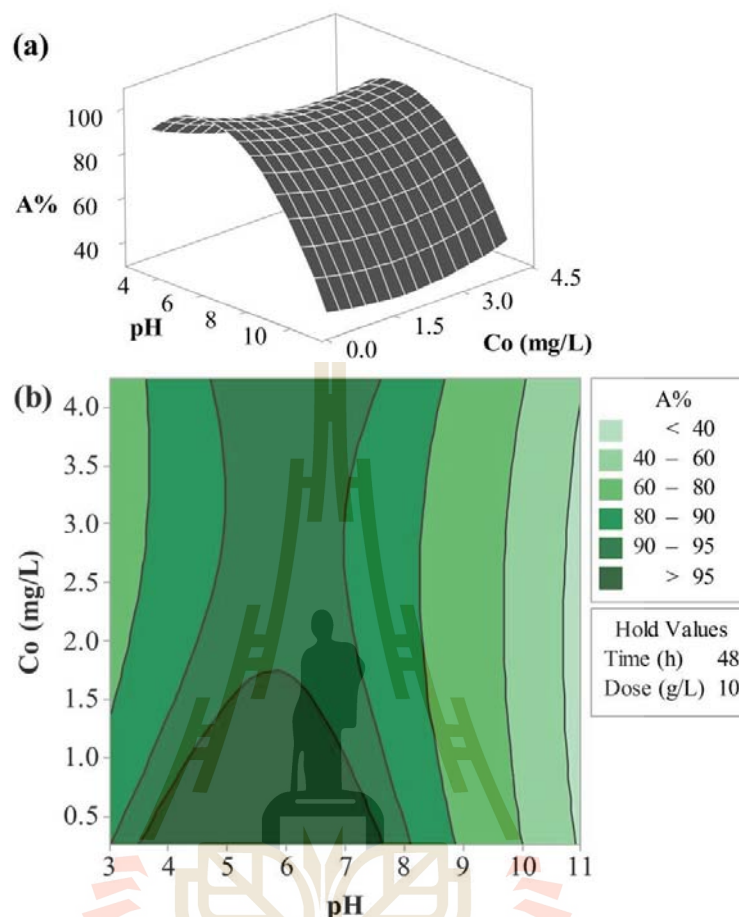
Figure 6.6   The 3D response surface (a) and 2D contour plots (b) of As(V+III) adsorption efficiency in terms of initial solution pH and initial adsorbate concentration

This implied that the unfavorable electrostatic interaction or the electrical repulsion between the adsorbent and the adsorbate occurs for the high pH regions and results in low adsorption efficiency. The occurrence of low adsorption efficiency region was observed when the initial concentration was greater than 1.5 mg/L. It could be due to insufficiency of active sites of the adsorbent surface at a fixed amount of 10 g/L in this case to adsorb more available adsorbate.

Figure 6.7a and 6.7b illustrates the 3D surface and 2D contour plots for the interactive effect of solution pH and adsorbent dose on the response by constantly holding

initial concentration and contact time, respectively. It can be clearly seen that increasing adsorbent dose to above 10 g/L produced the highest removal percentage region within the pH range of 4 to 8. It occurred as expected because increasing in dose leads to having more available reactive sites for enhancing the adsorption between adsorbate and adsorbent. However, the adsorption efficiency becomes low when the amount of adsorbent is further increased. This is due to the reduction of effective surface area and adsorbate/adsorbent ratio (Ahma and Hasan, 2016).
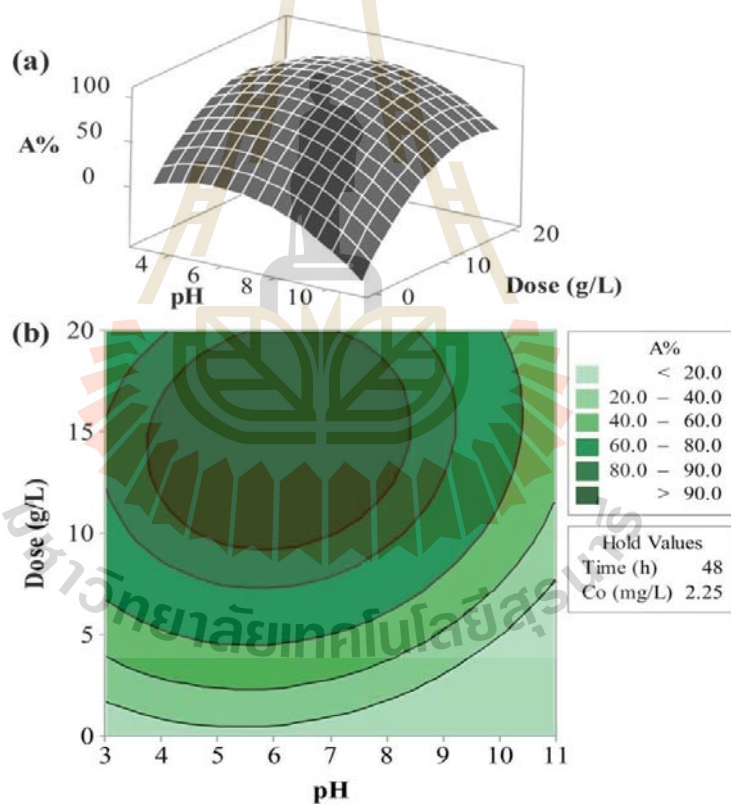
Figure 6.7   The 3D response surface (a) and 2D contour plots (b) of As(V+III) adsorption efficiency in terms of initial solution pH and adsorbent dose

The adsorbate adsorption efficiency in term of the combined effect of initial concentration and contact time at pH 7 and adsorbent dose 10 g/L is shown Figure 6.8a and 6.8b, respectively. As can be seen in the contour plot from this figure, the removal

efficiency increased with increasing in reaction time. Longer contact time means that it ensures to have enough amount of time for facilitating the interaction of adsorbate and adsorbent in the adsorption process.
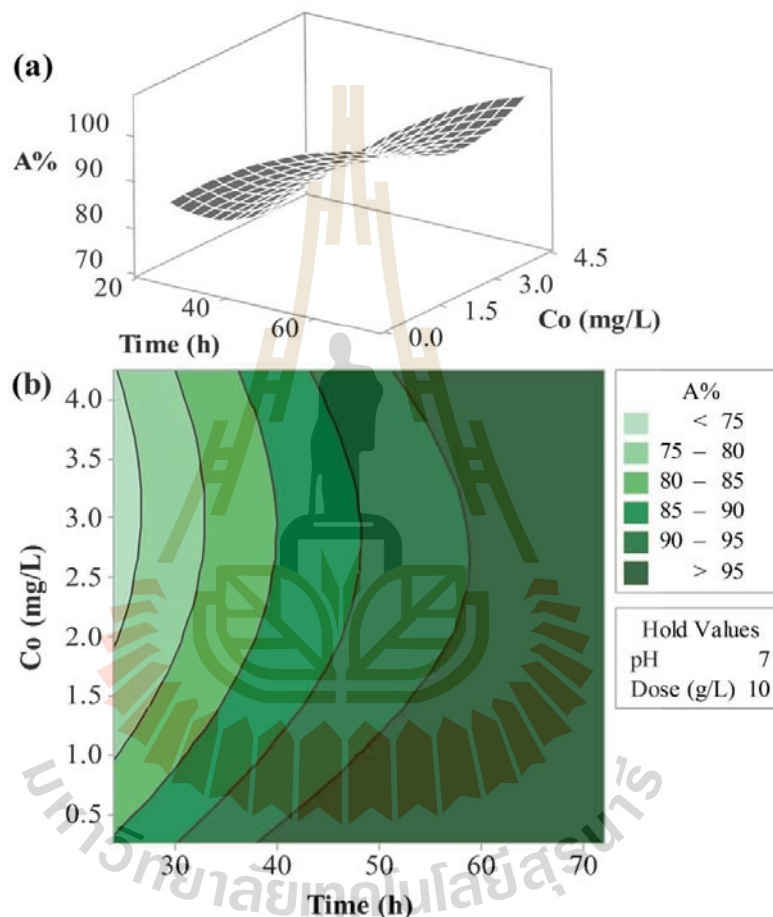
Figure 6.8   The 3D response surface (a) and 2D contour plots (b) of As(V+III) adsorption efficiency in terms of contact time and initial adsorbate concentration

It is also observed that the reaction time to achieve the maximum adsorption rate takes longer as the initial adsorbate concentration increase. This may be due to the increase of adsorbate/adsorption sites. For higher initial concentration, it has more available adsorbate ions to fill on the limited number of adsorption site which leads to increasing time

for removal. On the other hand, Alidokht et al. (2011) suggested that at high adsorbate concentration, it may create the passivation on the adsorbent surface with the consequent loss of its reactivity.

6.3.4 The process optimization and its validation

Response optimization involves defining independent variable settings that collaboratively produce the optimized arsenic adsorption efficiency, and its satisfactory is measured by the composite desirability (Rao and Baral, 2011). The desirability is scaled from 0.0 (undesirable) to 1.0 (very desirable) (Shahamirifard et al., 2016). In this work, the process optimization was evaluated by Response Optimizer of Minitab. Figure 6.9 presents the optimization plot of independent variables (contact time, solution pH, dose and initial concentration) affecting the predicted adsorption efficiency. Independent variable settings on the plot could be adjusted by moving the vertical red line to obtain more desirable predicted responses. The results suggested that the ideal condition to achieve the most desirable adsorption efficiency of 99.9321% is contact time (52h), solution pH (7), adsorbent dose (10g/L) and initial concentration (0.5mg/L). The predicted desirability (d and D) was found to be 1, implying that the selected optimized condition is suitable for production the maximum As(V+III) adsorption efficiency. The optimum condition has been applied in the batch experiment for removing coexisting arsenate and arsenite aqueous solution by the mesoporous pellet adsorbent to validate the model. The results indicated that the removal efficiency was 99.8%, comparable enough to the predicted value. It suggests that the process optimization on simultaneous removal of arsenate and arsenite from water using the new developed mesoporous adsorbent is valid and adequate in the range of investigated parameters.
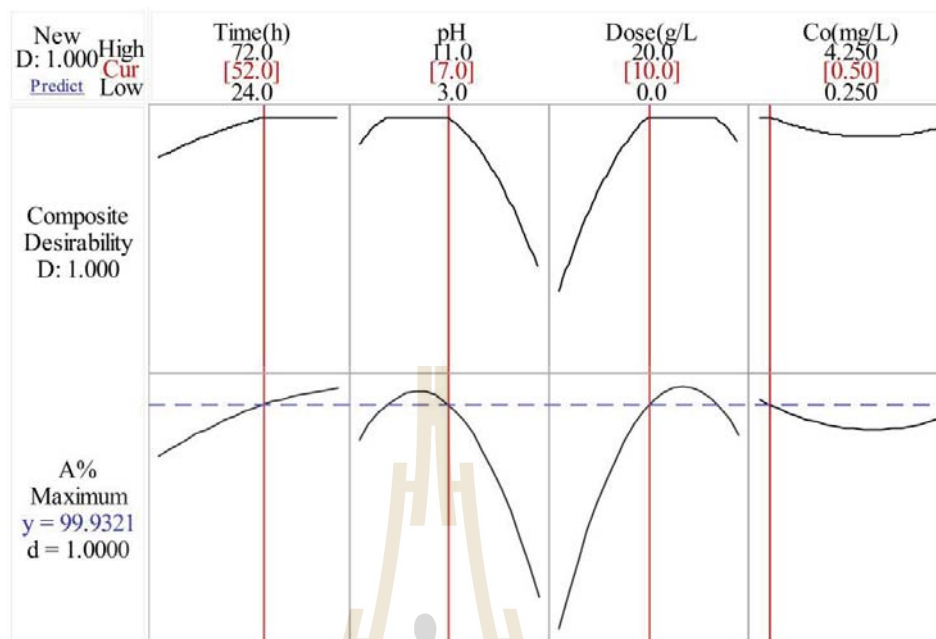
Figure 6.9   Response optimization plot for the adsorbate adsorption efficiency

6.4   Conclusion

The composite central design under response surface method was successfully applied to study the process optimization of the batch operational parameters. The ANOVA analysis suggested the second polynomial mathematical model should be used and its adequacy was supported by F-value, P-value, R^2 and R^2-adj. The residual data was confirmed to have a normal distribution by the residual and normality plots. Initial solution pH, adsorbent dose and initial concentration provided the most percentage effect on the response. The optimum values of contact time, initial pH, adsorbent dose and initial adsorbate concentration were 52 h, 7, 10 g/L and 0.5 mg/L, respectively. The confirmatory experiment is in agreement with the predicted model. The presented study process is simple, time saving and cost-effective to provide one specific optimum condition to remove highly toxic and carcinogenic pollutant by the adsorbent produced from the low cost and availability of raw materials.

CHAPTER VII

ADSORPTION OF ARSENIC FROM WATER BY IRON

MIXED CLAY POROUS PELLET IN A FIXED-BED

COLUMN

7.1 Introduction

Arsenic is a toxic and carcinogenic element, and it is necessary to treat elevated arsenic contaminated water to safe drinking level. Most studies of arsenic adsorption from aqueous solutions are primarily batch systems. The batch experiments are popularly conducted in the laboratory to determine adsorption capacity of adsorbents that can be used to design for a certain scale of treatment system; however, it is just more suitable for treating small volume of polluted water, requires large amount of adsorbents for a large volume of system, and is not popular in the real applications (Auta and Hameed, 2014; Lim and Aris, 2014). A fixed-bed adsorption is a dynamic system designed for allowing the introducing contamined liquid come in contact with a certain amount of adsorbent in a column (Malkoc and Nuhoglu, 2006). The dynamic system is easily scaled up, simple to operate, cost effective and practical for a treatment application (Lim and Aris, 2014; Nguyen et al., 2015). The continous fixed-bed adsorption column is generally performed to obtain the column breakthrough for determining the operation life span of the bed and some basic engineering data that provide accurate scale-up information regarding the column operation system (Maji et al., 2012).

However, a report on the removal of arsenic from water using clay supported metal oxides or elemental iron in a continuous fixed-bed column system is still limited.

Furthermore, the results of arsenic removal in the batch adsorption experiments by iron-mixed mesoporous pellet adsorbent were found to be encouraging (Te et al., 2017b). Therefore, arsenic adsorption from aqueous solutions in a dynamic system should be performed to obtain sufficient engineering data for designing the pilot scale filter for the filed test.

The main objective of the present research is to investigate the effect of bed height, flow rate, solution pH and initial concentration on the adsorption of arsenic from water by iron mixed mesoporous pellet in a continuous fixed-bed column. The obtained breakthrough profiles were fitted with various models.

7.2 Materials and methods

7.2.1 Reagents

Stock solutions (100 mg/L) of As(III) and As(V) were prepared by dissolving appropriate amount of sodium arsenite ($NaAsO_2$) and sodium hydrogen arsenate (Na_2HAsO_4) into deionized (DI) water, respectively. Further diluted As(III) or As(V) concentrations required in the experiment were freshly made. NaOH or HCl with appropriate concentrations was used to adjust the solution pH.

7.2.2 Adsorbent preparation and its characterization

The detail procedure of the adsorbent development is mentioned in previous work (Te et al., 2017b). Briefly, iron mixed porous pellet adsorbent was prepared by binding natural clay (NC) to iron oxide (Fe_2O_3), iron powder (IP) and rice bran (RB). The mixture was carried out at a ratio of 52.15% (NC):19.22% (Fe_2O_3):28.63% (IP) and 15% of RB was added for improving the porosity. The mixture was homogeneously mixed by adding deionized water slowly to produce a paste form. The paste was strongly stirred by hand for about 5-10min and dried at 104±1°C for 24h, and further heated at 600°C for 2-3h

in a muffle furnace to carbonize the presence of rice bran. After cooling down, the product was sized and sieved for desired particle size of 0.6-1.12mm. The adsorbent was kept in a dry and clean container for further experiments.

7.2.3 Fixed-bed adsorption experiments

The continuous fixed-bed adsorption experiments were conducted in polyethylene columns of 4.1 cm inner diameter and 31 cm height at room temperature ($25 \pm 1^{\circ}$C). The experimental set up of the continuous fixed-bed column system is presented in Figure 7.1. The columns were saturated with DI water for a certain period of time before the influent solutions were introduced upward to the columns at appropriate flow rates controlled by peristaltic pumps (WATSON MARLOW 505S, Watson-Marlow Fluid Technology Group, US). The first 1 cm at the bottom and top of the columns were filled with clean medium size sand to provide uniform and homogenous flow.
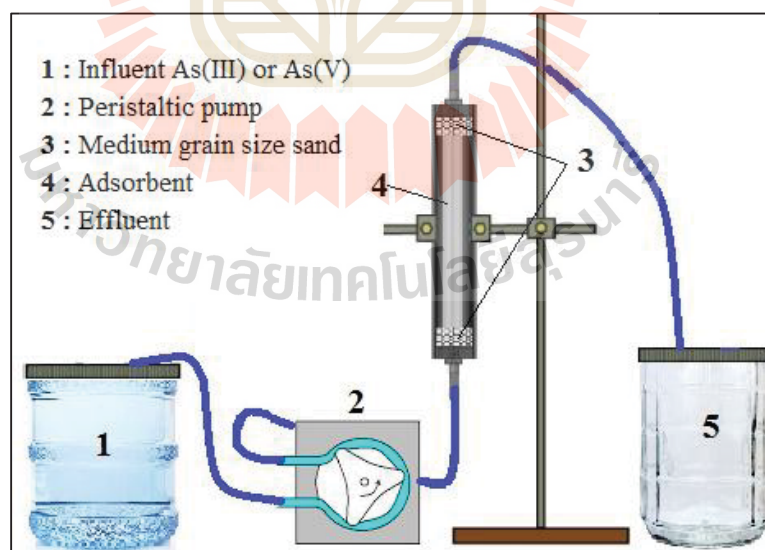
Figure 7.1 The schematic diagram of the continuous fixed-bed column packed with the adsorbent

In this study, the effects of influent feed flow rate (12.5, 17 and 20.5 mL/min), adsorbent bed height (5, 10, 15 cm), initial adsorbate concentration (500, 1000 and 2000 µg/L), and adsorbate solution pH (5, 7 and 9) were evaluated by the breakthrough curve. The summary of experimental conditions is summarized in Table 7.1. The samples were collected at preset time intervals, filtered through 0.22 µm syringe filter, acidified and analyzed for arsenic concentration by ICP-OES (Optima 8000, PerkinElmer, USA). Sampling of column effluent was done until a constant concentration of adsorbate was obtained.

7.2.4 Application to the real arsenic contaminated groundwater

The same column with iron mixed porous pellet adsorbent was used to treat arsenic contaminated groundwater in Cambodia. The physical-chemical water quality parameters of the raw groundwater were analyzed using various methods. The experimental conditions of the column were as follow: influent flow rate 7 mL/min; adsorbent bed depth 10 cm; and room temperature. Effluent samples were immediately preserved by acidification and stored at 4°C until arsenic analysis.

7.2.5 Fixed-bed column data analysis

The performance of column is usually evaluated with the concept of breakthrough curve. This curve can be obtained by plotting C_t/C_o (where C_t and C_o are the influent and effluent concentration of adsorbate, respectively) versus time (t). The adsorption capacity of adsorbate at breakthrough and saturation point can be calculated using the following equation (Lin et al., 2017):

$$q_t = \frac{QC_o}{M} \int_0^t (1 - \frac{C_t}{C_o}) dt \tag{7.1}$$

Table 7.1 Experimental conditions of the continuous fixed-bed column for As(III) or As(V) adsorption by iron mixed porous pellet adsorbent at room temperature

	H (cm)	Q (mL/min)	υ (cm/min)	C_o (μg/L)	Initial pH	M (g)	ρ_{bed} (g/cm^3)	ε_{bed}
Bed height	5	17	1.29	500	7	47.97	0.727	0.633
	10	17	1.29	500	7	95.94	0.727	0.633
	15	17	1.29	500	7	143.91	0.727	0.633
Flow rate	10	12.5	0.95	500	7	95.94	0.727	0.633
	10	20.5	1.55	500	7	95.94	0.727	0.633
	10	17	1.29	500	7	95.94	0.727	0.633
C_o	10	17	1.29	500	7	95.94	0.727	0.633
	10	17	1.29	1000	7	95.94	0.727	0.633
	10	17	1.29	2000	7	95.94	0.727	0.633
Initial pH	10	17	1.29	500	5	95.94	0.727	0.633
	10	17	1.29	500	7	95.94	0.727	0.633
	10	17	1.29	500	9	95.94	0.727	0.633

Note: H= bed height; Q= Feed flow rate; υ = superficial velocity; C_o = initial adsorbate concentration; M= Adsorbent mass; ρ_{bed} = bed density; ε_{bed}= bed porosity

where Q (L/h) is the volumetric flow rate; M (g) is the mass of adsorbent packed in the column; $\int_0^t (1-\frac{C_t}{C_o})dt$ is the numerical integration of the area above the breakthrough curve and could be estimated by trapeze method as follow:

$$\int_o^t \left(1-\frac{C_t}{C_o}\right)dt = \frac{1}{2}\sum_{n=0}^{t_s}(t_{n+1}-t_n)\left(2\left(\frac{C_{t_s}}{C_o}\right)-\left(\left(\frac{C_t}{C_o}\right)_{n+1}+\left(\frac{C_t}{C_o}\right)_n\right)\right) \qquad (7.2)$$

where C_{ts}/C_o is the saturation point; t_n and t_{n+1} are the nth and $(n+1)^{th}$ time point (h), respectively; $(C_t/C_o)_n$ and $(C_t/C_o)_{n+1}$ are the ratio of the nth and $(n+1)^{th}$ effluent concentrations over the initial influent concentration, respectively.

The mass transfer zone (MTZ) defined as the length of the adsorption zone in the column can be obtained from (Cruz-Olivares et al., 2013):

$$MTZ = H\left(1 - \frac{t_b}{t_s}\right) \tag{7.3}$$

where MTZ (cm) is the length of the mass transfer zone; t_b (min) is the breakthrough time; and t_s (min) is the exhaustion time.

The empty bed contact time (EBCT) in the column can be calculated by the following equation (Lin et al., 2017):

$$EBCT \text{ (min)} = \frac{\text{bed volume (mL)}}{\text{flow rate (mL/min)}} \tag{7.4}$$

The fractional bed utilization (FBU), defined as the ratio between the adsorption capacity at breakthrough time and at saturation time, can be expressed by the following equation (Lemus et al., 2017):

$$FBU \text{ (\%)} = \frac{q_b}{q_s} \times 100 \tag{7.5}$$

7.3   Results and discussion

7.3.1   Adsorbent characterization

The adsorbent exhibits a BET surface area of 19.393 m^2/g, total pore volume of 0.0978 cm^3/g and mean pore size of 20.169 nm (Table 7.2). The pore size distribution, as well as the mean pore size significantly presents between 2nm and 50nm, implying that it is a mesoporous adsorbent as defined by IUPAC classification for pore size ranges (Kuila and Prasad, 2013).

Table 7.2   The main physico-chemical characteristics of the adsorbent

Parameter	Value
Particle size (mm)	0.6-1.18
BET surface area (m^2/g)	19.393
Total pore volume (cm^3/g)	0.0978
Micropore volume (cm^3/g)	0.0011
Mesopore volume (cm^3/g)	0.0967
Mean pore size (nm)	20.169
Elemental analysis (wt. %)	
Si	21.829
Al	7.251
Fe	25.78
Point of zero charge (pH_{zpc})	7.50
Particle density, ρ_p, (g/cm^3)	1.986
Skeletal density, ρ_M, (g/cm^3)	2.465
Particle porosity, ε_p	0.194

Regardless the presence of oxygen, elemental composition analyzed by XRF indicated that the main constituent elements of porous pellet adsorbent were Si (21.829%), Al (7.251%), and Fe (25.780%).

7.3.2 Continuous fixed-bed column studies

The performance of the fixed-bed column systems has been evaluated through analyzing the plot of breakthrough curves. From the breakthrough curves constructed from the experimental data, the point with the effluent concentration (C_t) of 10 µg/L was defined as a breakthrough point and the point corresponding to 95% of the

influent concentration was considered as a saturation point. The breakthrough curves also provide the value of the breakthrough time (t_b), adsorption capacity in the breakthrough point (q_b), removal percentage in the breakthrough point (%R_b), saturation time (t_s), adsorption capacity in the saturation point (q_s), removal percentage in the saturation point (q_s), mass transfer zone (MTZ) and volume treated in the saturation time (V_s) (Table 7.3). The change in the column operating parameters, i.e., influent flow rate, adsorbent bed height, adsorbate initial concentration and initial solution pH, greatly affects the outcome of the breakthrough curve pattern.

7.3.3 Effect of flow rate

The effect of flow rates on adsorption of either As(III) or As(V) in the continuous fixed-bed column packed with iron-mixed porous pellet adsorbent was examined with the flow rate of 12.5, 17 and 20.5 mL/min at an initial concentration of 500 μg/L of As(III) or As(V) solution (pH = 7 ± 0.1) and at the adsorbent bed height of 10 cm. For both As(III) and As(V) adsorption, the breakthrough curves for lower flow rates appeared as more gradual curves and they became significant steeper when the flow rates were increased to 20.5 mL/min (Figure 2). As the flow rate increased from 10.2 to 20.5 mL/min, the breakthrough time of As(III) and As(V) decreased from 37.53 to 6.15 h and from 24.78 to 3.15 h, respectively, and the saturation time of As(III) and As(V) decreased from 137.53 to 59.07 h and from 124.35 to 49.23 h, respectively (Table 7.3). This is due to the amount of interaction time between adsorbate and adsorbent. Longer time that allows metal ions access to more binding sites within the pores of the adsorbent happens to slower flow rate (Cruz-Olivares et al., 2013), implying the gradual occupancy toward saturation point. Higher flow rate provides insufficient residence time for more effective interaction of metal ions with active sites and for diffusion into the pores to occur (Jain et al., 2013), leading to have a steeper inclination of the breakthrough profiles.

Table 7.3 Parameters in the fixed-bed column for arsenic adsorption by the adsorbent

	C_o (µg/L)	Q (mL/min)	H (cm)	pH	t_b (h)	t_s (h)	V_b (L)	V_s (L)	q_b (µg/g)	q_s (µg/g)	FBU (%)	EBCT (min)	MTZ (cm)
As(III)	500	12.5	10	7	37.53	137.53	28.15	103.15	124.19	338.93	36.64	10.53	7.27
	500	17	10	7	15.45	101.76	15.76	103.79	77.43	338.56	22.87	7.76	8.48
	500	20.5	10	7	6.15	59.07	7.56	72.66	37.13	187.86	19.77	6.45	8.96
	1000	17	10	7	10.69	77.49	10.90	79.04	107.57	453.65	23.71	7.76	8.62
	2000	17	10	7	5.16	57.76	5.26	57.89	104.01	465.96	22.32	7.76	9.11
	500	17	5	7	6.78	71.54	6.92	72.97	67.96	369.26	18.41	3.88	4.53
	500	17	15	7	31.28	141.44	31.91	144.27	104.51	314.63	33.33	19.35	11.68
	500	17	10	5	35.51	122.07	36.22	124.51	177.39	405.51	43.74	7.76	7.09
	500	17	10	9	11.26	77.41	11.49	78.96	56.57	240.32	23.54	7.76	8.55
As(V)	500	12.5	10	7	24.78	124.35	18.59	93.26	90.97	263.11	34.58	10.53	8.01
	500	17	10	7	11.36	91.50	11.59	93.33	56.97	255.75	22.27	7.76	8.76
	500	20.5	10	7	3.15	49.23	3.87	60.55	19.08	97.64	19.54	6.45	9.36
	1000	17	10	7	5.83	63.97	5.95	65.25	58.73	339.89	17.28	7.76	9.09
	2000	17	10	7	2.15	55.23	2.19	56.33	43.31	352.22	12.29	7.76	9.61
	500	17	5	7	5.18	56.48	5.28	57.61	51.95	256.61	20.25	3.88	4.54
	500	17	15	7	19.56	131.74	19.95	134.37	65.25	236.28	27.62	19.35	12.77
	500	17	10	5	33.18	112.25	33.84	114.49	165.68	393.84	42.07	7.76	7.04
	500	17	10	9	7.05	64.53	7.19	65.82	35.31	154.26	22.89	7.76	8.91
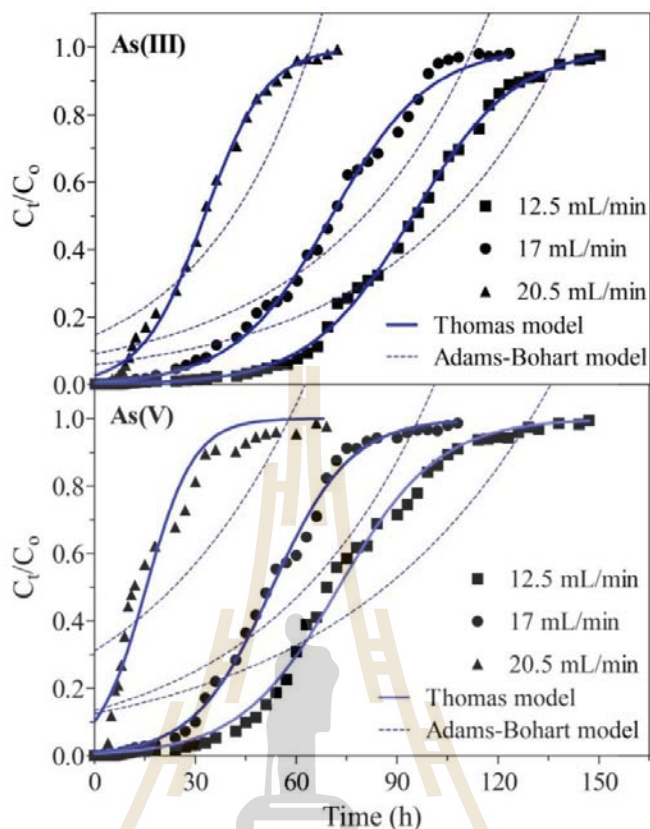
Figure 7.2 Effect of flow rate on adsorpton breakthrough curves of As(III) or As(V) by the adsorbent (initial As(III) or As(V) concentration: 500μg/L; initial solution pH: 7±0.1; temperature: 25±1°C; adsorbent bed height: 10 cm)

Increasing the flow rate from 12.5 to 20.5 mL/min allows decreasing the MTZ of As(III) and As(V) from 7.27 to 8.96 cm and from 8.01 to 9.36 cm, respectively, decreasing the FBU of As(III) and As(V) from 36.64 to 19.77% and from 34.58 to 19.54%, respectively, and also decreasing the EBCT of As(III) and As(V) from 10.53 to 6.45 min and from 10.53 to 6.45 min, respectively (Table 7.3). Ahmad and Hameed (2010) and Dutta and Basu (2013) suggested that the rate of mass transfer or mass transfer zone (MTZ) increases with increasing flow rate, resulting in faster breakthrough or saturation. With increasing in the flow rate, the saturation adsorption capacity of As(III) and As(V) decreased from 338.93 to 187 μg/L and from 263.11 to 97.64 μg/L, respectively (Table

7.3). Lower adsorption capacity at higher flow rate occurred because introducing influent into the column at a fast velocity rate makes the solute leave prior to reaching equilibrium and reduces the adhesion of adsorbate to the adsorbent due to the break of the film surrounded by adsorbent particle (Ahmad and Hameed, 2010; Singh and Pant, 2006).

7.3.4 Effect of bed height

The breakthrough curves of various adsorbent bed heights (5, 10, or 15cm) at initial As(III) or As(V) concentration of 500 µg/L (pH = 7 ± 0.1) and flow rate of 17 mL/min are presented in Figure 7.3. For both As(III) and As(V) adsorption cases, the behavior of the breakthrough curves looked similar and was observed to have lower inclination at higher bed heights, indicating the saturation point was reached slowly after passing the breakthrough point.

With the increase of the bed height from 5 to 15 cm, the breakthrough time increased from 6.78 to 31.28 h and from 5.18 to 19.56 h for As(III) and As(V) adsorption, respectively, and the saturation time increased from 71.54 to 141.44 h in case of As(III) and from 56.48 to 131.74 h in case of As(V) (Table 7.3). Higher bed height contains larger amount of adsorbent to provide more available adsorption binding sites, resulting in a longer time needed to reach the breakthrough and saturation points. A longer saturation time might contribute to the long residence time for a sufficient interaction between adsorbate and adsorbent, leading to increase in the adsorption capacity at a higher bed height (Jang and Lee, 2016). However, an increase in bed height from 5 to 15 cm led to a decrease of the saturation adsorption capacity of the adsorbent from 369.26 to 314.63 µg/L and from 256.61 to 236.28 µg/L for As(III) and As(V) adsorption, respectively (Table 7.3). This is probably due to inaccessibility of ions to all available surfaces of the adsorbent (Nazari et al., 2016). This suggested that a better and beneficial performance of the adsorption was with a relatively low bed height of the adsorbent.
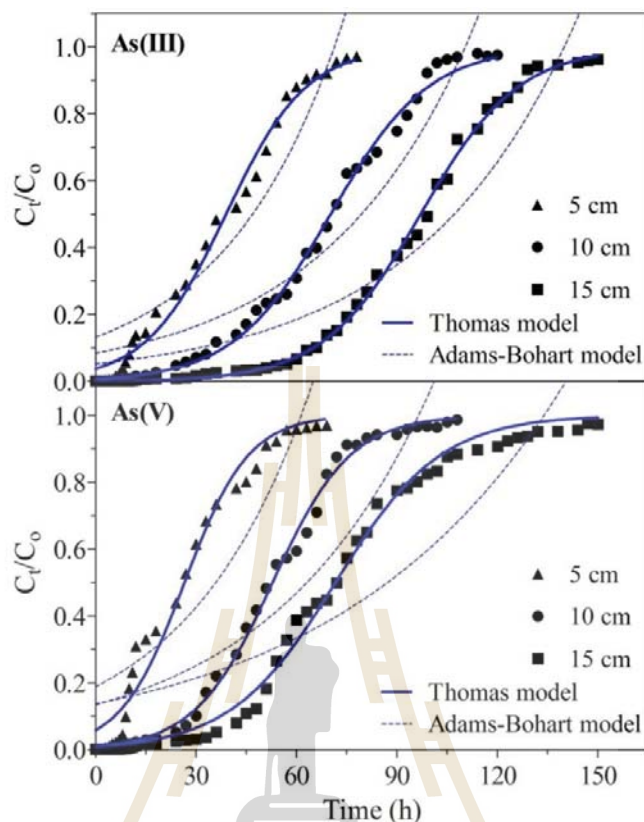
Figure 7.3 Effect of adsorbent bed height on adsorpton breakthrough curves of As(III) or As(V) by iron mixed porous pellet adsorbent (initial As(III) or As(V) concentration: 500μg/L; initial solution pH: 7±0.1; temperature: 25±1°C; influent flow rate: 17 mL/min)

7.3.5 Effect of initial concentration

Initial concentration is one of the main factors influencing on the performance of adsorption in the fixed-bed column because a certain amount of adsorbent can only uptake a particular amount of the solute. The effect of influent As(III) or As(V) concentrations (500, 1000 or 2000 μg/L) on the breakthrough curve, as shown in Figure 7.4, was investigated with the solution pH of 7 ± 0.1 at a constant flow rate of 17 mL/min and a bed height of 10 cm. For both As(III) and As(V) adsorptions, the breakthrough profiles were similar by having a relatively flatter shape for lower initial concentrations and having

a shaper shape for higher initial concentration. The flatter slope may attribute to a relatively wide use of MTZ suggesting a film controlled the adsorption process while the steeper slope may be due to a relatively small use of MTZ suggesting an intra-particle diffusion controlled the adsorption process (Afroze et al., 2015; Baral et al., 2009). For both cases, prolonged breakthrough and saturation times occurred at lower initial concentration whereas higher initial inlet concentration provided quicker breakthrough and saturation times (Table 7.3).
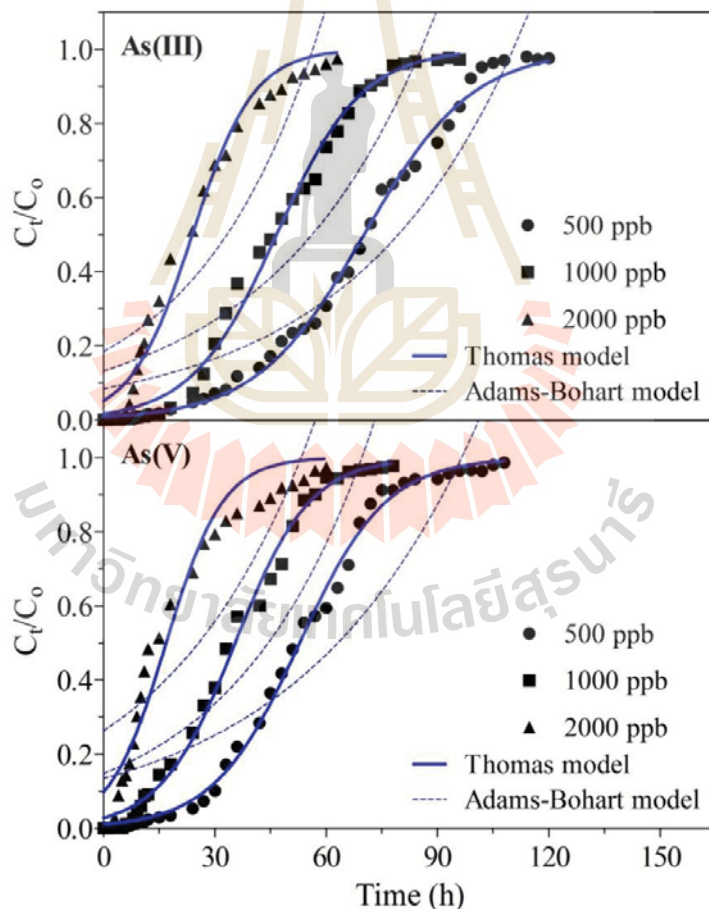
Figure 7.4   Effect of initial concentration on adsorpton breakthrough curves of As(III) or As(V) by the adsorbent (adsorbent bed height: 10 cm; initial solution pH: 7±0.1; temperature: 25±1°C; influent flow rate: 17 mL/min)

This can be reasoned by the fact that a lower initial concentration caused slower transport due to decreased diffusion coefficient and a higher initial concentration provided larger amount of solutes to cover available binding sites of adsorbent more quickly (Afroze et al., 2015). As the initial influent concentration increased from 500 to 2000 µg/L, the saturation adsorption capacity of the adsorbent increased from 453.65 to 465.96 µg/g and from 339.89 to 352.22 µg/g for As(III) and As(V) adsorption, respectively (Table 7.3). This might be attributed to the increase of driving force and the decrease in the mass adsorption transfer zone resulting from increasing initial influent concentration, implying that the driving force is strong enough for the transfer process to overcome the mass transfer resistance (Baral et al., 2009; Jang and Lee, 2016).

7.3.6 Effect of initial pH

The effect of initial pH on the adsorption of either As(III) or As(V) in the iron-mixed porous pellet adsorbent packed column was investigated at pH of 5, 7 and 9 (representing an acidic, neutral and alkaline condition, respectively) while keeping the adsorbent bed height of 10 cm, initial adsorbate concentration of 500 µg/L, and influent flow rate of 17 mL/min. For both cases, increasing the value of initial pH made the breakthrough curves shift from right to left, as shown in Figure 7.5, implying that the breakthrough and saturation points were obtained quicker when the influent solutions were becoming alkaline media. With the increase of pH from 5 to 9, the adsorption capacity decreased from 405.51 to 240.32 µg/g and from 393.84 to 154.26 µg/g for As(III) and As(V) adsorption, respectively (Table 7.3). The solution pH is one of the most important experimental factors for the adsorption process because of its influences on the ionic states of the functional groups of the adsorbent and metal species in the solution (Han et al., 2006). It is suggested that a solid surface is positively charged when the pH is below pH_{pzc} and predominates with negative charges when the pH is above pH_{pzc} (Wang et al., 2014). In this study, the point of zero charge of the adsorbent is 7.50.
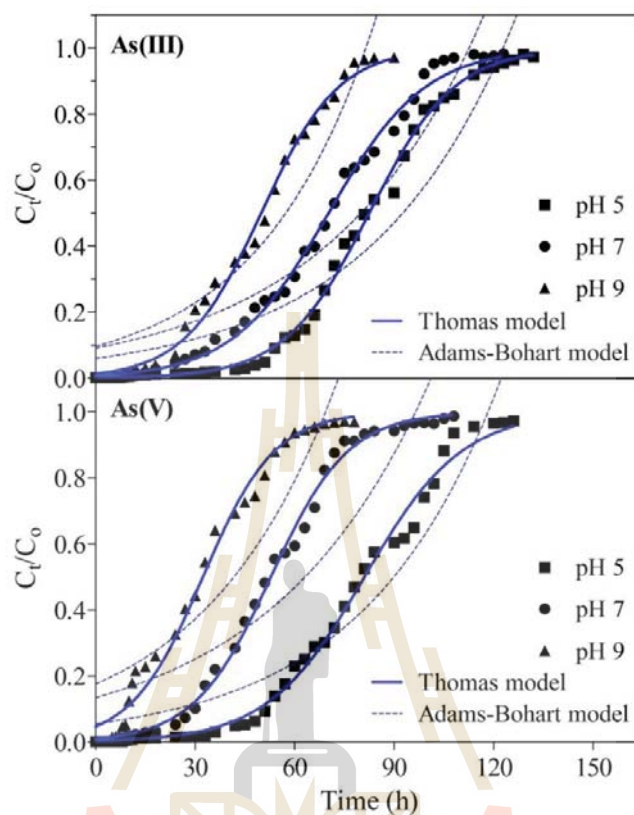
Figure 7.5   Effect of initial solution pH on adsorpton breakthrough curves of As(III) or
As(V) by iron mixed porous pellet adsorbent (adsorbent bed height: 10 cm;
initial As(III) or As(V) concentration: 500 µg/L; temperature: 25 ± 1°C;
influent flow rate: 17 mL/min)

On the other hand, in natural water, the As(III) species occur as H_3AsO_3 (pH <9.2) and
$H_2AsO_3^-$ (9<pH<12), and the As(V) species are mainly in the form of $H_2AsO_4^-$
(2.2<pH<6.98) and $HAsO_4^{2-}$ (6.98<pH<11.5) (Chang et al., 2010; Mohan and Pittman,
2007). Therefore, the repulsion between the negative species of both As(III) and As(V) and
the negative surface of the adsorbent with increase in initial pH to the alkaline condition
results in lower adsorption capacities.

7.3.7   Kinetic models of the fixed-bed column adsorption

Experimental continuous fixed-bed adsorption column can be used for designing and predicting the performance of practical full size columns. In the present study, Thomas, Adams-Bohart, Klinkenberg, and Bed Depth Service Time (BDST) models were applied for fitting the breakthrough curves, as well as the calculation of the column kinetic parameters and adsorption capacity of the fixed-bed columns.

7.3.7.1 The Thomas kinetic model

The Thomas model commonly used to fit the experimental data of a fixed-bed column assumes that the adsorption is limited by mass transfer at the interface and the adsorption experimental data is well described by Langmuir isotherms and second-order kinetics (Foo et al., 2013). The model has the non-linear form as follow (Thomas, 1944):

$$\frac{C_t}{C_o} = \frac{1}{1 + \exp\left(K_{Th} q_0 \frac{m}{Q} - K_{Th} C_o t\right)} \tag{7.5}$$

where K_{Th} (ml/min/mg) is the Thomas rate constant; q_0 (mg/g) is the As(III) or As(V) adsorption capacity; m (g) is the mass of adsorbent used in the column; and Q (mL/min) is the volumetric flow rate. The value of correlation coefficient (R^2) is used as an indicator for evaluating the performance of the model. The closer the correlation coefficient is close to 1, the better the performance of the model is to describe the data. Fitting the model to the experimental data of the breakthrough curves at different adsorption parameters such as the influent flow rate, adsorbent bed height, initial adsorbate concentration and initial solution pH is illustrated in Figure 2-5. The kinetic parameters of the Thomas model such as Thomas rate constant (K_{Th}), adsorption capacity (q_o) and correlation coefficient (R^2) determined by non-linear regression analysis are presented in Table 7.4.

Table 7.4 Parameters for the Thomas model with non-linear fitting in the fixed-bed column for As(III) and As(V) adsorption by the adsorbent

Parameters	C_o (μg/L)	Q (mL/min)	H (cm)	pH	As(III) K_{Th} (L/h/mg)	As(III) q_o (μg/g)	As(III) R^2	As(V) K_{Th} (L/h/mg)	As(V) q_o (μg/g)	As(V) R^2
Flow rate	500	12.5	10	7	0.1304	368.81	0.9984	0.1355	284.11	0.9957
	500	17	10	7	0.1375	373.26	0.9964	0.1721	280.89	0.9968
	500	20.5	10	7	0.2172	208.30	0.9964	0.2820	99.02	0.9505
Initial concentration	500	17	10	7	0.1375	373.26	0.9964	0.1721	280.89	0.9968
	1000	17	10	7	0.0873	496.08	0.9937	0.0997	377.24	0.9936
	2000	17	10	7	0.0608	509.27	0.9794	0.0657	359.19	0.9557
Bed height	500	17	5	7	0.1664	414.35	0.9902	0.2094	282.49	0.9763
	500	17	10	7	0.1375	373.26	0.9964	0.1721	280.89	0.9968
	500	17	15	7	0.1369	344.03	0.9982	0.1275	253.91	0.994
Initial pH	500	17	10	5	0.1567	438.55	0.9974	0.1364	430.89	0.9933
	500	17	10	7	0.1375	373.26	0.9964	0.1721	280.89	0.9968
	500	17	10	9	0.1719	265.45	0.9948	0.1855	171.96	0.9872

The non-linear fitting of the model provided with higher values of R^2 ranging from 0.9794 to 0.9984 and from 0.9557 to 0.9968 for As(III) and As(V) adsorption, respectively. Plus, the calculated adsorption capacities (in the ranges of 208.30-509.27 µg/g and 99.02-430.89 µg/g for As(III) and As(V) adsorption, respectively) are comparable enough to the experimental adsorption capacities (in the ranges of 187.86-466.27 µg/g and 154.26-393.84 µg/g for the adsorption of As(III) and As(V), respectively). This suggested that the Thomas model was more accurate and described well the performance of the experimental breakthrough curves for both cases. Better applicability of this model for these adsorption cases may be due to their batch adsorption data were well fitted to the Langmuir and second-order kinetic models (Te et al., 2017b).

Increasing in the influent flow rate of either As(III) or As(V) led to an increase of the K_{Th} values probably due to the decrease of mass transport resistance and axial dispersion (Roy et al., 2013). Contradictorily, with introducing higher initial adsorbate concentration in the column system, the value of K_{Th} decreased while the value of q_o increased because the driving force for adsorption is the concentration difference between the ions on the adsorbent surfaces and in the solution (Chen et al., 2012). For both cases, the values of K_{Th} and q_o decreased with the increase of the adsorbent bed height. This may be due to the increase of mass transport resistance and the axial dispersion (Ghosh et al., 2014).

7.3.7.2   The Adams-Bohart model

The Adams-Bohart model is typically used for describing the initial phase of a breakthrough curve ($C_t/C_o<0.5$) and its assumption is that the adsorption rate is controlled by external mass transfer and equilibrium is not instantaneous (Wang et al., 2015). Its non-linear form can be expressed as follow (Bohart and Adams, 1920):

$$\frac{C_t}{C_o} = \exp\left(K_{AB}C_o t - K_{AB}N_o \frac{H}{\upsilon} \right)$$

(7.6)

where K_{AB} (L/min/mg) is the kinetic constant; N_0 (mg/L) is the saturation concentration; H (cm) is the bed depth of column; υ (cm/min) is the linear velocity and can be calculated by dividing the flow rate to the column section area. Apparently, fitting the model to the whole range of experimental data provides worse performance of the model (Figure 7.2-7.5) compared to application of the model to only the breakthrough data less than 0.5 (Figure 7.6-7.9). It is supportive that this model is just appropriate for analyzing the initial part of a breakthrough curve.

The values of K_{AB} and N_o of the model applied to the breakthrough curve (Ct/Co <0.5) were calculated from the non-linear equation and are presented in Table 7.5. For both As(III) and As(V) adsorption cases, the constant K_{AB} increased, but N_o had an inconsistent change with an increase of the flow rate. Both K_{AB} and N_o decreased with an increase of the bed height for both adsorption cases. In case of As(III) adsorption, increasing the initial concentration tended to decreasing the value of K_{AB}, but increasing N_o.

Figure 7.6   Prediction of the Adam-Bohart model with different flow rate on adsorpton

breakthrough curves of As(III) or As(V) by iron mixed porous pellet

adsorbent (initial As(III) or As(V) concentration: 500μg/L; initial solution

pH: 7±0.1; temperature: 25±1°C; adsorbent bed height: 10 cm)

Figure 7.7 Prediction of the Adam-Bohart model with different adsorbent bed height on adsorpton breakthrough curves of As(III) or As(V) by iron mixed porous pellet adsorbent (initial As(III) or As(V) concentration: 500μg/L; initial solution pH: 7±0.1; temperature: 25±1°C; influent flow rate: 17 mL/min)

Figure 7.8   Prediction of the Adam-Bohart model with different initial concentration on adsorpton breakthrough curves of As(III) or As(V) by iron mixed porous pellet adsorbent (adsorbent bed height: 10 cm; initial solution pH: 7±0.1; temperature: 25±1°C; influent flow rate: 17 mL/min)

Figure 7.9   Prediction of the Adam-Bohart model with different initial solution pH on
adsorpton breakthrough curves of As(III) or As(V) by iron mixed porous
pellet adsorbent (adsorbent bed height: 10 cm; initial As(III) or As(V)
concentration: 500 μg/L; temperature: 25 ± 1°C; influent flow rate: 17
mL/min)

Table 7.5 Parameters for the Adam-Bohart model with non-linear fitting in the fixed-bed column for As(III) and As(V) adsorption by the adsorbent

Parameters	C_o (µg/L)	Q (mL/min)	H (cm)	pH	As(III)			As(V)		
					K_{AB} (L/mg/h)	N_o (mg/L)	R^2	K_{AB} (L/mg/h)	N_o (mg/L)	R^2
Flow rate	500	12.5	10	7	0.0956	306.77	0.9751	0.1349	224.25	0.9935
	500	17	10	7	0.0969	324.99	0.9820	0.1441	232.83	0.9826
	500	20.5	10	7	0.1774	180.94	0.9304	0.5138	62.55	0.9468
Initial concentration	500	17	10	7	0.0969	324.99	0.9820	0.1441	232.83	0.9826
	1000	17	10	7	0.0784	406.69	0.9415	0.0911	312.17	0.9575
	2000	17	10	7	0.0514	450.85	0.8167	0.1123	230.72	0.9642
Bed height	500	17	5	7	0.1453	348.59	0.9354	0.1929	238.64	0.7462
	500	17	10	7	0.0969	324.99	0.9820	0.1441	232.83	0.9826
	500	17	15	7	0.0907	291.75	0.9853	0.1065	212.96	0.9562
Initial pH	500	17	10	5	0.1303	350.59	0.9865	0.1104	351.31	0.9829
	500	17	10	7	0.0969	324.99	0.9820	0.1441	216.59	0.9826
	500	17	10	9	0.1204	238.79	0.9404	0.1609	149.72	0.8554

The correlation coefficients (R^2) obtained from the model were found to be higher than 0.9 (except for adsorption of As(III) at initial concentration of 2000 µg/L, for As(V) at bed height of 5 cm and for As(V) at initial pH of 9). This indicates that this model can provide a relatively satisfactory to fit the experimental breakthrough data of the column study.

7.3.7.3 The Klinkenberg model

The Klinkenberg model assumes that it has a constant fluid velocity, negligible axial dispersion, and the linear driving force mass-transfer model. This model is represented as below (Taamneh and Al Dwairi, 2013):

$$\frac{C}{C_0} \approx \frac{1}{2}\left[1 + erf\left(\sqrt{\tau} - \sqrt{\xi} + \frac{1}{8\sqrt{\tau}} + \frac{1}{8\sqrt{\xi}}\right)\right] \tag{7.7}$$

$$\xi = \left(kKZ/u\right)\frac{\left(1 - \varepsilon_b\right)}{\varepsilon_b} \tag{7.8}$$

$$\tau = k\left(t - \frac{Z}{u}\right) \tag{7.9}$$

where k (1/min) is the particle mass transfer coefficient; K is the Henry's constant of the linear isotherm equation; u (cm/min) in the interstitial fluid velocity; Z (cm) is the adsorbent bed height; t (min) is the time; ε_b is the adsorbent bed porosity. The fitting method of this model between experiment and calculation data was carried out using numerical method for error minimization by sum of square error (SSE), and for optimization of regression coefficient (R^2) close to 1. Fitting the model to the whole range of experimental data is illustrated in Figure 7.10-7.13. The obtained values of k and K for Klinkenberg model along with R^2 are presented in Table 7.6.
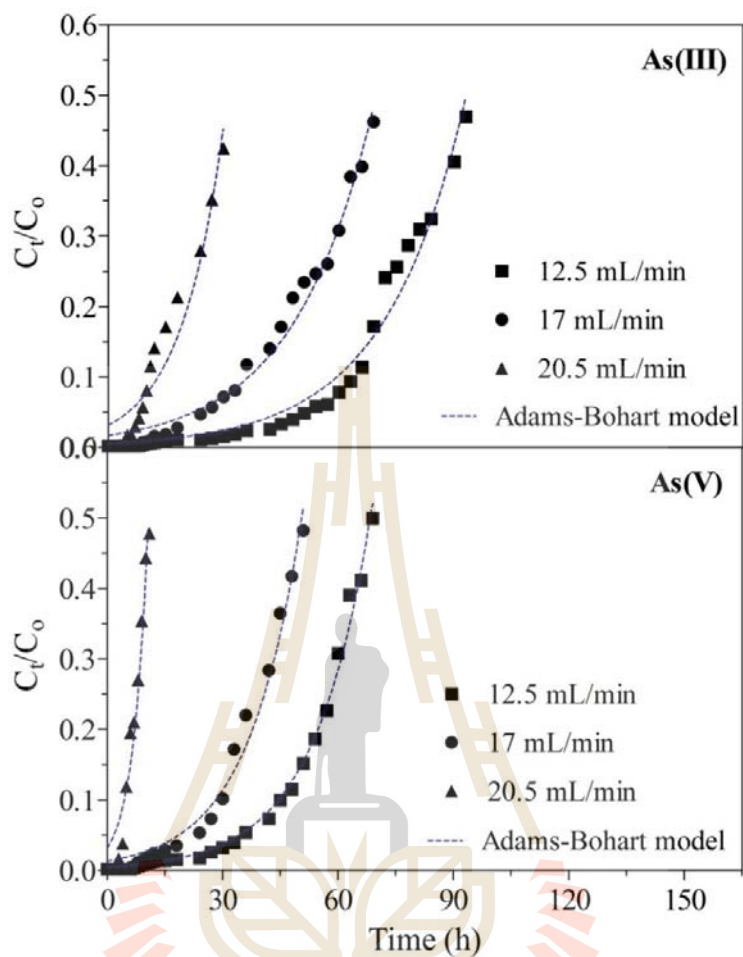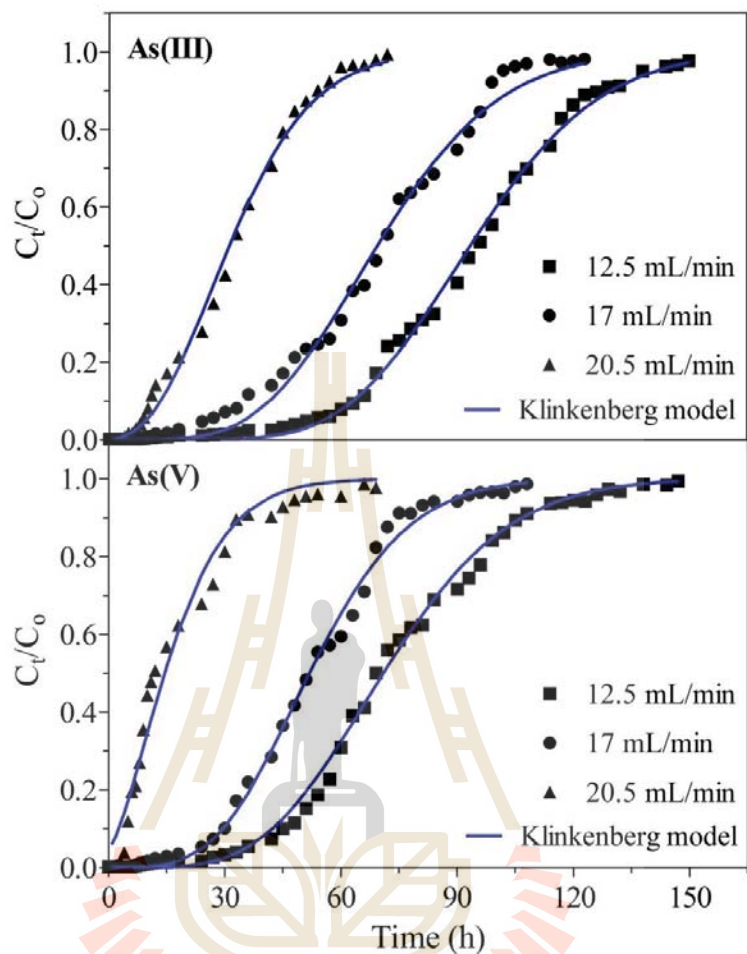
Figure 7.10 Prediction of the Klinkenberg model with different flow rate on adsorpton breakthrough curves of As(III) or As(V) by iron mixed porous pellet adsorbent (initial As(III) or As(V) concentration: 500µg/L; initial solution pH: 7±0.1; temperature: 25±1°C; adsorbent bed height: 10 cm)
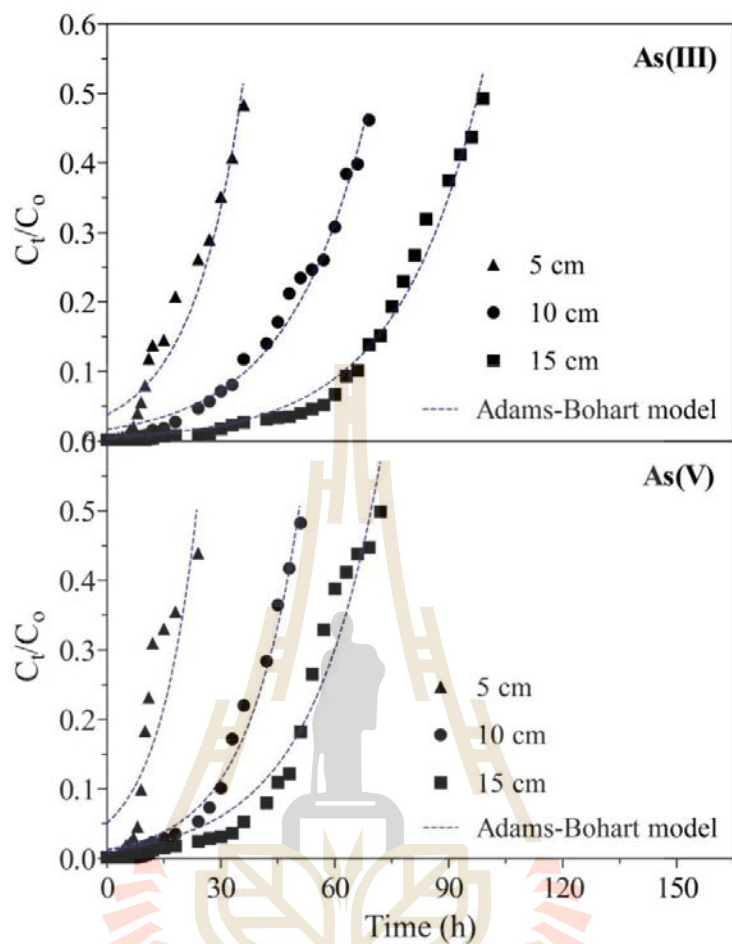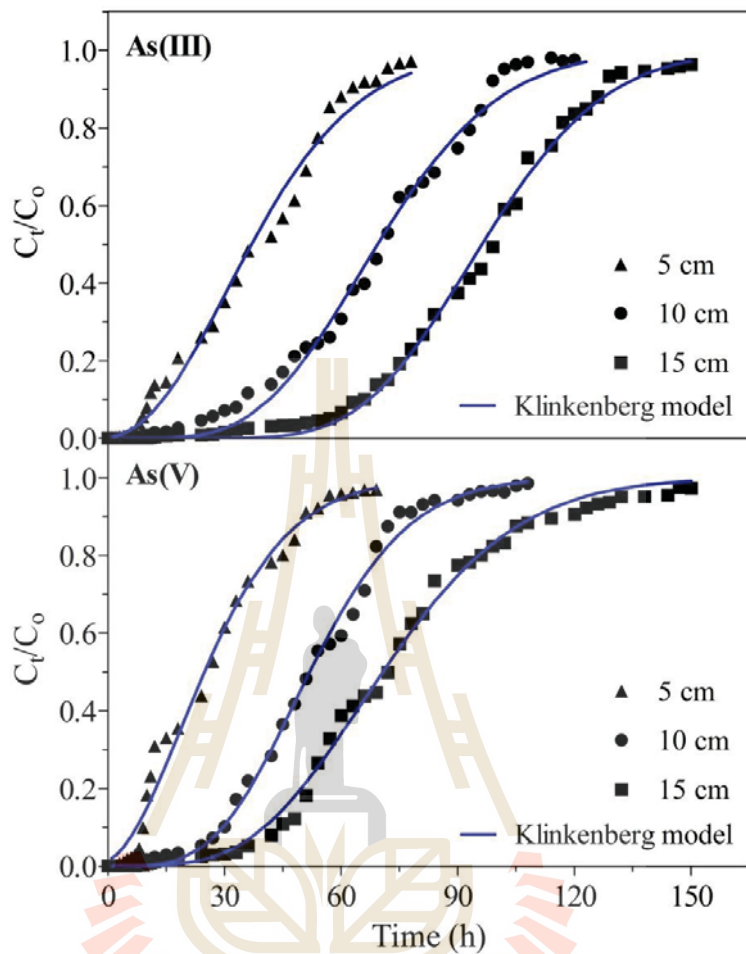
Figure 7.11 Prediction of the Klinkenberg model with different adsorbent bed height on adsorpton breakthrough curves of As(III) or As(V) by iron mixed porous pellet adsorbent (initial As(III) or As(V) concentration: 500μg/L; initial solution pH: 7±0.1; temperature: 25±1°C; influent flow rate: 17 mL/min)
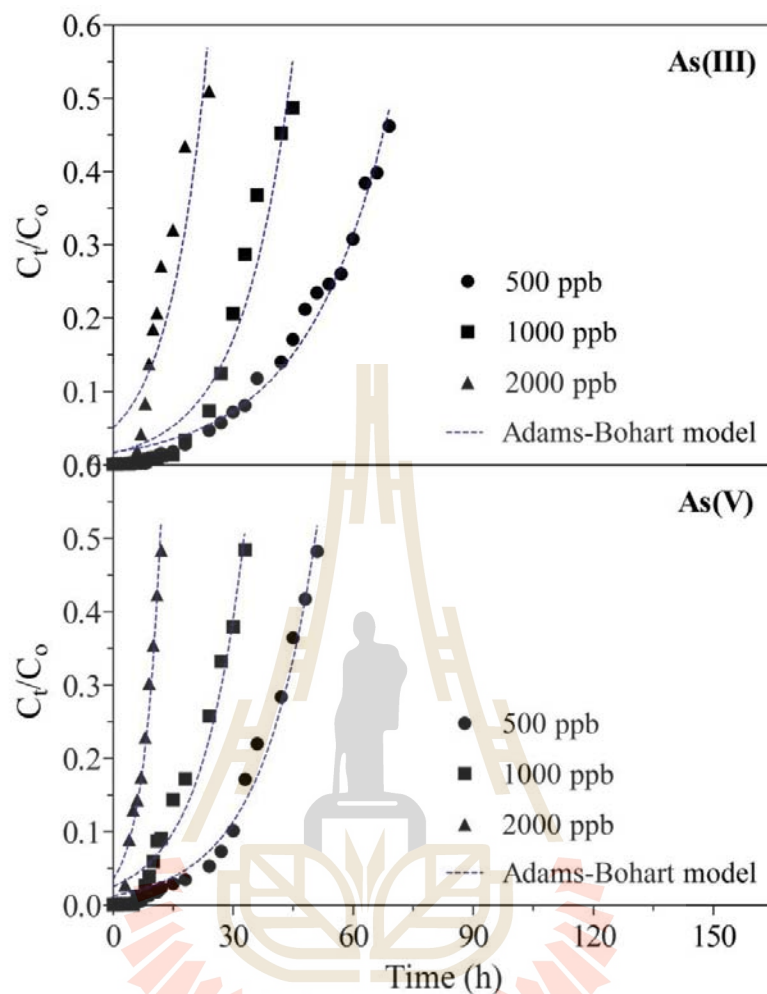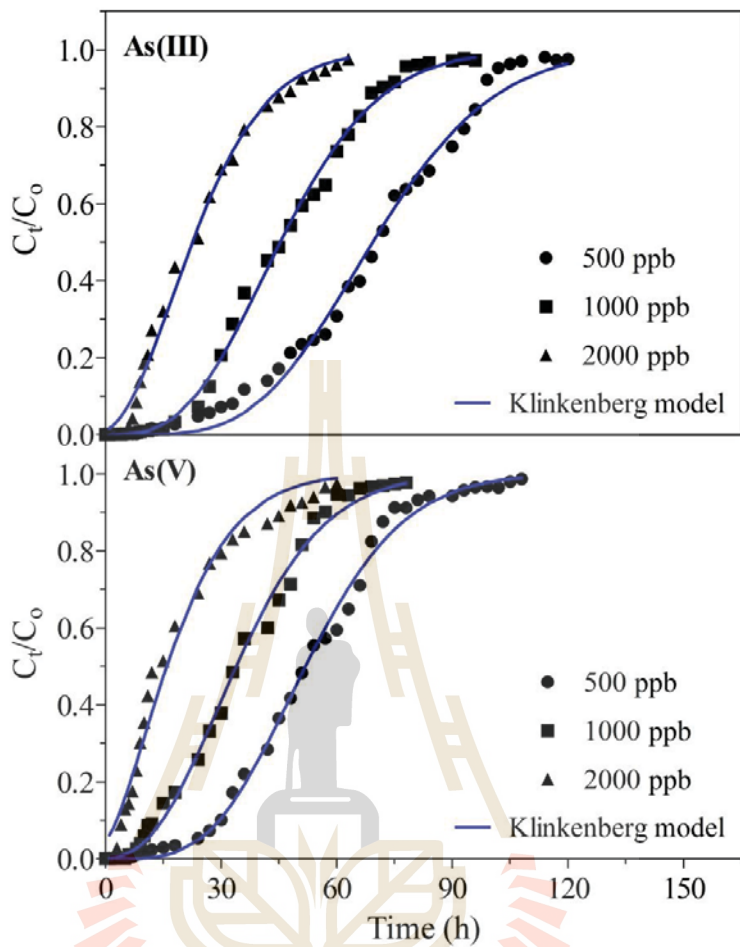
Figure 7.12 Prediction of the Klinkenberg model with different initial concentration on adsorpton breakthrough curves of As(III) or As(V) by iron mixed porous pellet adsorbent (adsorbent bed height: 10 cm; initial solution pH: 7±0.1; temperature: 25±1°C; influent flow rate: 17 mL/min)

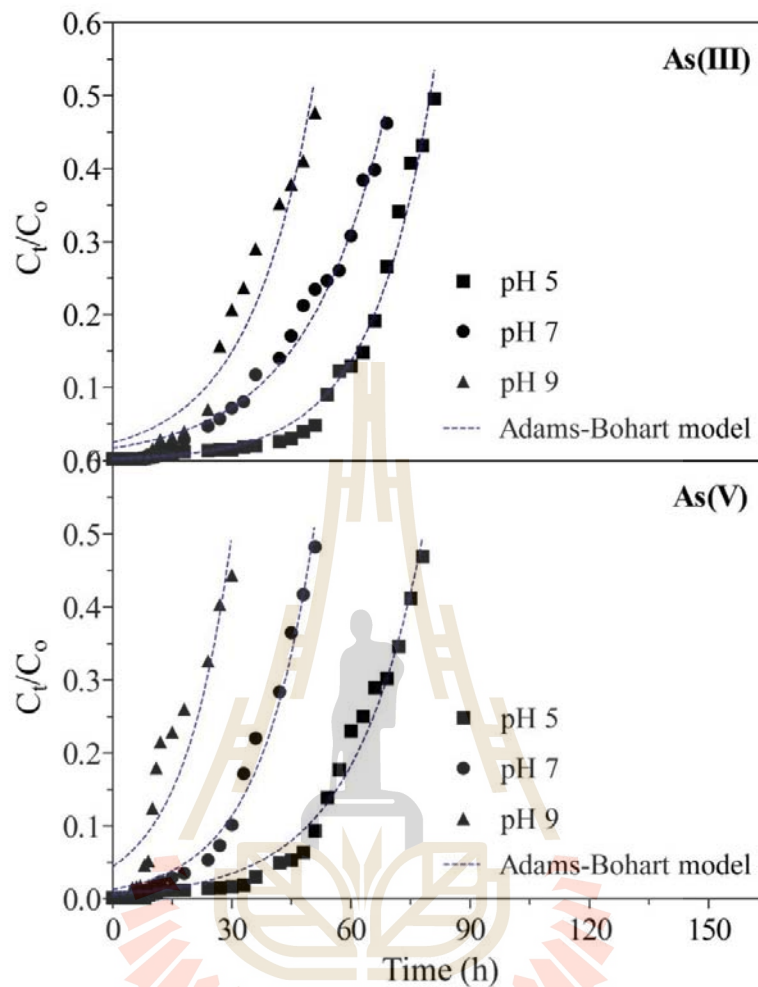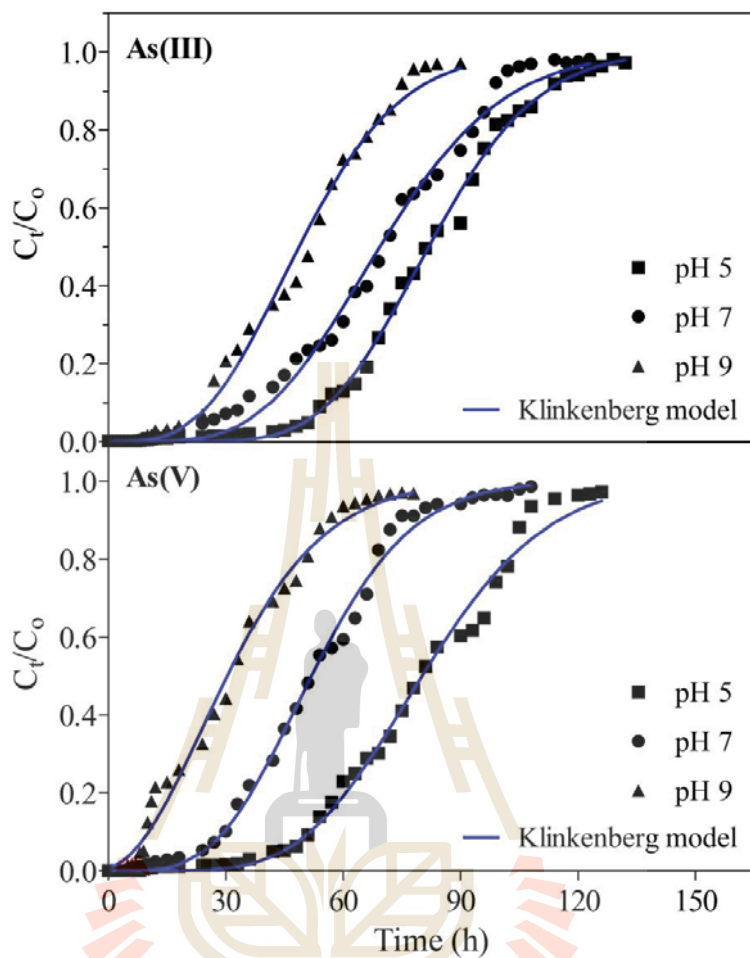**Figure 7.13** Prediction of the Klinkenberg model with different initial solution pH on adsorpton breakthrough curves of As(III) or As(V) by iron mixed porous pellet adsorbent (adsorbent bed height: 10 cm; initial As(III) or As(V) concentration: 500 μg/L; temperature: $25\pm1^{o}C$; influent flow rate: 17 mL/min)

Table 7.6 Parameters for the Klinkenberg model with non-linear fitting in the fixed-bed column for As(III) and As(V) adsorption by the adsorbent

Parameters	C_o (μg/L)	Q (mL/min)	H (cm)	pH	As(III)			As(V)		
					k (1/min)	K	R^2	k (1/min)	K	R^2
Flow rate	500	12.5	10	7	0.0046	931.28	0.9975	0.0038	715	0.9970
	500	17	10	7	0.0039	950.96	0.9913	0.0044	714.67	0.9965
	500	20.5	10	7	0.0038	532.29	0.9953	0.0035	269.96	0.9741
Initial concentration	500	17	10	7	0.0039	950.96	0.9931	0.0044	714.67	0.9965
	1000	17	10	7	0.0038	631.60	0.9970	0.0036	481.09	0.9952
	2000	17	10	7	0.0035	330.65	0.9929	0.0032	245.32	0.9803
Bed height	500	17	5	7	0.0027	1062.44	0.9892	0.0029	734.56	0.9882
	500	17	10	7	0.0039	950.96	0.9931	0.0044	714.67	0.9965
	500	17	15	7	0.0052	867.42	0.9965	0.0033	648.96	0.9966
Initial pH	500	17	10	5	0.0059	1107.71	0.9977	0.0044	1090.99	0.9929
	500	17	10	7	0.0039	950.96	0.9931	0.0044	714.67	0.9965
	500	17	10	9	0.0041	674.96	0.9931	0.0028	442.51	0.9922

For As(III) adsorption, the parameter k decreased with an increase of flow rate, but an inconsistent change of K was observed. Lower initial concentration and initial pH provided higher values of both k and K. Higher value of k was observed for higher bed height, but resulted in lower value of K. For As(V) adsorption, higher value of k and K occurred for lower flow rate. Increasing in an initial adsorbate concentration resulted in decreasing both the value of k and K. An inconsistent change of k was observed with an increase of bed height, but tended to decrease the K values. Lower initial solution pH provided higher values of both k and K. For both As(III) and As(V), the R^2 obtained from the model were found to be higher than 0.97, implying that Klinkenberg model is better for predicting the experimental data.

7.3.7.4 The Bed Depth Service Time (BDST) model

The BDST model is based on the assumptions that the intra-particle mass-transfer resistance and external film resistance are negligible. The model can be expressed as follow (Ghosh et al., 2014):

$$t_b = \frac{HN_b}{C_o \upsilon} - \frac{1}{K_b C_o} \ln\left(\frac{C_o}{C_b} - 1\right) \tag{7.10}$$

$$Z_b = \frac{\upsilon}{K_b N_b} \ln\left(\frac{C_o}{C_b} - 1\right) \tag{7.11}$$

where t_b (h) is the service time at the breakthrough point; H (cm) is the bed height; C_b (mg/L) is the As(III) or As(V) concentration at the breakthrough point; N_b (mg/L) is the column adsorption capacity; K_b (L/mg/h) is the rate constant of the adsorption reaction; υ (cm/h) is the linear flow velocity; Z_b (cm) is the critical bed height or the length of mass transfer zone.

The high values of the correlation coefficient R^2 (>0.95) indicated that the BDST model was valid and applicable for the adsorption of both As(III) and As(V) in this column system (Figure 7.14), implying that the variation of the time

period for the effluent As(III) or As(V) concentration reaching 0.01 mg/L for different bed height was highly linear. The constant parameters of the model and the corresponding critical bed height were evaluated and are presented in Table 7.7.
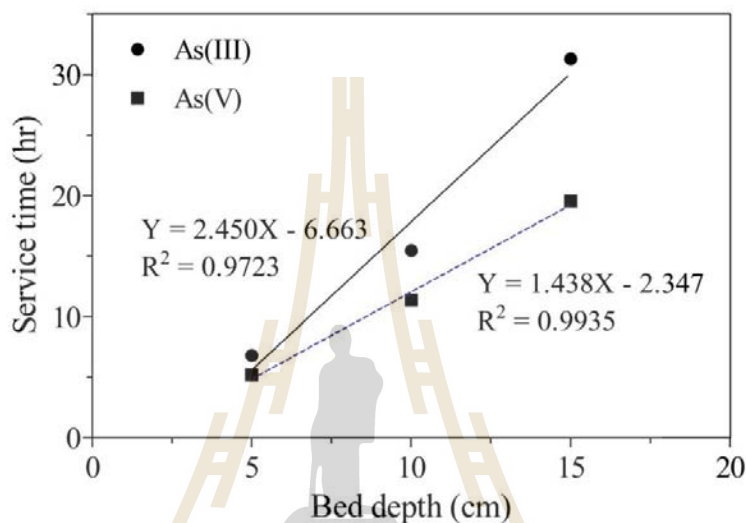
Figure 7.14   The plot of the Bed Depth Service Time (BDST) model on adsorpton of As(III) or As(V) by iron mixed porous pellet adsorbent (inital solution pH: 7±0.1; initial As(III) or As(V) concentration: 500 µg/L; temperature: 25±1°C; influent flow rate: 17 mL/min)

Table 7.7   Parameters for the BDST model in the fixed-bed column for As(III) and As(V) adsorption by the adsorbent

	K_b (L/mg/h)	N_b (mg/L)	Z_o (cm)	R^2
As(III)	1.1682	98.29	2.62	0.9723
As(V)	3.3164	55.62	1.63	0.9935

Generally, a shorter bed height is required to avoid the breakthrough for large value of K_b whereas a longer bed height is needed to avoid the breakthrough for small value of K_b

(Mohan et al., 2017). This suggests that the transfer of As(III) from aqueous solution to the adsorbent in this system required higher bed height compared to the As(V) solution to avoid breakthrough. The minimum bed height for producing As(III) or As(V) effluent within permissible limited concentration of 0.01 mg/L is only 2.62 cm and 1.63 cm for As(III) and As(V), respectively. The adsorption capacity (N_b) results suggested that this column system provided better performance toward As(III) by obtaining higher adsorption capacity of 98.29 mg/L, almost twice the As(V) adsorption capacity (55.62 mg/L).

7.3.8 Application to the real arsenic contaminated groundwater

The adsorbent packed in this column system was also applied for testing with the real arsenic contaminated groundwater collected from Kandal Province, Cambodia. The composition of groundwater was as follow: Arsenic (482.38 µg/L), Manganese (0.42 mg/L), Iron (6.36 mg/L), Fluoride (2.68 mg/L), Nitrate (0.83 mg/L), Chloride (12.08 mg/L), Sulfate (3.14 mg/L), Phosphate (3.15 mg/L), Turbidity (71.7 NTU), pH (7.4), Conductivity (700 µS/cm), and Total hardness (360 mg/L $CaCO_3$). The column was charged with arsenic contaminated groundwater using the flow rate of 17 mL/min in the up-flow mode. The breakthrough behavior obtained for the experimental data is presented in Figure 7.15. The profile indicated that the saturation point could not reach 95% of the influent As concentration, but only 75%. This can be explained by the occurrence of precipitation process between cation ions (Manganese and Iron) and As in the solution. The average iron concentration after adsorption was found to be 0.0216 mg/L. The breakthrough times were 10.63 h with WHO drinking water guideline for As (10µg/L) and 28.08 h with Cambodia drinking water guideline for As (50µg/L), resulting in treating As bearing groundwater 10.84 and 28.64 L, respectively. The saturation time was found to be 94.75 h with the corresponding volume of the treated As groundwater of 96.65 L.
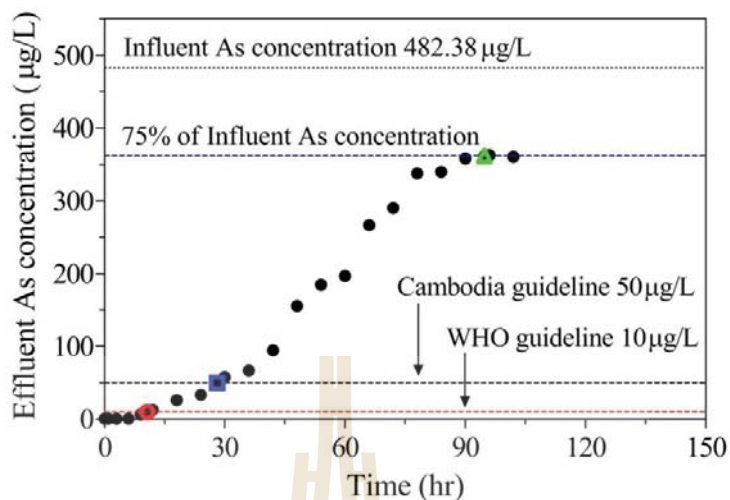
Figure 7.15 The breakthrough profile for treating real arsenic contaminated groundwater by iron mixed porous pellet adsorbent (adsorbent bed height: 10 cm; temperature: $25\pm1^{\circ}$C; influent flow rate: 17 mL/min)

The results suggested that both breakthrough and saturation points occurred shorter than those of the average of As(III) and As(V) adsorption (13.41 h and 96.63 h, respectively). This may be due to the competition for available binding sites on the surface of the adsorbent.

From the batch adsorption study, the presence of coexisting ions strongly influences on the adsorption efficiency of As(III) and As(V) (Te et al., 2017b). The impurities also interfere with the mass transfer between liquid and solid phases (Sun et al., 2014). Basically, a requirement of drinking water for a person is from 2 to 4.5 liters/day (Gleick, 1996). This proves that the adsorbent is capable of removing arsenic from elevated contaminated groundwater in the continuous fixed-bed column to provide enough safe drinking water.

7.3.9   A theoretical design based on experimental results

The design of a domestic filter from the experimental results of treating real arsenic contaminated groundwater is based on the assumption that any family with five members should drink 10 L water per day (2 L water per person). Thus, the water requirement per year will be 365 x 10 = 3650 L (1 year = 365 days). The experimental column was performed with the flow rate of 17 mL/min, and if the designed domestic filter is operated only 10 hours per day with the same flow rate, then the outlet water per day should be 10.2 L.

The arsenic concentration in feeding groundwater is 482.38 μg/L or approximately 0.48 mg/L, so the total arsenic concentration in the 3650 L raw water will be 0.48 mg/L x 3650 L = 1752 mg-As. The experimental results indicated that the breakthrough time of the column would be 10.63 h, corresponding for obtaining the adsorption capacity of 40.54 μg/g or approximately 0.04 mg-As/g-adsorbent. Thus, the total required amount of adsorbent to be used for treating 1752 mg-As will be 1752/0.04 = 43800 g-adsorbent or 43.8 kg-adsorbent. The expression of the required amount of adsorbent in terms of volume unit will be 43800/1.986 = 22054.4 cm^3 (particle density of adsorbent = 1.986 g/cm^3).

The dimension of domestic column filter should be selected to sufficiently hold approximately 22055 cm^3 adsorbent used. If the column diameter is 20 cm (approximately 5 times the lab scale column), then the required height of the column should be (4 x 22055 cm^3)/(3.14 x 20^2) = 70.23 cm. To provide enough space for supporting material like sand, the height can be chosen to be 100 cm. So, the designed column filter with diameter of 20 cm and height of 100 cm operated with flow rate of 17 ml/min at 10 hours per day will provide drinking water of potable standard for a period of 1 year.

7.4   Conclusion

Natural clay was successfully utilized as a binder on metal oxides or metal particles and developed to be iron-mixed porous pellet adsorbent for adsorption application on removing either As(III) or As(V) from water in a continuous fixed-bed column. Both As(III) and As(V) adsorption in the column packed with this adsorbent had similar breakthrough curve profiles while varying different adsorption parameters such as influent flow rate, adsorbent bed height, initial solution pH and initial adsorbate concentration. However, for most cases, a better performance toward removing As(III) compared to As(V) in this adsorbent packed column system was observed. The application of the same column system to treat a real As contaminated groundwater proves that the adsorbent still efficiently worked on removing As with approximate concentration 50 times higher than that of WHO guideline to the acceptable level.

CHAPTER VIII

ENCHANCING THE QUALITY OF ARSENIC CONTAMINATED GROUNDWATER USING BIO-SAND FILTER WITH IRON MIXED POROUS ADSORBENT

8.1 Introduction

The direct consumption of arsenic (As) contaminated drinking water, at any high concentration, can lead to the development of many incurable or fatal diseases. In Cambodia, large numbers of households, particularly in rural areas, still rely on groundwater from boreholes for drinking because it is considered relatively free of pathogens. In many regions, however, such as Kratie, Kandal, and areas south and southeast of Phnom Penh, elevated As concentrations, exceeding the WHO recommended guideline level of 10 µg/L, have been reported (Karagas et al., 2015; Luu et al., 2009). This may arise from natural enrichment by geothermal activity in the upper Mekong basin (Luu et al., 2009).

The concentration of As in groundwater in Kandal province has been reported at up to 1,543 µg/L, with As concentrations up to 6,000 µg/L elsewhere (Kang et al., 2014; Luu et al., 2009). Arsenic-poisoning (arsenicosis) is a major concern to millions in Cambodia as water consumption from tube wells is high (Kang et al., 2014). Thus, treating As-contaminated groundwater to provide potable supplies at household-scale is very necessary.

Numerous conventional, household-scale, water treatment systems are available, mostly for enhancing the microbial quality of water, and include filtration, flocculation,

chlorination and solar disinfection (Ahammed and Davra, 2011). Bio-sand filters (BSFs) have been gaining more attention for household water treatment since their initial design and development in the early 1990s, because of their high pollutant removal efficiency, technical simplicity, cost-effectiveness, low maintenance needs, ability to produce large volumes of treated water, and use of local materials (Baig et al., 2011; Mahmood et al., 2011; Stauber et al., 2012). The BSF is a small-scale, intermittently operated, slow sand filter with concrete filter bodies for household use (Ahammed and Davra, 2011; Stauber et al., 2012). Concrete BSFs use several types of material, take lots of time to build and are heavy, making them difficult to transport. The recently introduced plastic BSF may overcome those drawbacks.

The conventional BSF was initially designed to remove suspended solids and microbes using sand media, considered a non-reactive material in filtration (Baig et al., 2011; Noubactep and Caré, 2010). To improve its As-removal performance, more affinitive and active media must be used. The strong affinity between inorganic As species and iron is well known (Kang et al., 2014). Many iron-based adsorbents have shown promise in As removal, e.g., montmorillonite-supported nanoscale zero-valent iron, porous ceramic adsorbent, iron-mixed ceramic pellets, and iron-mixed porous pellet adsorbent (Bhowmick et al., 2014; Chen et al., 2010; Shafiquzzam et al., 2013; Te et al., 2017b). However, those studies were conducted in batch mode and no study has been made of the use of iron-mixed porous adsorbent in a BSF to treat a real As-contaminated groundwater.

In this study, a plastic BSF was used, with an iron-mixed porous pellet adsorbent as the active medium between the sand layers, to remove As from contaminated groundwater. Preferential flow rate, filtration rate, As adsorption efficiency, pH variation, turbidity removal, iron and organic carbon leaching, and dissolved oxygen were investigated.

8.2   Materials and Methods

8.2.1   Adsorbent preparation

The iron-mixed porous pellet adsorbent was prepared by binding iron oxide (19.22%), iron powder (28.63%) and rice bran (15%) with natural clay (52.15%). Iron oxide powder (Fe_2O_3) and iron powder (Fe^0) were purchased from Italmar chemical supply company (Thailand) and a local supply store, respectively. The natural clay used was collected from the field in Dankwian District, Nakhon Ratchasima 30000, Thailand. Deionized water was added slowly to the mixture to produce a homogeneous paste, which was stirred strongly by hand for 5 to 10 minutes and dried at $104\pm1°C$ for 24 hours, before further heating at $600°C$ for 2 to 3 hours in a muffle furnace to carbonize the rice bran. After cooling, the product was sieved to produce the desired particle size of 0.6 to 1.12 mm. The resulting adsorbent had a specific surface (BET) of 19.393 m^2/g, mean pore size 20.169 nm, particle density 1.986 g/cm^3, skeletal density 2.465 g/cm^3, and point of zero charge 7.50.

8.2.2   Filter installation and operation

The filter was built with 5 mm thick polyvinyl chloride (PVC) pipe bought from the local market. It was 1 m tall with internal diameter 20 cm. It is referred to herein as the lightweight modified bio-sand filter (LMBSF) and illustrated in Figure 8.1. The filter consisted of 5 cm of gravel (2 to 4 cm), 5 cm of coarse sand (1.5 to 3 mm), and 60 cm of fine sand (0.5 to 1.5 mm), the latter including a 10 cm iron-mixed porous pellet adsorbent layer in the middle. To minimize air space development and short circuiting, the media were placed in the filter with water present. A plastic diffusion plate, 5 cm above the retaining water, helped distribution of the daily influent water. The filter's maximum holding capacity was 31.4 L and it was operated intermittently using real As-contaminated
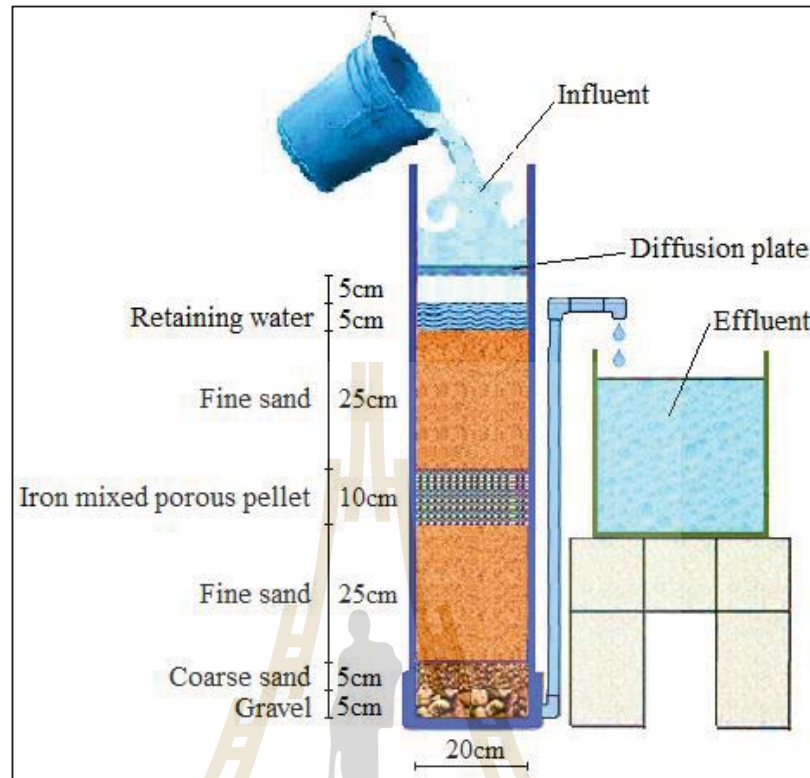
Figure 8.1   Schematic diagram of lightweight modified bio-sand filter (LMBSF)

groundwater collected from the field twice a day. The second charge was done 6 hours after the first and each charge comprised 15 L. The experiments were conducted at room temperature – i.e., 25 to 35°C. The raw water never stood, after collection, for more than 12 hours prior to being treated.

8.2.3   Influent water

The influent water was collected from a tube well at Dei Eith Primary School, Kien Svay district, Kandal province, Cambodia, which is in a well-known As contamination zone. The feed water characteristics are presented in Table 8.1, and it is noted that the water's As concentration is very high compared to the maxima recommended by both WHO (10 μg/L) and the Cambodian authorities (50 μg/L) (Kang et al., 2014).

Table 8.1   Characteristics of groundwater used in the experiments

Parameters	Value	Cambodian Standard
Arsenic (μg/L)	363.3-587	50
Manganese (mg/L)	0.42	0.10
Iron (mg/L)	4.1-6.62	0.30
Fluoride (mg/L)	2.68	1.50
Nitrate (mg/L)	0.83	50
Chloride (mg/L)	12.08	250
Sulfate (mg/L)	3.14	250
Phosphate (mg/L)	3.15	-
Turbidity (NTU)	42.5-75	5
pH	7.03-7.43	6.5-8.5
Conductivity (μS/cm)	700	1500
Total Hardness (mg/L CaCO$_3$)	360	300
Total Organic Carbon (mg/L)	31.2-74.1	-

8.2.4   Tracer test

The tracer test was conducted to evaluate the hydraulic performance of the filter, particularly with respect to preferential flow paths, if any. The test was run at the start of treatment before any As-contaminated water had been put through the system. The filter was fed with 2.5 L of 300 mg-NaCl/L solution (the tracer) after the retaining water was decanted, after which distilled water was poured in continuously to push the tracer further down in the media. Effluent samples were collected at pre-set time intervals and their electrical conductivity (EC) measured is a proxy for NaCl concentration.

8.2.5 Sample collection and parameter analysis

Influent and effluent samples were collected at the start of feeding and at the end of the last raw water feed, respectively. Sample portions were filtered immediately through a 0.22 μm syringe filter, acidified with concentrated HNO_3, and kept at $4\pm1°C$ for As determination. The remaining samples were analyzed for parameters including turbidity, pH, dissolved oxygen (DO), iron, and total organic carbon (TOC). The pH, DO and EC were measured using digital meters, and turbidity was measured with a Hach turbidimeter. Iron was analyzed by colorimetric spectrophotometry, and TOC was analyzed using the Walkley-Black titration method. The As concentration was determined by ICP-OES.

8.3   Results and discussion

8.3.1   Tracer test

The EC values from the tracer test produced a bell-shaped curve, indicating that the tracer concentration rose rapidly in the treated effluent and then dropped sharply to its initial concentration while being washed out (Figure 8.2). From the cumulative fraction data, the times for 10 and 90% tracer recovery from the filter were about 19 and 35 minutes, respectively. Using the technique, demonstrated by Tchobanoglous et al. (2003), the Morrill Dispersion Index (MDI) and volumetric efficiency were 1.82 and approximately 55%, respectively. The United States Environmental Protection Agency (USEPA) classifies flow with an MDI below 2.0 as effective plug flow, while the MDI of an ideal plug flow reactor is 1.0 (Bradley et al., 2011). Thus, preferential flow could be established for aqueous solutions through the media in LMBSF.
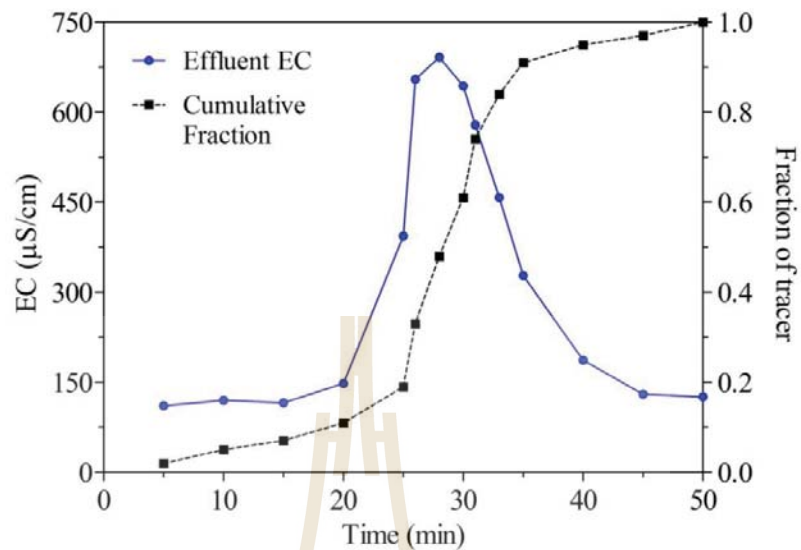
Figure 8.2   Tracer study results for the new introduced bio-sand filter

8.3.2   Filtration rate

The filtration rate was observed by measuring the flow rates at the start (immediately after charging), and 5 and 10 minutes after introduction of 5 L of influent. The results are presented in Figure 8.3. The starting flow rate declined progressively from 678 to 166 mL/min after 30 days of testing. The 5 and 10 minute flow rates fell gradually from 267 to 140 mL/min and 122 to 114.5 mL/min, respectively. The fall in hydraulic flow rate over time was caused by the drop in water level in the headspace. The fall observed over the test period is attributed to maturation and particle accumulation in the filter media. Head loss accumulation has a significant effect on the time needed to provide the desired effluent volume. The production of 15 L of As-treated groundwater was approximately 44 minutes for the first 3 operating days, but rose to about 3 hours on the last day.
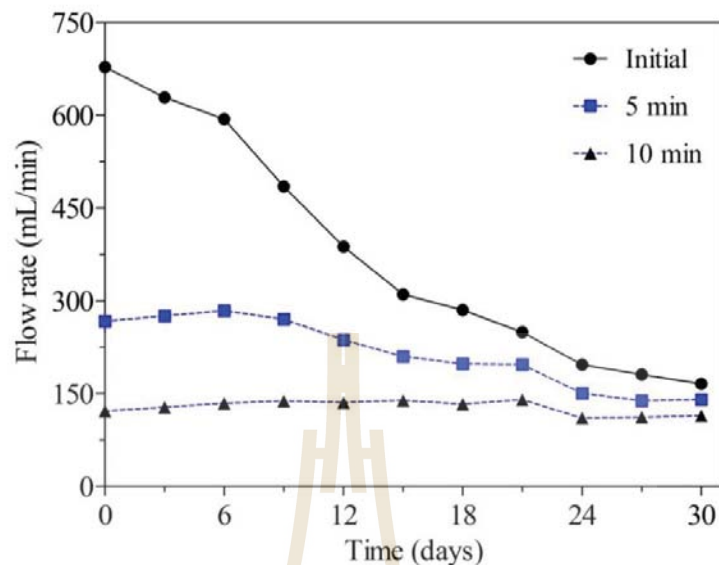
Figure 8.3   Variation of hydraulic flow rates of the filter during the treatment periods

8.3.3   Arsenic removal

The influent and effluent As concentrations, and the filter's As-removal efficiency are illustrated in Figure 8.4. The results show that, with the groundwater As-concentration in the range 355 to 587 µg/L, the filter achieved removal efficiencies of between about 97 and 99.5%, during the 30-day study period. For the first 24 days, As-removal efficiency varied little, fluctuating slightly at over 99%, with the effluent arsenic concentration within the WHO drinking water guideline. The removal efficiency decreased, with significant fluctuation, after 24 days, falling to about 97% on day 30. The effluent As-concentration on day 30 was about 16.5 µg/L, exceeding the WHO guideline, and the filter was stopped.
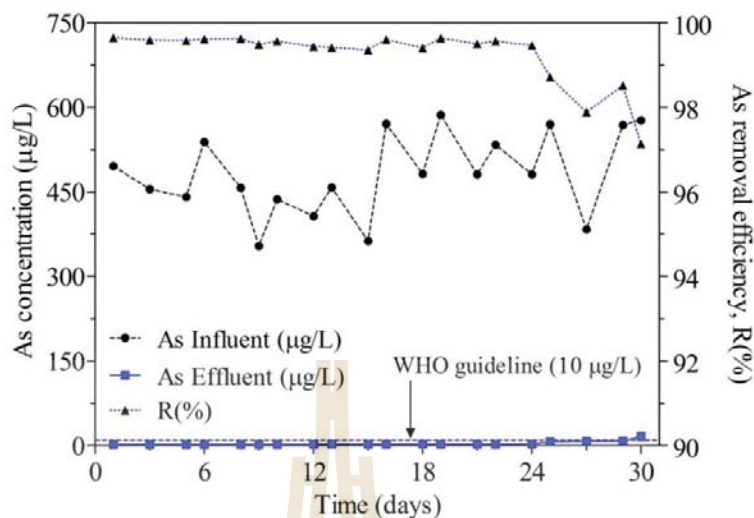
Figure 8.4   Arsenic removal from groundwater over the periods of operation

As-removal performance decreased with time, suggesting surface saturation in the filter media. The presence of Fe in groundwater can lead to arsenic removal through co-precipitation, when dissolved Fe is oxidized to form iron (hydro)oxide precipitates (Roberts et al., 2004; Smith et al., 2017). However, the contribution of Fe to arsenic removal can be altered by the presence of phosphate in groundwater, as the latter is well known as a competitor with arsenic for adsorption sites on iron oxide (Chiew et al., 2009; Tyruvola et al., 2006). Some previous researchers have attempted to introduce modified bio-sand filter for arsenic removal but the efficiency of their systems was low compared to that of LMBSF. Ngai et al. (2007) introduced brick chips and iron nails on the diffuser in the bio-sand filter to treat groundwater (> 50 μg-As/L) and achieved arsenic removal from 88 to 95%. Similarly, Chiew et al. (2009) found that a bio-sand filter containing iron nails could achieve As uptake efficiency between 39 and 75% from groundwater with As concentration exceeding 146 μg/L, phosphorus > 0.91 mg-P/L and iron < 5 mg-Fe/L.

Smith et al. (2017) report that nails embedded in the top sand layer treated influent As (226 to 240 μg/L) to achieve a maximum removal rate of 81%. Shah et al.

(2013) used Pinus bark and brick powder in the filter's middle sand layer to remove influent arsenic ranging from 50 to 350 µg/L, without involving co-existing ions, and obtained As-removal of between 80 and 100%. Baig et al. (2013) used iron-coated, honeycomb briquette cinders in the middle sand layer and demonstrated that the As-removal efficiency from an influent containing 200 µg/L of arsenic dropped to 60% after 24 days.

8.3.4 Variations of pH

The pH of the influent and effluent waters changed within the ranges 7.0 to 7.4 and 7.4 to 7.7, respectively (Figure 8.5). Increased effluent pH levels up to 9.0, from the influent level of 7.5, were observed in a sand filter containing iron filings and powder (Biterna et al., 2007). In an arsenic filter in Kanchan-Nepal, an increase of 0.37 pH units was reported after filtration (Ngai et al., 2007). Baig et al. (2013) reported that, using their sand filter containing iron-coated honeycomb briquette cinders, the effluent pH was in the range 7.5 to 8.1 when the influent pH was 7.1.
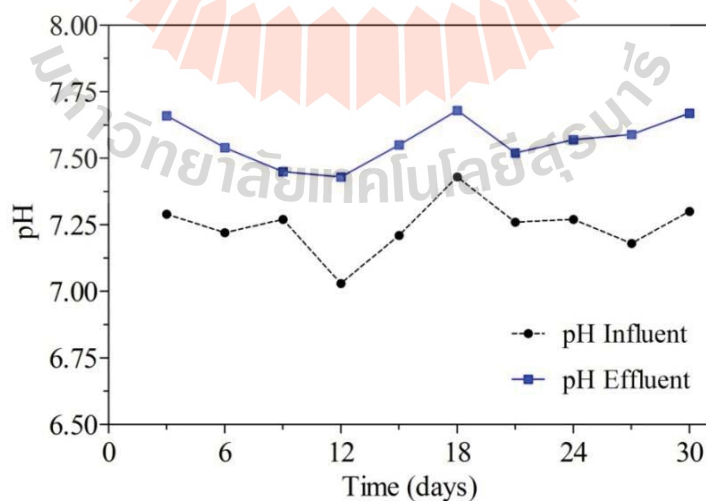
Figure 8.5   Influent and effluent pH during the operation period of the filter

The increases in pH after filtration could arise from carbonate mineral dissolution from the sand particles, and/or the release of OH⁻ groups as a result of ligand exchange during

adsorption onto the adsorbent surface (Biterna et al., 2007; Ngai et al., 2007; Tiwari and Lee, 2012).

8.3.5 Turbidity removal

The influent and effluent turbidities ranged from 42 to 75 NTU and 0.2 to 1.6 NTU, respectively, representing removal efficiency of 97 to 99% (Figure 8.6). The filter produced effluent turbidity below 5 NTU throughout the treatment period, perhaps because of pollutant-ion attachment on the filter media surface as well as the presence of precipitates from the influent. Turbidity removal by LMBSF exceeded that from some previous studies, e.g., 93% for Kanchan (Ngai et al., 2007), up to 96% for a bio-sand filter modified with iron oxide-coated sand (Ahammed and Davra, 2011), and up to 91.5% for a brass/zero valent iron filter (Yildiz, 2016).
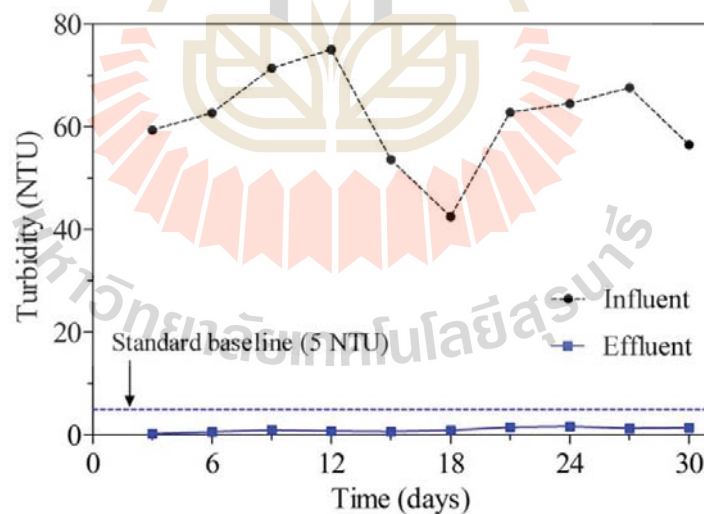
Figure 8.6   Turbidity removal for the influent and effluent

8.3.6 Leaching of iron and total organic carbon

The influent iron concentration varied between 4.1 and 6.6 mg/L. The effluent iron concentration, however, was between 0.01 and 0.03 mg/L, below the maximum recommended level (0.3 mg/L) for drinking water – see Figure 8.7. Iron removal

efficiency exceeded 99% throughout the treatment period. The dissolved iron in the influent groundwater could be oxidized and precipitated, and then trapped in the filter media layers. Low iron concentrations (< 0.3 mg/L) in the treated water improve its appearance and taste, and make its use socially acceptable (Ngai et al., 2007).

Figure 8.8 shows the TOC concentrations of the influent and effluent during the trial. The influent TOC varied between 31.2 and 74.1 mg/L – the limit of detection was 2 mg/L and TOC was never detected in the effluent. The filter removed TOC efficiently. Even using rice bran as the porosifier, there was no leaching of organic carbon to the treated water.
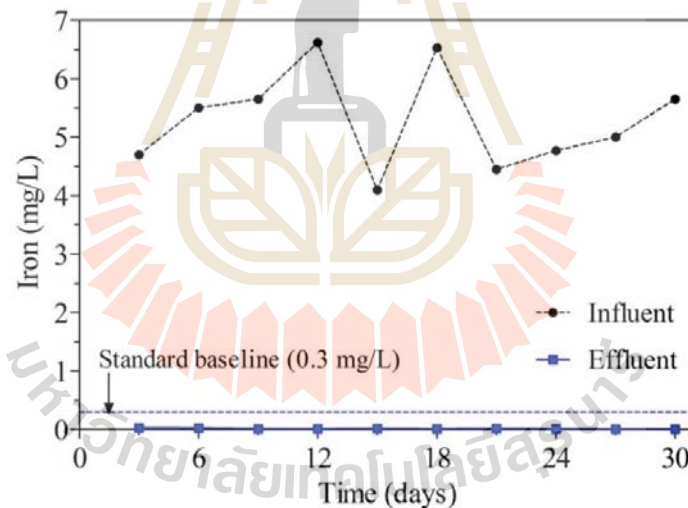
Figure 8.7 Variation of iron concentration in the influent and effluent water during the operation of the filter
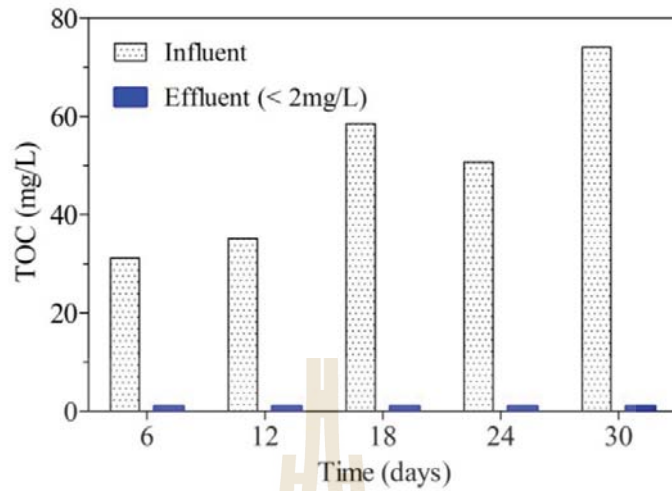
Figure 8.8   TOC variation in the influent and effluent water for the filter operation

8.3.7   Dissolved oxygen

The effluent DO concentration is shown in Figure 8.8. It appears that the oxygen concentration in water passing through the filter decreased during the 30-day treatment.
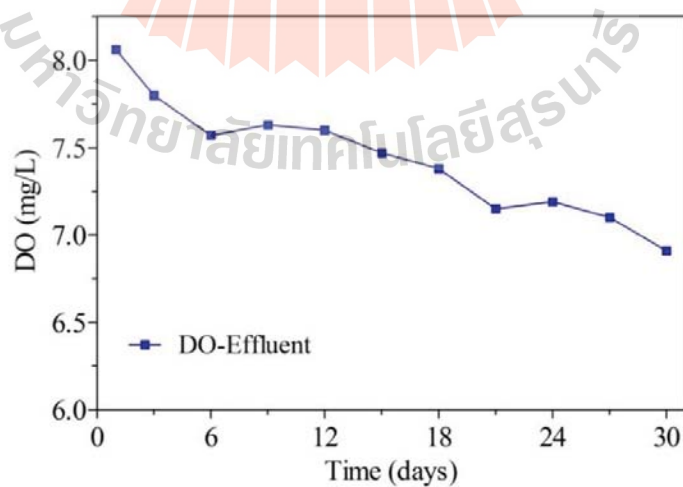
Figure 8.9   Dissolved oxygen variation for effluent during the treatment

Initially, the effluent DO was 8.1 mg/L, but it had fallen to 6.9 mg/L on the last day. DO concentrations exceeding 1 mg/L could imply aerobic conditions in the filter bed (Yildiz 2016) and this might contribute to improved As-removal. The predominant arsenic species found in groundwater is trivalent but it oxidizes quickly to pentavalent arsenic, which binds more strongly to iron hydroxides (Baig et al., 2013). However, the results obtained may not represent aerobic conditions within the filter bed, but rather interference from atmospheric oxygen at the outlet during sample collection. Further research is needed to develop suitable methods for measuring DO concentrations within the filter bed.

8.4 Conclusion

Iron mixed porous pellet adsorbent embedded in the middle sand layer of the lightweight bio-sand filter demonstrated to have an efficient arsenic removal. With the daily influent charge of 30 L, the effluent arsenic concentration after the filtration was lower than the WHO guideline (10 μg/L) over 29 days of treatment time. The breakthrough concentration would take longer than this if the Cambodian standard for arsenic (50 μg/L) were applied. The filter was also able to efficiently remove high turbidity from the groundwater. For a month period, turbidity of the treated water was lower than the WHO acceptable level (5 NTU) for drinking purposes. Applying iron oxide, iron powder and rice bran for developing the adsorbent used in the filter would not result in a health risk for their leaching in the filtered water. Therefore, introducing the surface amended adsorbent layer in lightweight bio-sand filter could be a sufficiently safe practice for providing arsenic safe drinking water at household scale in the arsenic contaminated areas in Cambodia. However, this study only accounted for one specific location as a raw groundwater source for feeding the filter.

CHAPTER IX

CONCLUSIONS AND RECOMMENDATIONS

9.1   General conclusions

This research initiates the idea of utilizing natural clays as hosts and binders to iron species, i.e., ferrous and ferric solutions, iron oxide, and zero valent iron (iron powder) to be a low-cost and effective adsorbent toward arsenic adsorption from aqueous solutions. This dissertation project consists of five main investigations: 1) preparing the iron-impregnated calcined natural clays as adsorbents for arsenic removal from water, 2) developing iron-mixed porous pellet adsorbent with a mixture design approach for As(III) and As(V) adsorption, 3) optimizing the batch experimental conditions for treating a combined As(III) and As(V) solution using response surface methodology, 4) removing As(III) and As(V) in a fixed-bed column study, and 5) treating a real As contaminated groundwater in Cambodia with a modified bio-sand filter. Their main findings are as follow:

Natural clay could be stabilized the particle size by a calcination technique. Iron impregnation on MC through a simple coating technique improved the iron oxide content for MC-FeII and MC-FeIII, as well as their adsorption efficiencies. The pseudo-second order rate is the most suitable model to describe both As(III) and As(V) adsorption by all adsorbents, except for As(III) removal by MC. In both adsorption cases, all adsorbents exhibited a significant decline in the uptake efficiency for pH greater than 9. The estimated maximum adsorption capacities of MC, MC-FeII, and MC-FeIII were 46.73, 354.99 and 230.47µg/g, respectively for As(III) adsorption, and 250, 747.38, and 429.7µg/g,

respectively for As(V) adsorption. Among added coexisting anions, phosphate (PO_4^{3-}) significantly decreased the arsenate adsorption capacity of all adsorbents in either As(III) or As(V) adsorption.

The augmented simplex-centroid mixture design method was a successful and useful tool to optimize the proportion of the constituent materials of the adsorbent. In the batch adsorption, the optimized adsorbent expressed a favorable adsorption toward both As(V) and As(III) even though the certain extent reduction of the efficiency occurred in the presence of some anions, especially phosphate. The adsorbent maintained high adsorption efficiency after several times of regeneration, was easily separated from the aqueous solution, and was non-hazardous solid waste after adsorption.

The new developed mesoporous pellet adsorbent has been used to adsorb simultaneously As(III) and As(V) from water in the batch mode experiment and the composite central design under response surface method was applied to study the process optimization based on the influence of the operational parameters such as contact time, solution pH, adsorbent dose and initial concentration. The ANOVA analysis suggested the second polynomial mathematical model should be used and its adequacy was supported by F-value, P-value, R^2 and R^2-adj. The residual data was confirmed to have a normal distribution by the residual and normality plots. Solution pH, adsorbent dose and initial concentration provided the most percentage effect on the response. The optimum values of contact time, initial pH, adsorbent dose and initial adsorbate concentration were 52h, 7, 10g/L and 0.5mg/L, respectively. The confirmatory experiment is in agreement with the predicted model.

Natural clay was successfully utilized as a binder on metal oxides or metal particles and developed to be iron-mixed porous pellet adsorbent for adsorption application on removing either As(III) or As(V) from water in a continuous fixed-bed column. Both As(III) and As(V) adsorption in the column packed with this adsorbent had similar

breakthrough curve profiles while varying different adsorption parameters such as influent flow rate, adsorbent bed height, initial solution pH and initial adsorbate concentration. However, for most cases, a better performance toward removing As(III) compared to As(V) in this adsorbent packed column system was observed. The application of the same column system to treat a real As contaminated groundwater proves that the adsorbent still efficiently worked on removing As with approximate concentration 50 times higher than that of WHO guideline to the acceptable level.

Iron mixed porous pellet adsorbent embedded in the middle sand layer of the lightweight bio-sand filter demonstrated to have an efficient arsenic removal. With the daily influent charge of 30 L, the effluent arsenic concentration after the filtration was lower than the WHO guideline (10 μg/L) over 29 days of treatment time. The breakthrough concentration would take longer than this if the Cambodian standard for arsenic (50 μg/L) were applied. The filter was also able to efficiently remove high turbidity from the groundwater. For a month period, turbidity of the treated water was lower than the WHO acceptable level (5 NTU) for drinking purposes. Applying iron oxide, iron powder and rice bran for developing the adsorbent used in the filter would not result in a health risk for their leaching in the filtered water. Therefore, introducing the surface amended adsorbent layer in lightweight bio-sand filter could be a sufficiently safe practice for providing arsenic safe drinking water at household scale in the arsenic contaminated areas in Cambodia.

9.2   Recommendations for future works

With regard to the utilization of natural materials like natural clays for developing cost-effective and efficient adsorbents for solving the problem of arsenic contaminated water, some aspects as supplements to this research project are worth to fulfill in the future works. Those are as follows.

- Collecting natural clays from other locations or different countries for developing clay-based adsorbents to investigate on the arsenic adsorption

- Applying modified bio-sand filter to many arsenic contaminated areas to solidify the sustainable use of this treatment system

- Investigating the performance of iron-mixed porous pellet adsorbents in a community-based water treatment plant for arsenic contaminated regions

- Investigating the possibility of arsenic leaching from arsenic-bearing iron-mixed porous pellet in the field environment and design a proper and sustainable arsenic-bearing solid waste management

- Treating wastewater containing high arsenic concentration using iron-mixed porous pellet adsorbent

REFERENCES

Abdullah, N., and Chin, N.L. (2010). Simplex-centroid mixture formulation for optimised composting of kitchen waste. **Bioresource Technology.** 101(21): 8205-8210.

Afroze, S., Sen, T.K., and Ang, H.M. (2015). Adsorption performance of continuous fixed bed column for the removal of methylene blue (MB) dye using Eucalyptus sheathiana bark biomass. **Research on Chemical Intermediates.** 42(3): 2343-2364.

Ahamed, M.M., and Davra, K. (2011). Performance evaluation of biosand filter modified with iron oxide-coated sand for household treatment of drinking water. **Desalination.** 276(1-3): 287-293.

Ahma, R., and Hasan, I. (2016). Optimiztion of the adsorption of Pb(II) from aqueous solution onto PAB nanocomposite using response surface methodology. **Enivronmental Nanotechnology, Monitoring and Management.** 6(2016): 116-129.

Ahmad, A.A., and Hameed, B.H. (2010). Fixed-bed adsorption of reactive azo dye onto granular activated carbon prepared from waste. **Journal of Hazardous Materials.** 175(1-3): 298-303.

Ali, I. (2012). New generation adsorbents for water treatment. **Chemical Reviews.** 112(10): 5073-5091.

Alidokht, L., Khataee, A.R., Reyhanitaba, A., and Oustan, S. (2011). Cr(VI) immobilization process in a Cr-spiked soil by zerovalent iron nanoparticle: Optimzation using response surface methodology. **Clean- Soil, Air, Water.** 39(7): 633-640.

Auta, M., and Hameed, B.H. (2014). Chitosan–clay composite as highly effective and low-cost adsorbent for batch and fixed-bed adsorption of methylene blue. **Chemical Engineering Journal.** 237: 352-361.

BahramParvar, M., Tehrani, M.M., Razavi, S.M., and Koocheki, A. (2015). Application of simplex-centroid mixture design to optimize stabilizer combinations for ice cream manufacture. **Journal of Food Science and Technology.** 52(3): 1480-1488.

Baig, S.A., Mahmood, Q., Nawab, B., Shafqat, M.N., and Pervez, A. (2011). Improvement of drinking water quality by using plant biomass through household biosand filter – A decentralized approach. **Ecological Engineering.** 37(11): 1842-1848.

Baig, S.A., Sheng, T., Hu, Y., Lv, X., and Xu, X. (2013). Adsorptive removal of arsenic in saturated sand filter containing amended adsorbents. **Ecological Engineering.** 60: 345-353.

Baig, S.A., Sheng, T., Hu, Y., Xu, J., and Xu, X. (2015). Arsenic removal from natural water using low cost granulated adsorbents: a review. **CLEAN - Soil, Air, Water.** 43(1): 13-26.

Barakat, M.A., and Ismat-Shah, S. (2013). Utilization of anion exchange resin Spectra/Gel for separation of arsenic from water. **Arabian Journal of Chemistry.** 6(3): 307-311.

Baral, S.S., Das, N., Ramulu, T.S., Sahoo, S. K., Das, S.N., and Chaudhury, G.R. (2009). Removal of Cr(VI) by thermally activated weed Salvinia cucullata in a fixed-bed column. **Journal of Hazardous Materials.** 161(2-3): 1427-1435.

Bentahar, Y., Hurel, C., Draoui, K., Khairoun, S., and Marmier, N. (2016). Adsorptive properties of Moroccan clays for the removal of arsenic(V) from aqueous solution. **Applied Clay Science.** 119: 385-392.

Bergaya, F., and Lagaly, G. (2001). Surface modification of clay minerals. **Applied Clay Science.** 19(2001): 1-3.

Bhatia, S., Balamurugan, G., and Baranwal, A. (2014). High arsenic contamination in drinking water hand-pumps in Khap Tola, West Champaran, Bihar, India. **Frontiers in Environmental Science.** 2(49): 1-8.

Bhattacharyya, K.G., and Gupta, S.S. (2008). Adsorption of a few heavy metals on natural and modified kaolinite and montmorillonite: a review. **Advances in Colloid and Interface Science.** 140(2): 114-131.

Bhowmick, S., Chakraborty, S., Mondal, P., Van Renterghem, W., Van den Berghe, S., Roman-Ross, G., Chatterjee, D., and Iglesias, M. (2014). Montmorillonite-supported nanoscale zero-valent iron for removal of arsenic from aqueous solution: Kinetics and mechanism. **Chemical Engineering Journal.** 243: 14-23.

Biterna, M., Arditsoglou, A., Tsikouras, E., and Voutsa, D. (2007). Arsenate removal by zero valent iron: batch and column tests. **Journal of Hazardous Materials.** 149(3): 548-552.

Bohart, G.S., and Adams, E.Q. (1920). Some aspects of the behavior of charcoal with respect to chlorine. **Journal of the American Chemical Society.** 42(3): 523-544.

Bradley, I., Straub, A., Maraccini, P., Markazi, S., and Nguyen, T.H. (2011). Iron oxide amended biosand filters for virus removal. **Water Research.** 45(15): 4501-4510.

Brammer, H., and Ravenscroft, P. (2009). Arsenic in groundwater: a threat to sustainable agriculture in South and South-east Asia. **Environment International.** 35(3): 647-654.

Chang, Q., Lin, W., and Ying, W.C. (2010). Preparation of iron-impregnated granular activated carbon for arsenic removal from drinking water. **Journal of Hazardous Materials.** 184(1-3): 515-522.

Chen, R., Lei, Z., Yang, S., Zhang, Z., Yang, Y., and Sugiura, N. (2012a). Characterization and modification of porous ceramic sorbent for arsenate removal. **Colloids and Surfaces A: Physicochemical and Engineering Aspects.** 414: 393-399.

Chen, R., Zhang, Z., Feng, C., Hu, K., Li, M., Li, Y., Shimizu, K., Chen, N., and Sugiura, N. (2010). Application of simplex-centroid mixture design in developing and optimizing ceramic adsorbent for As(V) removal from water solution. **Microporous and Mesoporous Materials.** 131(1-3): 115-121.

Chen, R., Zhang, Z., Lei, Z., and Sugiura, N. (2012b). Preparation of iron-impregnated tablet ceramic adsorbent for arsenate removal from aqueous solutions. **Desalination.** 286: 56-62.

Chen, S., Yue, Q., Gao, B., Li, Q., Xu, X., and Fu, K. (2012). Adsorption of hexavalent chromium from aqueous solution by modified corn stalk: a fixed-bed column study. **Bioresource Technology.** 113: 114-120.

Chen, Y., Parvez, F., Gamble, M., Islam, T., Ahmed, A., Argos, M., Graziano, J.H., and Ahsan, H. (2009). Arsenic exposure at low-to-moderate levels and skin lesions, arsenic metabolism, neurological functions, and biomarkers for respiratory and cardiovascular diseases: review of recent findings from the Health Effects of Arsenic Longitudinal Study (HEALS) in Bangladesh. **Toxicology and Applied Pharmacology.** 239(2): 184-192.

Chen, Z.X., Jin, X.Y., Chen, Z., Megharaj, M., and Naidu, R. (2011). Removal of methyl orange from aqueous solution using bentonite-supported nanoscale zero-valent iron. **Journal of Colloid and Interface Science.** 363(2): 601-607.

Chiban, M., Zerbet, M., Carja, G., and Sinan, F. (2012). Application of low-cost adsorbents for arsenic removal: A review. **Journal of Environmental Chemistry and Ecotoxicology.** 4(5): 91-102.

Chiew, H., Sampson, M.L., Huch, S., Ken, S., and Bostick, B.C. (2009). Effect of Groundwater Iron and Phosphate on the Efficacy of Arsenic Removal by Iron-Amended BioSand Filters. **Environmental Science and Technology.** 43(16): 6295-6300.

Choong, T.S.Y., Chuah, T.G., Robiah, Y., Gregory Koay, F.L., and Azni, I. (2007). Arsenic toxicity, health hazards and removal techniques from water: an overview. **Desalination.** 217(1-3): 139-166.

Churchman, G.J., Gates, W.P., Theng, B.K.G., and Yuan, G. (2006). Clays and clay minerals for pollution control. In **Developments in Clay Science** (vol. 1, pp. 625-675): Elsevier Science Publishers.

Chutia, P., Kato, S., Kojima, T., and Satokawa, S. (2009). Arsenic adsorption from aqueous solution on synthetic zeolites. **Journal of Hazardous Materials.** 162(1): 440-447.

Cornell, J.A. (2011). **Experiments with Mixtures: Designs, Models, and the Analysis of Mixture Data.** John Wiley and Sons: New York.

Cruz-Olivares, J., Pérez-Alonso, C., Barrera-Díaz, C., Ureña-Nuñez, F., Chaparro-Mercado, M.C., and Bilyeu, B. (2013). Modeling of lead (II) biosorption by residue of allspice in a fixed-bed column. **Chemical Engineering Journal.** 228: 21-27.

Das, R.P., and Anand, S. (1999). Precipitation of arsenic in the Fe (II)–NH_3–$(NH_4)_2$ SO_4–O_2 system. **Hydrometallurgy.** 53(3): 267-277.

Dodd, M.C., Vu, N.D., Ammann, A., Le, V.C., Kissner, R., Pham, H.V., Cao, T.H., Berg, M., and von Gunten, U. (2006). Kinetics and mechanistic aspects of As (III) oxidation by aqueous chlorine, chloramines, and ozone: relevance to drinking water treatment. **Environmental science and technology.** 40(10): 3285-3292.

Dousova, B., Fuitova, L., Grygar, T., Machovic, V., Kolousek, D., Herzogova, L., and Lhotka, M. (2009). Modified aluminosilicates as low-cost sorbents of As(III) from anoxic groundwater. **Journal of Hazardous Materials.** 165(1-3): 134-140.

Dousova, B., Grygar, T., Martaus, A., Fuitova, L., Kolousek, D., and Machovic, V. (2006). Sorption of As(V) on aluminosilicates treated with Fe(II) nanoparticles. **Journal of Colloid and Interface Science.** 302(2): 424-431.

Dutta, M., and Basu, J.K. (2013). Fixed-bed column study for the adsorptive removal of acid fuchsin using carbon–alumina composite pellet. **International Journal of Environmental Science and Technology.** 11(1): 87-96.

Ezzatahmadi, N., Ayoko, G.A., Millar, G.J., Speight, R., Yan, C., Li, J., Li, S., Zhu, J., and Xi, Y. (2017). Clay-supported nanoscale zero-valent iron composite materials for the remediation of contaminated aqueous solutions: A review. **Chemical Engineering Journal.** 312: 336-350.

Far, L. B., Souri, B., Heidari, M., and Khoshnavazi, R. (2012). Evaluation of iron and manganese-coated pumice application for the removal of as (v) from aqueous solutions. **Iranian Journal of Environmental Health Science and Engineering.** 9(1): 21.

Foo, K.Y., and Hameed, B.H. (2010). Insights into the modeling of adsorption isotherm systems. **Chemical Engineering Journal.** 156(1): 2-10.

Foo, K.Y., Lee, L.K., and Hameed, B.H. (2013). Preparation of tamarind fruit seed activated carbon by microwave heating for the adsorptive treatment of landfill leachate: A laboratory column evaluation. **Bioresource Technology.** 133: 599-605.

Fufa, F., Alemayehu, E., and Lennartz, B. (2014). Sorptive removal of arsenate using termite mound. **Journal of Environmental Management.** 132: 188-196.

Gallegos-Garcia, M., Ramírez-Muñiz, K., and Song, S. (2012). Arsenic removal from water by adsorption using iron oxide minerals as adsorbents: a review. **Mineral Processing and Extractive Metallurgy Review.** 33(5): 301-315.

Gang, D.D., Deng, B., and Lin, L. (2010). As(III) removal using an iron-impregnated chitosan sorbent. **Journal of Hazardous Materials.** 182(1-3): 156-161.

Garelick, H., Dybowska, A., Valsami-Jones, E., and Priest, N. (2005). Remediation technologies for arsenic contaminated drinking waters. **Journal of Soils and Sediments.** 5(3): 182-190.

Ghosh, A., Chakrabarti, S., and Ghosh, U.C. (2014). Fixed-bed column performance of Mn-incorporated iron(III) oxide nanoparticle agglomerates on As(III) removal from the spiked groundwater in lab bench scale. **Chemical Engineering Journal.** 248: 18-26.

Ghurye, G., and Clifford, D. (2004). As (III) oxidation using chemical and solid-phase oxidants. **Journal (American Water Works Association).** 96(1): 84-96.

Gleick, P.H. (1996). Basic Water Requirements for Human Activities: Meeting Basic Needs. **Water International.** 21(2): 83-92.

Glocheux, Y., Pasarín, M.M., Albadarin, A.B., Allen, S.J., and Walker, G.M. (2013). Removal of arsenic from groundwater by adsorption onto an acidified laterite by-product. **Chemical Engineering Journal.** 228: 565-574.

Goldberg, S., and Johnston, C.T. (2001). Mechanisms of arsenic adsorption on amorphous oxides evaluated using macroscopic measurements, vibrational spectroscopy, and surface complexation modeling. **Journal of Colloid and Interface Science.** 234(1): 204-216.

Grossl, P.R., Eick, M., Sparks, D.L., Goldberg, S., and Ainsworth, C.C. (1997). Arsenate and chromate retention mechanisms on goethite. 2. Kinetic evaluation using a pressure-jump relaxation technique. **Environmental Science and Technology.** 31(2): 321-326.

Hamayun, M., Mahmood, T., Naeem, A., Muska, M., Din, S.U., and Waseem, M. (2014). Equilibrium and kinetics studies of arsenate adsorption by FePO(4). **Chemosphere.** 99: 207-215.

Henke, K. (2009). **Arsenic: Environmental Chemistry, Health Threats and Waste Treatment**. John Wiley and Sons: West Sussex.

Holl, W.H. (2010). Mechanisms of arsenic removal from water. **Environmental Geochemistry and Health.** 32(4): 287-290.

Hossain, M.M., and Piantanakulchai, M. (2013). Groundwater arsenic contamination risk prediction using GIS and classification tree method. **Engineering Geology.** 156: 37-45.

Hsu, J.C., Lin, C.J., Liao, C.H., and Chen, S.T. (2008). Evaluation of the multiple-ion competition in the adsorption of As(V) onto reclaimed iron-oxide coated sands by fractional factorial design. **Chemosphere.** 72(7): 1049-1055.

Hu, C., Liu, H., Chen, G., and Qu, J. (2012). Effect of aluminum speciation on arsenic removal during coagulation process. **Separation and Purification Technology.** 86: 35-40.

Hua, M., Zhang, S., Pan, B., Zhang, W., Lv, L., and Zhang, Q. (2012). Heavy metal removal from water/wastewater by nanosized metal oxides: a review. **Journal of Hazardous Materials.** 211-212: 317-331.

Hughes, M.F. (2002). Arsenic toxicity and potenital mechanisms of action. **Toxicology Letters.** 133(2002): 1-16.

Jain, C.K., and Singh, R.D. (2012). Technological options for the removal of arsenic with special reference to South East Asia. **Journal of Environmental Management.** 107: 1-18.

Jain, M., Garg, V.K., and Kadirvelu, K. (2013). Cadmium(II) sorption and desorption in a fixed bed column using sunflower waste carbon calcium-alginate beads. **Bioresource Technology.** 129: 242-248.

Jang, J., and Lee, D.S. (2016). Enhanced adsorption of cesium on PVA-alginate encapsulated Prussian blue-graphene oxide hydrogel beads in a fixed-bed column system. **Bioresource Technology.** 218: 294-300.

Jiang, M.Q., Wang, Q.P., Jin, X.Y., and Chen, Z.L. (2009). Removal of Pb(II) from aqueous solution using modified and unmodified kaolinite clay. **Journal of Hazardous Materials.** 170(1): 332-339.

Jung, K.W., and Ahn, K.H. (2016). Fabrication of porosity-enhanced MgO/biochar for removal of phosphate from aqueous solution: application of a novel combined electrochemical modification method. **Bioresource Technology.** 200: 1029-1032.

Kakavandi, B., Jahangiri-rad, M., Rafiee, M., Esfahani, A.R., and Babaei, A.A. (2016). Development of response surface methodology for optimzation of phenol and *p*-chlorophenol adsorption on magnetic recoverable carbon. **Microporous and Mesoporous Materials.** 231(2016): 192-206.

Kang, Y., Takeda, R., Nada, A., Thavarith, L., Tang, S., Nuki, K., and Sakurai, K. (2014). Removing arsenic from groundwater in Cambodia using high performance iron adsorbent. **Environmental Monitoring and Assessment.** 186(9): 5605-5616.

Kango, S., and Kumar, R. (2016). Low-cost magnetic adsorbent for As (III) removal from water: adsorption kinetics and isotherms. **Environmental Monitoring and Assessment.** 188(1): 1-14.

Karagas, M.R., Gossai, A., Pierce, B., and Ahsan, H. (2015). Drinking Water Arsenic Contamination, Skin Lesions, and Malignancies: A Systematic Review of the Global Evidence. **Current Environmental Health Reports.** 2(1): 52-68.

Katsoyiannis, I.A., and Zouboulis, A.I. (2002). Removal of arsenic from contaminated water sources by sorption onto iron-oxide-coated polymeric materials. **Water Research.** 36(2002): 5141-5455.

Khan, T.A. and Khan, E.A. (2015). Removal of basic dyes from aqueous solution by adsorption onto binary iron-manganese oxide coated kaolinite: Non-linear isotherm and kinetics modeling. **Applied Clay Science.** 107: 70-77.

Khataee, A.R., Dehghan, G., Ebadi, E., and Pourhassan, M. (2010). Central composite design optimization of biological dye removal in the presence of macroalgae *Chara sp.* **Clean- Soil, Air, Water.** 38(8): 750-757.

Kim, M.J., and Nriagu, J. (2000). Oxidation of arsenite in groundwater using ozone and oxygen. **Science of the Total Environment.** 247(1): 71-79.

Kuila, U., and Prasad, M. (2013). Specific surface area and pore-size distribution in clays and shales. **Geophysical Prospecting.** 61(2): 341-362.

Lemus, J., Moya, C., Gilarranz, M.A., Rodriguez, J.J., and Palomar, J. (2017). Fixed-bed adsorption of ionic liquids onto activated carbon from aqueous phase. **Journal of Environmental Chemical Engineering.** 5(6): 5347-5351.

Lenoble, V., Laclautre, C., Deluchat, V., Serpaud, B., and Bollinger, J.C. (2005). Arsenic removal by adsorption on iron(III) phosphate. **Journal of Hazardous Materials.** 123(1-3): 262-268.

Li, S., Wang, W., Liang, F., and Zhang, W.X. (2017). Heavy metal removal using nanoscale zero-valent iron (nZVI): Theory and application. **Journal of Hazardous Materials.** 322(Pt A): 163-171.

Li, S., Wu, P., Li, H., Zhu, N., Li, P., Wu, J., Wang, X. and Dang, Z. (2010). Synthesis and characterization of organo-montmorillonite supported iron nanoparticles. **Applied Clay Science.** 50(3): 330-336.

Li, X., Zhao, Y., Xi, B., Mao, X., Gong, B., Li, R., Peng, X. and Liu, H. (2016). Removal of nitrobenzene by immobilized nanoscale zero-valent iron: Effect of clay support and efficiency optimization. **Applied Surface Science.** 370: 260-269.

Li, Y., Cai, X., Guo, J., Zhou, S., and Na, P. (2015). Fe/Ti co-pillared clay for enhanced arsenite removal and photo oxidation under UV irradiation. **Applied Surface Science.** 324: 179-187.

Lim, A.P., and Aris, A.Z. (2014). Continuous fixed-bed column study and adsorption modeling: Removal of cadmium (II) and lead (II) ions in aqueous solution by dead calcareous skeletons. **Biochemical Engineering Journal.** 87: 50-61.

Lin, X., Huang, Q., Qi, G., Shi, S., Xiong, L., Huang, C., Chen, X., Li, H., and Chen, X. (2017). Estimation of fixed-bed column parameters and mathematical modeling of breakthrough behaviors for adsorption of levulinic acid from aqueous solution using SY-01 resin. **Separation and Purification Technology.** 174: 222-231.

Litter, M.I., Morgada, M.E., and Bundschuh, J. (2010). Possible treatments for arsenic removal in Latin American waters for human consumption. **Environmental Pollution.** 158(5): 1105-1118.

Liu, X., Ao, H., Xiong, X., Xiao, J., and Liu, J. (2012). Arsenic removal from water by iron-modified bamboo charcoal. **Water, Air, and Soil Pollution: Focus.** 223(3): 1033-1044.

Luengo, C., Puccia, V., and Avena, M. (2011). Arsenate adsorption and desorption kinetics on a Fe(III)-modified montmorillonite. **Journal of Hazardous Materials.** 186(2-3): 1713-1719.

Luu, T.T., Sthiannopkao, S., and Kim, K.W. (2009). Arsenic and other trace elements contamination in groundwater and a risk assessment study for the residents in the Kandal Province of Cambodia. **Environment International.** 35(3): 455-460.

Mahmood, Q., Baig, S.A., Nawab, B., Shafqat, M.N., Pervez, A., and Zeb, B.S. (2011). Development of low cost household drinking water treatment system for the earthquake affected communities in Northern Pakistan. **Desalination.** 273(2-3): 316-320.

Mahmood, T., Din, S.U., Naeem, A., Mustafa, S., Waseem, M., and Hamayun, M. (2012). Adsorption of arsenate from aqueous solution on binary mixed oxide of iron and silicon. **Chemical Engineering Journal.** 192: 90-98.

Maiti, A., Agarwal, V., De, S., and Basu, J.K. (2010). Removal of As(V) using iron oxide impregnated carbon prepared from Tamarind hull. **Journal of Environmental Science and Health Part A.** 45(10): 1203-1212.

Maji, S.K., Kao, Y.-H., Wang, C.-J., Lu, G.-S., Wu, J.-J., and Liu, C.-W. (2012). Fixed bed adsorption of As(III) on iron-oxide-coated natural rock (IOCNR) and application to real arsenic-bearing groundwater. **Chemical Engineering Journal.** 203: 285-293.

Mak, M.S., Rao, P., and Lo, I.M. (2011). Zero-valent iron and iron oxide-coated sand as a combination for removal of co-present chromate and arsenate from groundwater with humic acid. **Environmental Pollution.** 159(2): 377-382.

Malik, A.H., Khan, Z.M., Mahmood, Q., Nasreen, S., and Bhatti, Z.A. (2009). Perspectives of low cost arsenic remediation of drinking water in Pakistan and other countries. **Journal of Hazardous Materials.** 168(1): 1-12.

Maliyekkal, S.M., Philip, L., and Pradeep, T. (2009). As(III) removal from drinking water using manganese oxide-coated-alumina: Performance evaluation and mechanistic details of surface binding. **Chemical Engineering Journal.** 153(1-3): 101-107.

Malkoc, E., and Nuhoglu, Y. (2006). Fixed bed studies for the sorption of chromium(VI) onto tea factory waste. **Chemical Engineering Science.** 61(13): 4363-4372.

Mandal, B.K., and Suzuki, K.T. (2002). Arsenic round the world: a review. **Talanta.** 58(2002): 201-235.

Mandal, N.K., Pal, M., Sinha, B.K., and Das, P. (2008). Optimum mixture designs under constraints on mixing components. **Statistics and Applications.** 6(1): 189-205.

Masih, D., Izumi, Y., Aika, K., and Seida, Y. (2007). Optimization of an Iron Intercalated Montmorillonite Preparation for the Removal of Arsenic at Low Concentrations. **Engineering in Life Sciences.** 7(1): 52-60.

Massoudinejad, M., Ghaderpoori, M., Shahsavani, A., and Amini, M.M. (2016). Adsorption of fluoride over a metal organic framework Uio-66 functionalized with amine groups and optimization with response surface methodology. **Journal of Molecular Liquids.** 221(2016): 279-286.

174

Mishra, T., and Mahato, D.K. (2016). A comparative study on enhanced arsenic(V) and arsenic(III) removal by iron oxide and manganese oxide pillared clays from ground water. **Journal of Environmental Chemical Engineering.** 4(1): 1224-1230.

Mohan, D., and Pittman, C.U.,Jr. (2007). Arsenic removal from water/wastewater using adsorbents-A critical review. **Journal of Hazardous Materials.** 142(1-2): 1-53.

Mohan, S., Singh, D.K., Kumar, V., and Hasan, S.H. (2017). Effective removal of Fluoride ions by rGO/ZrO2 nanocomposite from aqueous solution: Fixed bed column adsorption modelling and its adsorption mechanism. **Journal of Fluorine Chemistry.** 194: 40-50.

Mohapatra, D., Mishra, D., Chaudhury, G.R., and Das, R.P. (2007). Arsenic(V) adsorption mechanism using kaolinite, montmorillonite and illite from aqueous medium. **Journal of Environmental Science and Health Part A.** 42(4): 463-469.

Mondal, P., Bhowmick, S., Chatterjee, D., Figoli, A., and Van der Bruggen, B. (2013). Remediation of inorganic arsenic in groundwater for safe water supply: a critical assessment of technological solutions. **Chemosphere.** 92(2): 157-170.

Muniz, G., Fierro, V., Celzard, A., Furdin, G., Gonzalez-Sanchez, G., and Ballinas, M.L. (2009). Synthesis, characterization and performance in arsenic removal of iron-doped activated carbons prepared by impregnation with Fe(III) and Fe(II). **Journal of Hazardous Materials.** 165(1-3): 893-902.

Murray, H. H. (2006). Structure and composition of the clay minerals and their physical and chemical properties. In **Developments in Clay Science** (vol. 2, pp. 7-31). Elsevier Science Publishers.

Na, P., Jia, X., Yuan, B., Li, Y., Na, J., Chen, Y., and Wang, L. (2010). Arsenic adsorption on Ti-pillared montmorillonite. **Journal of Chemical Technology and Biotechnology.** 85(5): 708-714.

Nair, A.T., Makwana, A.R., and Ahammed, M.M. (2014). The use of response surface methodology for modelling and analysis of water and wastewater treatment process: a review. **Water Science and Technology.** 69(3): 464-478.

Nayak, P.S., and Singh, B.K. (2007). Instrumental characterization of clay by XRF, XRD and FTIR. **Bulletin of Materials Science.** 30(3): 235-238.

Nazari, G., Abolghasemi, H., Esmaieli, M., and Sadeghi Pouya, E. (2016). Aqueous phase adsorption of cephalexin by walnut shell-based activated carbon: A fixed-bed column study. **Applied Surface Science.** 375: 144-153.

Ng, J.C., Wang, J., and Shraim, A. (2003). A global health problem caused by arsenic from natural sources. **Chemosphere.** 52(9): 1353-1359.

Ngai, T.K., Shrestha, R.R., Dangol, B., Maharjan, M., and Murcott, S.E. (2007). Design for sustainable development-household drinking water filter for arsenic and pathogen treatment in Nepal. **Journal of Environmental Science and Health Part A.** 42(12): 1879-1888.

Nguyen, T.A., Ngo, H.H., Guo, W.S., Pham, T.Q., Li, F.M., Nguyen, T.V., and Bui, X.T. (2015). Adsorption of phosphate from aqueous solutions and sewage using zirconium loaded okara (ZLO): Fixed-bed column study. **Science of the Total Environment.** 523: 40-49.

Noubactep, C., and Caré, S. (2010). Enhancing sustainability of household water filters by mixing metallic iron with porous materials. **Chemical Engineering Journal.** 162(2): 635-642.

O'Day, P.A., and Vlassopoulos, D. (2010). Mineral-Based Amendments for Remediation. **Elements (Que).** 6(6): 375-381.

Ouadjenia-Marouf, F., Marouf, R., Schott, J., and Yahiaoui, A. (2013). Removal of Cu(II), Cd(II) and Cr(III) ions from aqueous solution by dam silt. **Arabian Journal of Chemistry.** 6(4): 401-406.

Öztel, M.D., Akbal, F., and Altaş, L. (2015). Arsenite removal by adsorption onto iron oxide-coated pumice and sepiolite. **Environmental Earth Sciences.** 73(8): 4461-4471.

Pallier, V., Feuillade-Cathalifaud, G., Serpaud, B., and Bollinger, J.C. (2010). Effect of organic matter on arsenic removal during coagulation/flocculation treatment. **Journal of Colloid and Interface Science.** 342(1): 26-32.

Petala, E., Dimos, K., Douvalis, A., Bakas, T., Tucek, J., Zbořil, R., and Karakassides, M. A. (2013). Nanoscale zero-valent iron supported on mesoporous silica: characterization and reactivity for Cr (VI) removal from aqueous solution. **Journal of Hazardous Materials.** 261: 295-306.

Pillewan, P., Mukherjee, S., Roychowdhury, T., Das, S., Bansiwal, A., and Rayalu, S. (2011). Removal of As(III) and As(V) from water by copper oxide incorporated mesoporous alumina. **Journal of Hazardous Materials.** 186(1): 367-375.

Prakash, O., Talat, M., Hasan, S.H., and Pandey, R.K. (2008). Factorial design for the optimization of enzymatic detection of cadmium in aqueous solution using immobilized urease from vegetable waste. **Bioresource technology.** 99(16): 7565-7572.

Qi, J., Zhang, G., and Li, H. (2015). Efficient removal of arsenic from water using a granular adsorbent: Fe–Mn binary oxide impregnated chitosan bead. **Bioresource Technology.** 193: 243-249.

Ramesh, A., Hasegawa, H., Maki, T., and Ueda, K. (2007). Adsorption of inorganic and organic arsenic from aqueous solutions by polymeric Al/Fe modified montmorillonite. **Separation and Purification Technology.** 56(1): 90-100.

Rao, P.V., and Baral, S.S. (2011). Experimental design of mixture for the anaerobic co-digestion of sewage sludge. **Chemical Engineering Journal.** 172: 977-986.

Ren, X., Zhang, Z., Luo, H., Hu, B., Dang, Z., Yang, C., and Li, L. (2014). Adsorption of arsenic on modified montmorillonite. **Applied Clay Science.** 97-98: 17-23.

Rivera-Hernandez, J.R., and Green-Ruiz, C. (2014). Geosorption of As(III) from aqueous solution by red clays: kinetic studies. **Bulletin of Environmental Contamination and Toxicology.** 92(5): 596-601.

Roberts, L.C., Hug, S.J., Ruettimann, T., Billah, M.M., Khan, A.W., and Rahman, M.T. (2004). Arsenic removal with iron (II) and iron (III) in waters with high silicate and phosphate concentrations. **Environmental Science and Technology.** 38(1): 307-315.

Roosta, M., Ghaedi, M., Daneshfar, A., and Sahraei, R. (2014). Experimental design based response surface methodology optimization of ultrasonic assisted adsorption of safaranin O by tin sulfide nanoparticle loaded on activated carbon. **Spectrochimica Acta Part A: Molecular and Biomolecular Spectroscopy.** 122: 223-231.

Rosales, E., Ferreira, L., Sanromán, M.Á., Tavares, T., and Pazos, M. (2015). Enhanced selective metal adsorption on optimised agroforestry waste mixtures. **Bioresource Technology.** 182: 41-49.

Rostamiyan, Y., Hamed, M.A., and SalmanKhani, A. (2014). Optimization of mechanical properties of epoxy-based hybrid nanocomposite: Effect of using nano silica and high-impact polystyrene by mixture design approach. **Materials and Design.** 56: 1068-1077.

Roy, P., Mondal, N.K., Bhattacharya, S., Das, B., and Das, K. (2013). Removal of arsenic(III) and arsenic(V) on chemically modified low-cost adsorbent: batch and column operations. **Applied Water Science.** 3(1): 293-309.

Sabbatini, P., Yrazu, F., Rossi, F., Thern, G., Marajofsky, A., and Fidalgo de Cortalezzi, M.M. (2010). Fabrication and characterization of iron oxide ceramic membranes for arsenic removal. **Water Research.** 44(19): 5702-5712.

Salameh, Y., Al-Lagtah, N., Ahmad, M.N.M., Allen, S. J., and Walker, G.M. (2010). Kinetic and thermodynamic investigations on arsenic adsorption onto dolomitic sorbents. **Chemical Engineering Journal.** 160(2): 440-446.

Sarkar, A., and Paul, B. (2016). The global menace of arsenic and its conventional remediation - A critical review. **Chemosphere.** 158: 37-49.

Scheffe, H. (1963). The simplex-centroid design for experiments with mixtures. **Journal of the Royal Statistical Society. Series B (Methodological).** 235-263.

Sdiri, A., Higashi, T., Hatta, T., Jamoussi, F., and Tase, N. (2011). Evaluating the adsorptive capacity of montmorillonitic and calcareous clays on the removal of several heavy metals in aqueous systems. **Chemical Engineering Journal.** 172(1): 37-46.

Sen Gupta, S., and Bhattacharyya, K.G. (2011). Kinetics of adsorption of metal ions on inorganic materials: a review. **Advances in Colloid and Interface Science.** 162(1): 39-58.

Shafiquzzam, M., Hasan, M.M., and Nakajima, J. (2013). Iron mixed ceramic pellet for arsenic removal from groundwater. **Environmental Engineering Research.** 18(3): 163-168.

Shah, S.H., Mahmood, Q., Raja, I. A., Pervez, A., and Kalsoom, A. (2013). Bio-Sand filter to treat arsenic contaminated drinking water. **Desalination and Water Treatment.** 53(11): 2999-3006.

Shahamirifard, S.A.R., Ghaedi, M., Rahimi, M.R., Hajati, S., Montazerozohori, M., and Soylak, M. (2016). Simultaneous extraction and preconcentration of Cu^{2+}, Ni^{2+} and Zn^{2+} ions using Ag nanoparticle-loaded activated carbon: response surface methodology. **Advanced Powder Technology.** 27(2): 426-435.

Sharma, A.K., Tjell, J.C., Sloth, J.J., and Holm, P.E. (2014). Review of arsenic contamination, exposure through water and food and low cost mitigation options for rural areas. **Applied Geochemistry.** 41: 11-33.

Sharma, V.K., Dutta, P.K., and Ray, A.K. (2007). Review of kinetics of chemical and photocatalytical oxidation of Arsenic(III) as influenced by pH. **Journal of Environmental Science and Health Part A.** 42(7): 997-1004.

Šiljeg, M., Foglar, L., and Gudelj, I. (2012). The removal of arsenic from water with natural and modified clinoptilolite. **Chemistry and Ecology.** 28(1): 75-87.

Singh, R., Singh, S., Parihar, P., Singh, V.P., and Prasad, S.M. (2015). Arsenic contamination, consequences and remediation techniques: a review. **Ecotoxicology and Environmental Safety.** 112: 247-270.

Singh, T.S., and Pant, K.K. (2006). Experimental and modelling studies on fixed bed adsorption of As(III) ions from aqueous solution. **Separation and Purification Technology.** 48(3): 288-296.

Smedley, P.L., and Kinniburgh, D.G. (2002). A review of the source, behaviour and distribution of arsenic in natural waters. **Applied Geochemistry.** 17(5): 517-568.

Smith, K., Li, Z., Chen, B., Liang, H., Zhang, X., Xu, R., Li, Z., Dai, H., Wei, C., and Liu, S. (2017). Comparison of sand-based water filters for point-of-use arsenic removal in China. **Chemosphere.** 168: 155-162.

Srilomsak, S., Pattanasiriwisawa, W., Somphon, W., Tanthanuch, W., and Meethong, N. (2014). Effect of firing conditions on properties of Dan Kwian pottery. **Suranaree Journal of Science and Technology.** 21(3): 125-135.

Srinivasan, R. (2011). Advances in application of natural clay and its composites in removal of biological, organic, and inorganic contaminants from drinking water. **Advances in Materials Science and Engineering.** 2011: 1-17.

Srivastava, V., Sharma, Y.C., and Sillanpaa, M. (2015). Response surface methodological approach for the optimization of adsorption process in the removal of Cr(VI) ions by Cu₂(OH)₂CO₃ nanoparticles. **Applied Surface Science.** 326(257-270).

Stauber, C.E., Printy, E.R., McCarty, F.A., Liang, K.R., and Sobsey, M.D. (2012). Cluster randomized controlled trial of the plastic BioSand Water filter in Cambodia. **Environmental Science and Technology.** 46(2): 722-728.

Su, C., and Puls, R.W. (2001). Arsenate and arsenite removal by zerovalent iron: kinetics, redox transformation, and implications for in situ groundwater remediation. **Environmental Science and Technology.** 35(7): 1487-1492.

Su, J., Huang, H.G., Jin, X.Y., Lu, X.Q., and Chen, Z.L. (2011). Synthesis, characterization and kinetic of a surfactant-modified bentonite used to remove As(III) and As(V) from aqueous solution. **Journal of Hazardous Materials.** 185(1): 63-70.

Sullivan, C., Tyrer, M., Cheeseman, C.R., and Graham, N.J. (2010). Disposal of water treatment wastes containing arsenic -a review. **Science of the Total Environment.** 408(8): 1770-1778.

Sun, X., Imai, T., Sekine, M., Higuchi, T., Yamamoto, K., Kanno, A., and Nakazono, S. (2014). Adsorption of phosphate using calcined Mg3–Fe layered double hydroxides in a fixed-bed column study. **Journal of Industrial and Engineering Chemistry.** 20(5): 3623-3630.

Taamneh, Y., and Al Dwairi, R. (2013). The efficiency of Jordanian natural zeolite for heavy metals removal. **Applied Water Science.** 3(1): 77-84.

Tandon, P.K., Shukla, R.C., and Singh, S.B. (2013). Removal of arsenic (III) from water with clay-supported zerovalent iron nanoparticles synthesized with the help of tea liquor. **Industrial and Engineering Chemistry Research.** 52(30): 10052-10058.

Tchobanoglous, G., Burton, F.L., and Stensel, H.D. (2003). **Wastewater Engineering: Treatment and Reuse.** McGraw-Hill Higher Education: New York.

Te, B., Wichitsathian, B., and Yossapol, C. (2015). Modification of natural common clays as low cost adsorbents for arsenate adsorption. **International Journal of Environmental Science and Development.** 6(11): 799-804.

Te, B., Wichitsathian, B., and Yossapol, C. (2016). Uptake behavior of arsenate from aqueous solution using ferric-coated mesoporous ceramic adsorbent. **Jurnal Teknologi.** 78(5-3): 65-71.

Te, B., Wichitsathian, B., and Yossapol, C. (2017a). Adsorptive behavior of low-cost modified natural clay adsorbents for arsenate removal from water. **International Journal of GEOMATE.** 12(33): 1-7

Te, B., Wichitsathian, B., Yossapol, C., and Wonglertarak, W. (2017b). Development of low-cost iron mixed porous pellet adsorbent by mixture design approach and its application for arsenate and arsenite adsorption from water. **Adsorption Science and Technology.** 36(1-2): 372-392.

Thomas, H.C. (1944). Heterogeneous ion exchange in a flowing system. **Journal of the American Chemical Society.** 66(10): 1664-1666.

Tiwari, D., and Lee, S.M. (2012). Novel hybrid materials in the remediation of ground waters contaminated with As(III) and As(V). **Chemical Engineering Journal.** 204-206: 23-31.

Tran, H.N., You, S.J., Hosseini-Bandegharaei, A., and Chao, H.P. (2017). Mistakes and inconsistencies regarding adsorption of contaminants from aqueous solutions: A critical review. **Water Research.** 120: 88-116.

Tyruvoda, K., Nikolaidis, N.P., Veranis, N., Kallithrakas-Kontos, N., and Koulouridakis, P.E. (2006). Arsenic removal from geothermal waters with zero-valent iron--effect of temperature, phosphate and nitrate. **Water Research.** 40(12): 2375-2386.

Vaishya, R.C., and Gupta, S.K. (2010). Arsenic (III) adsorption by mixed-oxide-coated sand: kinetic modeling and desorption studies. **Journal of Hazardous, Toxic, and Radioactive Waste.** 15(3): 199-207.

Villaescusa, I., and Bollinger, J.-C. (2008). Arsenic in drinking water: sources, occurrence and health effects (a review). **Reviews in Environmental Science and Bio/Technology.** 7(4): 307-323.

Wang, C., Luo, H., Zhang, Z., Wu, Y., Zhang, J., and Chen, S. (2014). Removal of As(III) and As(V) from aqueous solutions using nanoscale zero valent iron-reduced graphite oxide modified composites. **Journal of Hazardous Materials.** 268: 124-131.

Wang, S., and Mulligan, C.N. (2006). Occurrence of arsenic contamination in Canada: sources, behavior and distribution. **Science of the Total Environment.** 366(2-3): 701-721.

Wang, W., Li, M., and Zeng, Q. (2015). Adsorption of chromium (VI) by strong alkaline anion exchange fiber in a fixed-bed column: Experiments and models fitting and evaluating. **Separation and Purification Technology.** 149: 16-23.

Worch, E. (2012). **Adsorption Technology in Water Treatment: Fundamentals, Processes, and Modeling.** Walter de Gruyter: Berlin.

Yagub, M.T., Sen, T.K., Afroze, S., and Ang, H.M. (2014). Dye and its removal from aqueous solution by adsorption: a review. **Advances in Colloid and Interface Science.** 209: 172-184.

Yaqubzadeh, A.R., Ahmadpour, A., Bastami, T.R., and Hataminia, M.R. (2016). Low-cost preparation of silica aerogel for optimized adsorptive removal of naphthalene from aqueous solution with central composite design (CCD). **Journal of Non-Crystalline Solids.** 447(2016): 307-314.

Yildiz, B.S. (2016). Performance assessment of modified biosand filter with an extra disinfection layer. **Journal of Water Supply: Research and Technology - Aqua.** 65(3): 266-276.

Yin, H., Kong, M., Gu, X., and Chen, H. (2017). Removal of arsenic from water by porous charred granulated attapulgite-supported hydrated iron oxide in bath and column modes. **Journal of Cleaner Production.** 166: 88-97.

Yuan, L., and Liu, Y. (2013). Removal of Pb (II) and Zn (II) from aqueous solution by ceramisite prepared by sintering bentonite, iron powder and activated carbon. **Chemical Engineering Journal.** 215: 432-439.

Zehhaf, A., Benyoucef, A., Quijada, C., Taleb, S., and Morallón, E. (2015). Algerian natural montmorillonites for arsenic (III) removal in aqueous solution. **International Journal of Environmental Science and Technology.** 12(2): 595-602.

Zhao, S., Feng, C., Huang, X., Li, B., Niu, J., and Shen, Z. (2012). Role of uniform pore structure and high positive charges in the arsenate adsorption performance of Al13-modified montmorillonite. **Journal of Hazardous Materials.** 203-204: 317-325.

Zhou, C.H., and Keeling, J. (2013). Fundamental and applied research on clay minerals: From climate and environment to nanotechnology. **Applied Clay Science.** 74: 3-9.
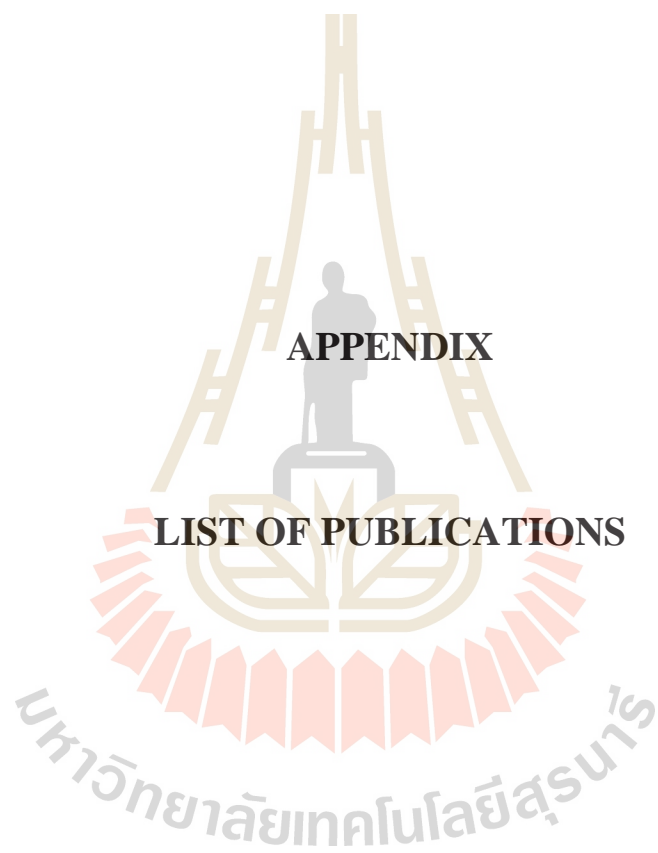
APPENDIX

LIST OF PUBLICATIONS

LIST OF PUBLICATIONS

International Publications

Te, B., Wichitsathian, B., and Yossapol, C. (2015). Modification of natural common clays as low cost adsorbents for arsenate adsorption. **International Journal of Environmental Science and Development.** 6(11): 799-804.

Te, B., Wichitsathian, B., and Yossapol, C. (2016). Uptake behavior of arsenate from aqueous solution using ferric-coated mesoporous ceramic adsorbent. **Jurnal Teknologi.** 78(5-3): 65-71.

Te, B., Wichitsathian, B., and Yossapol, C. (2017). Adsorptive behavior of low-cost modified natural clay adsorbents for arsenate removal from water. **International Journal of GEOMATE**. 12(33): 1-7

Te, B., Wichitsathian, B., Yossapol, C., and Wonglertarak, W. (2017). Development of low-cost iron mixed porous pellet adsorbent by mixture design approach and its application for arsenate and arsenite adsorption from water. **Adsorption Science and Technology.** 36(1-2): 372-392.

Te, B., Wichitsathian, B., Yossapol, C., and Wonglertarak, W. (2018). Coexisting arsenate and arsenite adsorption from water using iron mixed porous pellet adsorbents: Optimization by response surface methodology. **Global Journal of Environmental Science and Management.** 4(2): 141-152.

Te, B., Wichitsathian, B., Yossapol, C., and Wonglertarak, W. (2018). Enchancing the quality of elevated arsenic contaminated groundwater in Cambodia using a household biosand filter with iron mixed porous pellet as active media. **Water Practice and Technology.** (Accepted)

International Conference Proceedings

Wichitsathian, B., Yossapol, C., and Te, B. (2015). Isotherm study for the uptake of As(V) from aqueous solution by local pottery clay. **Fourth International Conference on Environmental Engineering, Science and Management.** Chiang Mai, Thailand.

Te, B., Wichitsathian, B., and Yossapol, C. (2016). Adsorptive behavior of low-cost modified natural clay adsorbents for arsenate removal from water. **Second International Conference on Science, Engineering, and Environment (SEE-2016)**. Osaka, Japan.

Poster Publication

Wichitsathian, B., Yossapol, C. and Te, B. (2016). Modification of calcined-natural clays as low-cost adsorbents for arsenite adsorption from water. **Asia-Pacific Conference on Engineering and Applied Science (APCEAS-2016).** Tokyo, Japan.

BIOGRAPHY

Mr. Borano Te was born on December 12, 1987 in Kampong Cham Province, Cambodia. He obtained a bachelor degree of technology in Civil Construction from Preah Kossomak Polytechnic Institute, Phnom Penh, Cambodia in 2008 under the government scholarship. He graduated with a senior technical instructor diploma from National Technical Training Institute, Phnom Penh in 2009, and has been appointed by the Ministry of Labour and Vocational Training as a senior technical instructor for a teachning position at Preah Kossomak Polytechnic Institute since then. In 2010, he graduated with a bachelor degree of science in Environmental Science from Paññāsāstra University of Cambodia, Phnom Penh under the supportive university scholarship in accordane with a great achiement in academic. In 2012, he won a SUT-ASEAN Ph.D. Scholarship program to pursue a graduate study of doctoral level in School of Environmental Engineering, Institute of Engineering, Suranaree University of Technology (SUT), Nakhon Ratchasima 30000, Thailand. Within conducting his Ph.D., he has published several scientific research articles in international journals with regard to environmental pollution remediations.